

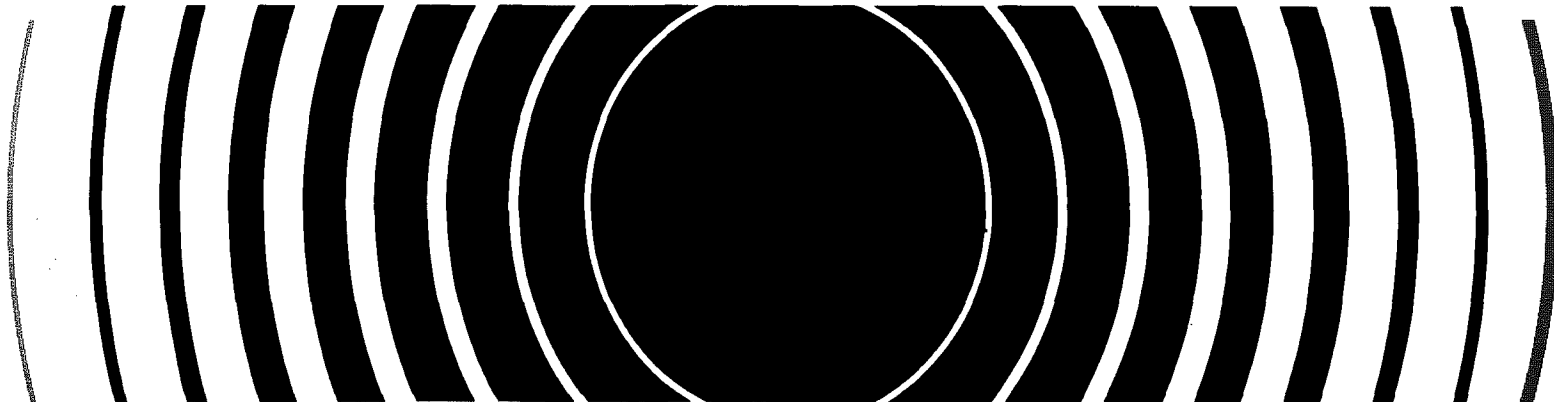
---

Radiation

---



# **Analysis and Evaluation of a Radioactive Waste Package Retrieved from the Atlantic 2800 Meter Disposal Site**



#### EPA REVIEW NOTICE

This report has been reviewed by the Office of Radiation Programs, U.S. Environmental Protection Agency (EPA) and approved for publication. Approval does not signify that the contents necessarily reflect the views and policies of the EPA. Neither the United States Government nor the EPA makes any warranty, expressed or implied, or assumes any legal liability or responsibility for any information, apparatus, product or process disclosed, or represents that its use would not infringe on privately owned rights.

ANALYSIS AND EVALUATION OF A RADIOACTIVE WASTE PACKAGE  
RETRIEVED FROM THE ATLANTIC 2800 METER DISPOSAL SITE

BY

P. COLOMBO, R.M. NEILSON, JR. AND M.W. KENDIG  
NUCLEAR WASTE MANAGEMENT RESEARCH GROUP  
DEPARTMENT OF NUCLEAR ENERGY  
BROOKHAVEN NATIONAL LABORATORY  
ASSOCIATED UNIVERSITIES, INC.  
UPTON, NEW YORK 11973

SEPTEMBER 1979

REVISED MAY 1982

THIS REPORT WAS PREPARED AS AN ACCOUNT OF WORK SPONSORED  
BY THE UNITED STATES ENVIRONMENTAL PROTECTION AGENCY  
UNDER INTERAGENCY AGREEMENT NO. EPA-IAG-D6-0166

PROJECT OFFICER  
ROBERT S. DYER

OFFICE OF RADIATION PROGRAMS  
U.S. ENVIRONMENTAL PROTECTION AGENCY  
WASHINGTON, D.C. 20460

## Table of Contents

	<u>Page</u>
Foreword	x
Summary	xi
I. Introduction	1
II. Retrieval, Storage, and Transport of the 80-Gallon Radioactive Waste Package	2
A. Retrieval Operation	2
B. Storage and Transfer	3
III. Analysis of the Waste Form	4
A. Description of the Retrieved Waste Package	4
B. Radiography	5
C. Concrete Coring	6
D. Radiochemical Analysis	9
E. Concrete Integrity	13
IV. Corrosion Analysis of the Waste Container	16
A. Visual Inspection	16
B. Corrosion Rates as a Function of Position	18
C. Microscopic Examination of Local Effects	20
D. Chemical Analysis	24
V. Conclusions	25
References	27

## List of Tables

1. Major U.S. Radioactive Waste Disposal Sites <sup>(1)</sup>	29
2. Analysis of Liquid Found in the Inner Steel Container and Bottom Seawater	30
3. Core Specific Activity - Curies/Gram $\pm \sigma$ (%)	31
4. Cement Specific Activity - Curies/Gram $\pm \sigma$ (%)	34



### List of Tables (Cont'd)

	<u>Page</u>
5. Cesium-137 Content in Annular Volumes of the Concrete Waste Form as a Function of Depth	37
6. Concrete Core Compressive Strength	38
7. Mild Steel Corrosion Rates in Ocean Environments	39
8. X-Ray Diffraction Identification of Surface Scrapings	40
9. Trace Element Analyses of Container Materials	41

### List of Figures

1(a). Approximate Location of the Atlantic 2800 m Radioactive Waste Disposal Site. <sup>(2)</sup>	42
1(b). Location of the Retrieved 80-Gallon Radioactive Waste Package. <sup>(2)</sup>	43
2. Schematic Diagram of the Hoist System Used for the Retrieval of the Waste Package from the Ocean Floor at a Depth of 2783 Meters. <sup>(2)</sup>	44
3(a). Open End of Radioactive Waste Package Immediately after Surfacing from the Atlantic 2800 m Disposal Site.	45
3(b). Side View of Radioactive Waste Package Prior to Being Brought Aboard.	46
4(a). A Modified H47 Jet Engine Container Used for the Encapsulation and Shipment of the Retrieved Radioactive Waste Package.	47
4(b). An Open H47 Jet Engine Container Showing Rubber Faced Interior Clamp Rings Provided to Hold the Radioactive Waste Package Against Shock and Vibration.	47
5. Surface Markings on the Exposed Concrete Face of the Waste Package.	48
6. Orientation System Used to Describe the Waste Package.	49
7. Montage of Waste Package Radiographs. The Top of the Figure Shows the Flanged End of the Internal Container Which Was Located Approximately 5.5 Inches from the Open End of the Container (on the right edge in this figure) Which Resulted from Implosion During Descent in Sea Disposal. Film was Positioned Along 270° Axis.	50

List of Figures (Cont'd)

	<u>Page</u>
8. Radiograph of the Flanged End of the Internal Container.	51
9. View of the Concrete Waste Form with the Steel Drum Removed (00° axis).	52
10. View of the Concrete Waste Form with the Steel Drum Removed (90° axis).	53
11. View of the Concrete Waste Form with the Steel Drum Removed (180° axis).	54
12. View of the Concrete Waste Form with the Steel Drum Removed (270° axis).	55
13. Core Drilling of the Concrete Waste Form. The Worker on the Right is Moving the Drill Bit into the Waste Form While the Worker on the Left Holds the Pneumatic Chisel Used to Remove the Steel Drum.	56
14. Letter Designation of Core Locations as Shown Along the 00° and 200° Longitudinal Axis.	57
15. Letter Designation of Core Locations Along the 90° Longitudinal Axis.	58
16. Letter Designation of Core Locations Along the 180° Longitudinal Axis.	59
17. Letter Designation of Core Locations Along the 270° Longitudinal Axis.	60
18. Schematic Showing the Letter Designation of Core Holes as Related to (ø,x,r) Location Coordinates.	61
19. Closed End of the Waste Form after Removal of the Five Inch Thick Initial Concrete Pouring.	62
20. Waste Form after Removal of the Upper Eight Inches of Concrete from the Open End, Exposing the Flanged End of the Inner Container.	63
21. View of the Exposed Flange End of the Inner Container. Note the Gap Between the Container and the Concrete Formed by Implosion of the Inner Container Wall During Descent.	64

List of Figures (Cont'd)

	<u>Page</u>
22. Concrete Waste Form after Removal of the Inner Container.	65
23. Inner Steel Vessel after Removal from the Waste Form. Note Implosion of the Container Walls Along the 0° Longitudinal Axis.	66
24. Inner Steel Vessel Viewed Along the 180° Longitudinal Axis.	67
25. Inner Steel Vessel with the Cover Removed, Showing the Enclosed Wound Filter Assemblies.	68
26. Close up View of the Inner Container Cover, Flange and Enclosed Filter Assemblies.	69
27. Cesium-137 Content in Concrete Cores Along the 0° Longitudinal Axis.	70
28. Cesium-137 Content in Concrete Cores Along the 90° Longitudinal Axis.	71
29. Cesium-137 Content in Concrete Cores Along the 180° Longitudinal Axis.	72
30. Cesium-137 Content in Concrete Cores Along the 270° Longitudinal Axis.	73
31. Cesium-134 Content in Concrete Cores Along the 0° Longitudinal Axis.	74
32. Cesium-134 Content in Concrete Cores Along the 270° Longitudinal Axis.	75
33. Cobalt-60 Content in Concrete Cores Along the 0° Longitudinal Axis.	76
34. Cobalt-60 Content in Concrete Cores Along the 90° Longitudinal Axis.	77
35. Cobalt-60 Content in Concrete Cores Along the 180° Longitudinal Axis.	78
36. Cobalt-60 Content in Concrete Cores Along the 270° Longitudinal Axis.	79

List of Figures (Cont'd)

	<u>Page</u>
37. A Map of the Surface of the Container.	80
38. The Entire Length of the Container.	81
39. A Schematic Illustrating Specific Features of the Container as Seen in Figure 38.	82
40. An Exterior View of the Upper Portion of the Container - Sediment Facing Side.	83
41. An Exterior View of the Upper Portion of the Container - Sea Facing Side.	84
42. An Exterior View of the Mid-Section of the Container.	85
43. An Exterior View of General Attack Adjacent to a Chime within the Mid-Section.	86
44. Sediment Side Perforation Adjacent to a Chime as Viewed from the Inside of the Carbon Steel Sheath.	87
45. Sea Side Perforation Adjacent to a Chime as Viewed from the Inside of the Carbon Steel Sheath.	88
46. The Interior Surface of the Carbon Steel Sheath.	89
47. The Concrete Waste Form. The Upper Portion of the Form is to the Right in the Photograph.	90
48. Attack Adjacent to the Weld in the Upper Container.	91
49. Attack Adjacent to the Weld in the Lower Container.	92
50. Macroscopic Pits Covering the Carbon Steel Surface at the Closed End of the Container.	93
51. The metal end of the Container.	94
52. An Example of Filiform Corrosion.	95
53. The Sheath Thickness vs. Container Position.	96
54. A Typical Metallographic Cross Section of the Upper Container.	97
55. A Typical Metallographic Cross Section of the Lower Container.	98

List of Figures (Cont'd)

	<u>Page</u>
56. Attack within a Rim Fold.	99
57. Attack at a Chime.	100
58. The Coated Interface.	101
59. A Pit Formed within the Coated Region of the Mid-Section of the Container.	102
60. Scanning Electron Micrograph of the Disbonding of the Interfacial Oxide.	103
61. Micrograph of the Attack upon the Upper Container.	104
62. A Perforation Formed at the Upper Container Sheathing.	105

## Foreword

The Environmental Protection Agency was given a Congressional mandate to develop criteria and regulations governing the ocean disposal of all forms of wastes pursuant to Public Law 92-532, the Marine Protection, Research and Sanctuaries Act. Within this Congressional mandate, EPA has initiated a specific program to develop these regulations and criteria to control the ocean disposal of radioactive wastes.

EPA has taken an active role both domestically and within the international nuclear regulatory arenas to develop the effective controls necessary to protect the health and safety of man and the marine environment. The EPA Office of Radiation Programs first initiated feasibility studies to determine whether current technologies could be applied toward determining the fate of radioactive wastes dumped in the past. After successfully locating actual radioactive waste disposal containers in the disused dumpsites, the Office of Radiation Programs has developed an intensive program of site-characterization studies to look at the biological, chemical and physical characteristics and the presence and distribution of radionuclides within the sites, and is conducting a performance evaluation of past packaging techniques and materials. During the 1976 Atlantic 2800 meter radioactive waste disposal site survey, the first recovery of a radioactive waste package from a radioactive waste disposal site was performed by the EPA Office of Radiation Programs. Under Interagency Agreement Number EPA-180-D6-0166, Brookhaven National Laboratory has performed container corrosion and matrix leach rate and degradation studies on the recovered radioactive waste container. This report presents the results of laboratory analyses performed.

These studies have helped to focus attention on the problems associated with past and present nuclear waste disposal activities concomitant with the growing national and international concern for the long-term effects of this low-level waste disposal option.

### Acknowledgment

The authors wish to thank R.S. Dyer of the U.S. Environmental Protection Agency for the many helpful suggestions and discussions during the course of this work.

The assistance of W.M. Becker, W. Vogel, and A.E. Lukas in performing the numerous tasks associated with the ocean retrieval and subsequent core sampling of the radioactive drum is acknowledged with thanks.

The authors also wish to acknowledge the assistance of A.J. Weiss, L. Milian, and S. Garber in the preparation and performance of chemical and radiochemical tests on the concrete core specimens.

Also contributing was J.R. Weeks, who furnished guidance on corrosion studies for the metal container.

### Summary

On July 31, 1976, an 80-gallon radioactive waste package was retrieved from the Atlantic Ocean 2800 meter depth disposal site. This site which is centered at coordinates  $38^{\circ}30'N$ ,  $72^{\circ}06'W$  is located approximately 120 miles (190 km) east of the Maryland-Delaware coast. The radioactive waste package was transported to Brookhaven National Laboratory where container corrosion and matrix leach rate and degradation studies were conducted.

The retrieved waste package comprised an eighty gallon mild steel drum with no lid which contained a concrete waste form. Markings on the concrete surface indicated that it had been disposed in 1961. Within the concrete matrix, a sealed steel vessel was found which contained some liquid and three wound filter assemblies. Although this vessel had a major indentation running along its length resulting from the pressure differential during or after descent to the sea floor, it had not leaked. The integrity of the concrete matrix had not degraded appreciably during fifteen years in the disposal environment as evidenced by visual observation, weight loss, and compression strength measurements. A conservative estimate indicates that it would require a minimum of 300 years in this ocean environment before the waste form would lose its integrity and provide no barrier to activity release due to cement phase dissolution. Radiochemical analysis indicated the presence of cesium-137, cesium-134 and cobalt-60 in both the concrete matrix and the inner vessel. Based on the measured cesium-137 distribution in concrete core samples, an average cesium-137 release rate of 3.7% per year was calculated.

Corrosion rates for general attack on the upper portion of the 80-gallon mild steel drum were 0.0013-0.0019 in/yr (0.032-0.049 mm/yr) assuming a constant rate with no induction period. A lower limit for the rate of local pitting corrosion of 0.0026 in/yr (0.067 mm/yr) was determined. Based on observations after 15 years in ocean disposal, general thinning attack appears to be the most important process. Using the range of general attack rates, an 18 gauge (nominal 0.0476 inch thickness) mild steel drum would require 25-37 years in this disposal environment before corrosion would cause the container to lose its effectiveness as a barrier to activity migration.



## I. INTRODUCTION

Sea disposal of low-level radioactive waste began in the United States in 1946, under the licensing authority of the Atomic Energy Commission (AEC). In 1962, the first commercial land disposal site was licensed in Beatty, Nevada, and as land disposal operations expanded, ocean dumping was phased out in 1970.

Most of the radioactive wastes were packaged in used 55 gallon drums filled with concrete so that the average package density was sufficiently greater than sea water to assure sinking. Generally, the drums were capped with "clean" concrete and were disposed without tops.

Although radioactive wastes were dumped in various areas of the Pacific and the Atlantic Oceans, three deepsea disposal sites received the majority of wastes dumped between 1946 and 1959. The location of these sites and the estimated amounts of waste disposed are given in Table 1.

Recently, there has been renewed interest in sea disposal as a waste management alternative to land burial of low-level radioactive wastes. The U.S. Environmental Protection Agency (EPA) has been designated to establish controls governing ocean disposal of wastes. To develop ocean disposal regulations, it is considered important to assess past packaging techniques and to determine the effects of ocean environments on the waste packages. In 1974 and 1975, EPA conducted survey studies at the Pacific-Farallons 900 m and 1700 m depth sites and the Atlantic 2800 m depth site<sup>(1)</sup> using submersibles to locate and identify radioactive waste packages.

As part of this effort, Brookhaven National Laboratory (BNL) conducted container corrosion and matrix leach-rate and degradation studies on an 80-gallon radioactive waste package retrieved from the Atlantic 2800 meter radioactive waste disposal site in July 1976.

This report includes analytical methods, results, conclusions, and preliminary estimates relevant to the expected life of the metal container - concrete matrix packaging system in the ocean environment.

## II. RETRIEVAL, STORAGE, AND TRANSPORT OF THE 80-GALLON RADIOACTIVE WASTE PACKAGE

On July 31, 1976, an 80-gallon radioactive waste drum was retrieved from the Atlantic 2800 meter disposal site, centered at coordinates  $38^{\circ}30'N$ ,  $72^{\circ}06'W$ . This site, Figure 1(a) is located approximately 120 miles (190 km) east of the Maryland-Delaware Coast, and occupies an area of 98.8 square miles ( $256 \text{ km}^2$ ).

### A. Retrieval Operation

The retrieval operation was a coordinated effort involving the R/V Lulu, support ship for the deep submersible ALVIN, the DSV ALVIN, and the R/V Cape Henlopen, escort ship for the ALVIN underwater survey operations.

During the morning of July 29, 1976, ALVIN located a clearly labeled 80-gallon radioactive waste drum, deemed suitable for recovery, at a depth of 9131 ft (2783 m). The location of the drum is shown in Figure 1(b).

The actual drum retrieval operation required a specially designed drum attachment device, a computerized navigation system, and a synthetic lift line. Figure 2 shows a schematic diagram of the hoist system. The plan was to position a lift line close enough to the waste package to allow ALVIN to attach them together for retrieval aboard the R/V Cape Henlopen.

A 1500 lb. clump anchor and a transponder were lowered by the synthetic Kevlar line\* to a depth approximately 50-100 meters from the ocean bottom in close proximity to the waste package. At this point, the R/V Lulu was able to guide the R/V Cape Henlopen towards the container by monitoring the transponder position with an acoustic array previously placed on the ocean bottom. The details of this procedure have been described previously.<sup>(3)</sup> During the early morning of July 30th, the clump anchor was positioned on the ocean floor 295 ft (90 m) from the waste package. To maintain the position of the anchor, the end of the Kevlar line was buoyed off to two-48 inch diameter floats.

---

\* Manufactured by Philadelphia Resin, Inc.

Immediately after positioning the anchor, ALVIN dove carrying the drum grab mechanism and a 100 m length of 1 inch diameter nylon line. ALVIN attached the grab to the drum, and then ran the 100 m length of nylon line between the drum and the clump anchor. The clump anchor was detached after one end of the line was attached to the grab and the other to the lift line below the transponder in preparation for the final hoist procedure.

The retrieval procedure started aboard the Cape Henlopen at 0200 on July 31st with the recovery of the two 48-inch floats. At 0800 the waste package surfaced and the radiation level was monitored before being lifted aboard, as shown in Figures 3(a) and 3(b). Once aboard it was carefully documented photographically, sampled for corrosion products and biological growth, and finally sealed in a shipping container, which was flushed with dry argon. The elapsed time from the moment the waste package broke the surface until it was sealed in the shipping container was two hours.

#### B. Storage and Transfer

The container used for storage and transfer of the drum to BNL was designed for the shipment of H47 jet engines. It is a hermetically sealed cylinder of welded heavy gauge steel construction having outside dimensions 75 inches long x 40 inches wide x 43 inches high, as shown in Figure 4(a). The container stands horizontally on heavily reinforced legs and has a gasketed, bolted flange which is on the plane of the central axis of the cylinder. Thus, the top and bottom form half cylinders which are fastened at the mid-section (Figure 4(b)). Hermetic sealing is certified at interior pressures of 7.5 psia to 30 psia. The container was modified to provide access for introducing an inert cover gas (argon) and removal of the initial air atmosphere. The purpose for inert gas was to remove oxygen and thus minimize corrosion of the metal drum in transit. The oxygen content in the sealed container was reduced to  $\sim 0.5\%$  by successive evacuation (-5 psig) and argon pressurization (+1 psig).

A BNL health physicist aboard the R/V Cape Henlopen maintained radioactive surveillance from the point of recovery in the Atlantic Ocean to arrival at BNL.

### III. ANALYSIS OF THE WASTE FORM

#### A. Description of the Retrieved Waste Package

The retrieved waste package\* comprised an eighty gallon mild steel drum filled with cement concrete. The waste form was 50.1 inches (127 cm) in length with a diameter of 22.9 inches (58.3 cm). According to identification markings stamped into the lower drum head, the 55 gallon drum was made from 18 gauge (nominal 0.0476 inch thickness) steel and was manufactured in June 1959. The drum did not have a lid and that portion of the exposed drum lip which was not in intimate contact with the concrete was almost completely separated from the drum body by corrosion. Markings scratched into the exposed top surface of the concrete are shown in Figure 5. These markings indicate that the Army Chemical Corps was the source of this waste package which had a radiation dose level of 40 and 3 mr/hr at the surface and at one meter, respectively, at the time of disposal. The surface dose rate measured after recovery ranged from 0.1 to 4.0 mr/hr with the highest reading at the open end portion of the drum buried in the sediment. Background levels were measured at a distance of one meter. The drum was designated package 28, dated 1961, and weighed 1682 pounds at the time of disposal. The markings also seem to indicate that the package contains cobalt-60.

After sufficient time had been allowed for drainage after recovery, the retrieved drum weighed 1600 pounds. This is an apparent weight loss of approximately 5% since disposal. Weight loss may be attributed to several factors: (1) dissolution of calcium hydroxide (a hydration product) and some of the cement phase from the waste form, (2) loss of water by evaporation during concrete curing, (3) erosion of the waste form in disposal and (4) the accuracy of the initial weighing. Since the weight of the package was written in the concrete surface, the concrete was apparently "wet" during weighing. Because hydration of the cement phase requires substantial time (hours or days), both hydration and evaporation compete during curing for water and appreciable loss of unreacted water due to evaporation is possible.

---

\*In this and subsequent discussion, waste form refers to the solidified solid enclosed in the eighty gallon mild steel drum which is the waste container. The waste package is comprised of the waste form and its container.

Figure 6 is a schematic of the retrieved drum and the orientation system used in describing the waste package. In this system, one point on the drum circumference at the open end was arbitrarily assigned to be the zero degree reference point. Looking at the open end of the drum, an angle ( $\theta$ ) measured clockwise about the longitudinal axis of the drum is used to describe any radius about this axis. In taking metal samples and concrete cores, coordinates of any point in the waste form are described by ( $\theta$ , x, r) where x is the distance (in inches) along the longitudinal axis from the open end concrete surface and r is the distance (in inches) along a radius from the circumferential surface towards the longitudinal axis. The diameter of the waste package (22.9 inches) is such that one inch along the circumference is equivalent to a theta ( $\theta$ ) of 5 degrees. Note in Figure 6 that the sediment line is indicated for both the open and closed ends of the drum. Above these lines (as indicated in the figure) the drum was buried in sediment at the time of retrieval.

#### B. Radiography

Information supplied by the site where the waste was packaged indicates that the 80 gallon drum was formed by welding one half of a 55 gallon drum to the end of another 55 gallon drum to increase its length. The added length was necessary to accommodate a sealed metal container used to encapsulate demineralized resin or filter material containing cobalt-60. This container was centered in the 80 gallon mild steel drum and the surrounding space was filled with concrete containing radioactive cesium and possibly cobalt-60. The waste package was radiographed to determine the exact position of the internal vessel since knowledge of the location was necessary prior to proceeding with the concrete coring operation.

The radiographs were produced by the Consolidated Testing Laboratories, Inc., New Hyde Park, New York, at Brookhaven National Laboratory using a 45 curie cobalt-60 source. Two series of radiographs were taken along the length of the drum; one in which the source was positioned on the drum circumference along the 180 degree longitudinal axis with the film located along the zero

degree axis and a second series with the source located on the 90 degree longitudinal axis with the film along the 270 degree axis. The second series, along an axis displaced 90 degrees from the first, was necessary to define the location and shape of internal items. Fiducial markers were placed on the drum to allow the subsequent positioning of one radiograph relative to another. Initially, thirty minute exposure times were used to locate the upper flange of the inner vessel. Subsequently, one hour exposures were employed to enhance detail. Figure 7 illustrates a montage of the radiographs in which the film was positioned along the 270 degree longitudinal axis. Figure 8 shows the flanged end of the inner container alone.

Interpretation of the radiographs by BNL personnel satisfied the prime objective, the location of the inner vessel. This permitted the calculation of the maximum depth cores that could be taken at various positions without impacting the inner vessel. The radiographs indicated that the inner steel vessel was approximately 39 inches (100 cm) in length, with an outside diameter of 6.3 inches (16 cm) and a wall thickness of 0.25 inches (0.64 cm). The flanged end was located approximately 5.5 inches from the open end of the waste package. These values proved to be quite close to the actual dimensions of the inner container measured after it had been removed from the concrete. In addition to the inner container, the radiographs indicated the presence of other objects, including two pipes located near the inner container. The radiographs also indicated a large indentation along the longitudinal axis of the inner container. This was ascribed to bending of the wall of the inner container due to implosion during descent.

### C. Concrete Coring

After the eighty gallon steel drum was removed with a power chisel, the concrete waste form was cored. Cores were taken to determine the type, quantity, and distribution of contained activity in the waste form. In addition, the presence of the core holes facilitated the subsequent removal of the inner steel vessel.

Figures 9-12 show sequential views ( $0^{\circ}$ ,  $90^{\circ}$ ,  $180^{\circ}$ ,  $270^{\circ}$  longitudinal axes) of the concrete waste form after removal of the steel drum. Observation disclosed that two concrete pourings were made. An interface five inches from the closed end (bottom) of the waste form delineated the two pourings. Since the radiographs indicated that the non-flange end of the inner steel vessel was also approximately five inches from the closed end of the waste form, it was assumed that the first concrete pouring was made to position the inner vessel that distance from the end of the waste form, probably for shielding purposes. The integrity of the concrete waste form was good. Some dissolution of the cement phase on the open end and on the sides of the waste form near the open end had occurred leaving aggregate exposed. However, the exposed aggregate still adhered to the waste form indicating the dissolution of the cement phase was not extensive. Some deposits resulting from corrosion of the steel drum were apparent on the portion of the waste form near the open end. Circular markings in Figures 9-12 resulted during sampling of metal from the steel drum for corrosion studies.

Coring of the concrete waste form was performed using a Target<sup>\*</sup> concrete hole saw with a dual speed motor (500/1000 rpm) on a swivel base. Impregnated diamond core bits (2-1/4 inch diameter) were used to produce two inch diameter concrete cores. Although water is normally used during concrete coring as both a lubricant and to flush out coring debris, water was not used during the coring of the retrieved waste form since the water potentially could remove activity from the core and also create substantial volumes of contaminated liquid waste. A commercial teflon spray lubricant was occasionally applied to the outside of the coring bit. An attempt was made to take two inch long cores from each core hole until the inner steel container was closely approached. After a core hole was started, drilling would continue until the bit had progressed approximately two inches into the concrete. At this point, the drilling was stopped and the coring bit backed out which usually broke off the concrete core at the two inch depth. Drilling would begin again until

---

\* Robert G. Evans Company, Kansas City, Missouri 64130

the core bit had cut an additional two inches into the concrete (four inch total depth) at which point drilling would stop and the two inch long core of the concrete from a depth of 2-4 inches into the waste form was removed. The coring operation was performed inside a hot cell (primarily for dust control purposes) as shown in Figure 13. Cores were taken along the  $0^{\circ}$ ,  $90^{\circ}$ ,  $180^{\circ}$ , and  $270^{\circ}$  longitudinal axis as shown in Figures 14-17 respectively. Although individual cores could be described by the  $(\theta, x, r)$  coordinates, the core holes were also designated by a letter for ease of identification. The center of any particular letter designated core hole was the same distance from the open end concrete surface ( $x$ ) independent of the theta ( $\theta$ ) for that axis. Figure 18 gives the  $x$  distances for the letter designated core holes. Cores were described as, for example, 90C6, which indicates the core was taken along the  $90^{\circ}$  longitudinal axis, from core hole C ( $x = 10$  inches) and to a depth ( $r$ ) of six inches. Since cores were normally two inches in length, the material in this core was obtained at a depth of 4-6 inches. A core designated 0C7.5, however, had a length of 1-1/2 inches since drilling for the prior core (0C6) stopped at a depth of six inches.

Core drilling was done slowly to prevent the bit from heating up excessively and thus releasing diamonds and also to provide an indication of the presence of foreign objects before substantial damage occurred. During coring, the presence of wide mesh wire, two steel pipes and a cavity which occurred along the  $0^{\circ}$  longitudinal axis at a depth of 7.5 inches for much of the length of the waste form were observed. A vacuum system was used to pick up the dust and coring debris created.

After core samples were taken for activity analysis and compression testing, the concrete waste form was dissected using a power chisel to free the inner steel vessel. The progress of this dissection is shown in Figures 19-22. In Figure 19, the five inch thick concrete pouring at the closed end of the waste form has been removed. Note the presence of the two concentric rings of wide mesh wire and the two steel pipes. At this point, work was continued at the open end of the waste form. Figure 20 shows the open end of the waste form with the upper eight inches of concrete removed, exposing the inner container flanged end and the two steel pipes which traverse almost the entire length



of the waste form. The upper flange is observed in Figure 21 at a different angle showing the indentation which runs the length of the inner container on the side which imploded. The concrete debris after removal of the inner container are shown in Figure 22. The lower end of the steel pipe in the upper portion of this photograph was cut off during concrete removal. Figure 23 is a photograph of the inner steel vessel after removal from the waste form. This vessel had a mass of 96 lbs (43.5 kg) with a length of 39 inches (99 cm), and a body diameter of 6.5 inches (16.5 cm). The 0° marking on the edge of the flange corresponds to the 0° longitudinal axis of the concrete waste form. Note the implosion of the inner container along the 0° axis which occurred during or after descent to the sea floor. Figure 24 shows the inner container from the 180° orientation. The flange was removed from this container in an enclosed area using non-sparking tools because of the possibility of hydrogen pressurization due to radiolysis. No pressurization of the container was noted. Three wound filter assemblies were contained within as shown in Figures 25 and 26. Metal samples cut from this vessel for corrosion studies indicated a container wall thickness of 0.25 inches (0.64 cm). In addition, the vessel contained 1.74 liters of liquid which was collected for subsequent analysis. The cation constituents of this liquid were determined using a Perkin Elmer model 360 atomic absorption spectrophotometer. Sulfate content was measured with a Technicon Autoanalyzer II. This composition is compared in Table 2 to the composition of bottom seawater obtained in the vicinity of the retrieved waste package. These analyses indicate that the liquid in the inner steel vessel had significantly lower sodium, magnesium, and sulfate contents than the bottom seawater and that these constituents were not present in the same ratios. As such, it was determined that the liquid in the inner seal container was not seawater.

#### D. Radiochemical Analysis

The concrete cores taken to determine the radionuclide distribution in the waste form were dissolved in aqua regia prior to analysis. The aqua regia was made by combining 3 parts of 12 M hydrochloric acid, 1 part of 16 M nitric acid, and 1 part of distilled water by volume. Distilled water was added to inhibit the interaction of the two acids during storage. Since

the concrete was composed of portland cement, sand, and quartz aggregate, only the cement phase dissolved in the aqua regia. However, the activity in the cores did go into solution since it is associated predominantly with the cement phase and any activity on the aggregate is cleaned off during the dissolution. No activity was noted in any aggregate samples counted.

In the dissolution process, the concrete core to be dissolved was weighed and then placed in a glass beaker to which aqua regia and a Teflon stirring bar were added. The solution was stirred until the sample was dissolved and present in the solution as a suspended floc with the exception of the aggregate which settled out on the bottom of the beaker. The solution containing the floc was then poured into a 500 ml volumetric flask, which in all cases exceeded the volume of the dissolved sample. The beaker and aggregate were washed with additional aqua regia to remove any residual solution and/or activity. This rinse was also added to the volumetric flask. Sufficient additional aqua regia was then added to the volumetric flask to bring the liquid level up to the calibrated volume. The liquid in the volumetric flask was mixed thoroughly and a fifteen milliliter sample taken for analysis. The fifteen milliliter samples thus obtained were placed into twenty plastic screw cap polyethylene counting vials for analysis. It was observed that the suspended floc solution was very stable, facilitating the removal of homogeneous aliquots. The core aggregate was weighed after drying to determine, by subtraction, the cement mass in the core.

Core dissolution samples were analyzed using an Ortec<sup>\*</sup> coaxial Ge(Li) detector. The detector was horizontally mounted with an integral FET pre-amplifier whose signal was fed into an Ortec 472A spectroscopy amplifier. The detector has an efficiency of 20% with a resolution of 2 keV at 1.33 MeV. The energy spectrum was analyzed using a Tracor Northern<sup>\*\*</sup> TN 1700 multi-channel analyzer in the pulse height analysis mode. A hardwired peak search routine (ALI) was used for peak identification and peak area determination.

---

\* Ortec, Inc., 100 Midland Road, Oak Ridge, Tennessee 37830

\*\* Tracor Northern, 3551 W. Beltline Highway, Middleton, Wisconsin 53562

Strontium-90 was measured using a low-level beta counter to determine the in-growth of yttrium-90 after a radiochemical separation of strontium. Plutonium analysis was performed by alpha spectroscopy using a surface barrier silicon detector after radiochemical separation and electrodeposition on to a disk.

Cesium-137, cesium-134, and cobalt-60 were found in the concrete cores as indicated in Tables 3 and 4. Table 3 expresses the activity concentration in terms of curies/gram of core mass, while the values in Table 4 indicate the curies/gram of cement mass in the respective cores. The data in Table 4, that is the activity concentration relative to the core cement mass, are shown plotted as a function of position in the waste form in Figures 27-36. Concentration in curies/gram of cement mass is believed to be more meaningful than considering the entire core mass because the activity is associated with the cement phase and the aggregate portion of the cores vary considerably depending upon the location from where the core was taken. These figures show that the cesium-137 ( $t_{1/2} = 30.2$  years) concentration increases with core depth and reaches an approximately equal level for the 4-6 inch and 6-7.5 inch cores depths. The cesium-137 concentration levels were highest in the  $0^0$  and  $270^0$  core orientations. Cesium-134 ( $t_{1/2} = 2.1$  year) was present in concentrations below  $10^{-12}$  curies/gram cement in most cores. It was measured above this level only in the  $0^0$  and  $270^0$  orientations and primarily in 4-6 inch depth cores. Since disposal (fifteen years), the cesium-134 has gone through approximately seven half-lives. With no loss due to leaching, only 0.64% of the initially contained quantity could be present at the time of analysis. Cobalt-60 ( $t_{1/2} = 5.3$  years) was found to be present in approximately equal concentrations for all orientations and core depths. The OH2 core was analyzed to determine its strontium-90 and plutonium content. This core contained less than  $2.4 \times 10^{-12}$  curies/gram strontium-90 (limit of detection) and  $6.7 \times 10^{-13}$  curies/gram plutonium-239. These values should be evaluated relative to background fallout levels.

The results from the concrete coring can be considered in terms of annular volume elements. The average cesium-137 content of the concrete in annular volume elements has been determined and is shown in Table 5. The thickness of these volume elements correspond to the position of core series depths, i.e.,

0-2, 2-4, 4-6, and 6-7.5 inches (this final volume element has a thickness of 1-1/2 inches). While these elements only consider the concrete to a depth of 7.5 inches from the surface, this represents 88% of the drum volume, and the majority of the volume not considered was occupied by the inner concrete container. An average volume weighted cesium-137 activity concentration of  $2.48 \times 10^{-10}$  curies/gram was measured to a depth of 7.5 inches. Since the density of the concrete waste form (neglecting the inner concrete) is  $2.21 \text{ g/cm}^3$ , the sum of the concrete annular masses is  $6.52 \times 10^5 \text{ g}$ , resulting in a total cesium-137 content of  $1.62 \times 10^{-4}$  curies at the time of analysis. This number could be related to the original cesium-137 content of the waste form (considering decay) to determine the radionuclide release during disposal if the total initially contained activity were known. However, if the original activity distribution was homogeneous and the inner container released no activity, an estimate of the minimum cesium-137 release can be made. This is accomplished by noting that the activity concentration increases from the outside to a depth of four inches and that for the 4-6 and 6-7.5 inch depth cores, the average activity concentration are approximately equal with a volume weighted average of  $5.65 \times 10^{-10}$  curies/gram. As such, leaching can be assumed to have removed activity only from the outer four inches of the waste form and the constant activity concentration at core depths of 4-7.5 inches represents the initial waste form concentration after decay. Using a decay time of 15 years from waste form disposal to analysis, cesium-137 decays to 70.9% of its original quantity ( $t_{1/2} = 30.2$  years). This suggests an initial homogeneous activity concentration of  $7.97 \times 10^{-10}$  curies/gram or a total waste form activity of  $5.20 \times 10^{-4}$  curies of cesium-137 at the time of disposal. The calculated loss of activity (corrected to the time of disposal) from the outer two volume elements to produce an activity concentration of  $7.97 \times 10^{-10}$  curies/gram is  $2.92 \times 10^{-4}$  curies. The waste form is calculated to have lost  $2.92 \times 10^{-4}$  curies of cesium-137 from a total content of  $5.20 \times 10^{-4}$  curies (both corrected to the time of disposal). This corresponds to a release of 56.2% of the cesium-137 contained at the time of disposal. The calculated bulk leach rate,  $L_B$ , of the waste form is  $2.38 \times 10^{-3} \text{ g/(cm}^2\text{-day)}$  where  $L_B$  is defined by:

$$L_B = \frac{\sum a_n}{A_0} \times \frac{m}{S \cdot t} \quad (1)$$

where  $\frac{\sum a_n}{A_0}$  = cumulative fraction release of the species of interest (corrected to the time of disposal)  
 $m$  = waste form mass, g  
 $S$  = external geometric surface area,  $\text{cm}^2$   
 $t$  = cumulative time since disposal, days

Note that cesium is one of the most leachable radionuclides in a cement waste form. The release rates for other radionuclides, particularly cobalt-60 are typically appreciably lower. This calculation shows that for cesium-137 the release is dominated by leachability and not waste form dissolution.

The inner flanged container when opened was found to contain 1740 milliliters of liquid. This liquid was counted on the Ge(Li) detector after the addition of 24 ml of 12 M HCl and 2 ml of distilled water. The measured specific activities in this liquid were  $2.00 \times 10^{-7}$  curies/ml Cs-137,  $5.48 \times 10^{-10}$  curies/ml Cs-134,  $2.37 \times 10^{-9}$  curies/ml Co-60 and  $1.47 \times 10^{-8}$  curies/ml Sr-90.

During removal of the waste form from its shipping container at BNL, approximately 7.5 liters of liquid was present in the bottom of the shipping container. Upon analysis, this liquid was found to contain  $3.53 \times 10^{-10}$  curies/ml Cs-137,  $1.55 \times 10^{-11}$  curies/ml Cs-134,  $2.4 \times 10^{-13}$  curies/ml Sr-90 and  $1.4 \times 10^{-13}$  curies/ml Pu-239. The one sigma counting uncertainty for the plutonium analysis was  $\pm 50\%$ .

#### E. Concrete Integrity

Concrete cores were taken to evaluate the integrity of the concrete as measured by its compressive strength using ASTM Standard C 39-72, "Method of Test for Compressive Strength of Cylindrical Concrete Specimens." A Soiltest\* CT-710 compressive tester was used to make the compression strength measurements. Table 6 lists the compressive strengths of the cores tested, which averaged 1,710 psi. These cores had a diameter of 1.73 inches and varied in length from 2.17-3.58 inches. The sample diameter is less than

\*Soiltest, Inc. Evanston, Illinois 60602

the minimum diameter typically used in compression testing (2 inches). Core drilled samples for construction material compression strength verification typically use larger core diameters (3-6 inches). Small sample diameter can lead to misleading low compression strength values as the drilling operation may introduce substantial imperfections such as surface microcracking, especially when water cooling and flushing is not employed during coring. Inaccuracies can also occur if the size of the concrete aggregate approaches the diameter of the core sample. The concrete was also tested using an impact test hammer (Soiltest, CT-320). With this method, a weighted hammer is impacted against the concrete surface and the hammer rebound measured. This rebound is directly related to the compression strength. Rebound is expressed in terms of compression strength by the use of conversion tables. Available conversion tables are applicable to ordinary construction concrete. For other types of concrete (that differ appreciably in composition in terms of type and quantity of aggregate, cement and water), one must first establish the relationship between rebound and compression strength to derive an appropriate conversion table. Applying this method and construction concrete conversion tables to the concrete waste form, an average compression strength of 4,100 psi was obtained. As such, the core samples used in actual compression testing may have been adversely affected during the drilling operation, although this can not be definitively verified since the original concrete composition is not known.

It is difficult to estimate if the strength of the concrete has decreased as a result of ocean disposal since no control exists for comparison purposes. Certainly, the concrete exhibits good integrity in that it has a reasonably high compression strength and does not indicate appreciable mechanical degradation such as exfoliation or cracking. The only visually observed degradation consisted of a small amount of cement phase dissolution near the open end of the waste form which exposed some aggregate. This aggregate, however, remained bound to the cement matrix. Minimum average concrete compression strength values are available as a function of water/cement weight ratio.<sup>(4)</sup> A value of 4,300 psi is obtained with a water/cement weight ratio of 0.5 (4,900 and 3,800 for  $w/c = 0.45$  and  $0.55$  respectively). This is a common concrete mix, and as such, it may indicate no significant change in waste form compression strength since disposal.

Any deterioration of the concrete would most likely be attributed to sulfate attack. Solutions containing sodium, calcium and magnesium sulfates can react chemically with hydrated lime and calcium aluminate in cement to form calcium sulfate and calcium sulfoaluminate. These reactions lead to an increase in volume, accompanied by mechanical disruption of the cement phase. This expansion type of degradation, typically associated with on-land sulfate attack, is not observed with cement in seawater. The cause for the lack of expansion is not known. Instead, seawater sulfate attack, particularly by sodium or calcium sulfate, is of a surface softening type. This is a localized attack and will not progress unless the soft surface layer is removed (wave action, abrasion, etc.). This may account for the cement phase dissolution near the open end of the waste form. In any case, the concrete did not exhibit significant deterioration as a result of sulfate attack.

The concrete waste form will lose integrity as the cement phase dissolves. The maximum weight loss that could be ascribed to cement phase dissolution (hydrated silicate and aluminate compound and calcium hydroxide) is 5% after fifteen years in disposal. As mentioned previously, other factors may have contributed to this apparent weight loss. The most satisfactory explanation for the weight loss is measurement error at the time of disposal. As a result, the assumption of a 5% weight loss over 15 years due to cement phase dissolution is conservative. Assuming a constant 0.33%/yr weight loss due solely to cement phase dissolution, a period of 300 years would be required for the cement phase to completely dissolve. During this time, the waste form would demonstrate a gradual loss of integrity. This estimate of the time during which the waste form will retain at least some integrity is conservative. The dissolution rate is likely to decrease substantially with time as the relatively soluble calcium hydroxide is removed leaving the less soluble hydrated calcium silicate and aluminate compounds which bind the sand and aggregate together and are the primary contributors to concrete integrity. Conversely, although a substantial decrease in the rate of weight loss is expected as relatively soluble products are removed, some increase above this low rate may occur as the waste container corrodes away exposing more of the waste form surface area to attack.

#### IV. CORROSION ANALYSIS OF THE WASTE CONTAINER

Corrosion analysis of the eighty gallon carbon steel drum was performed using the experimental procedures recommended by NACE<sup>(5)</sup> whenever practicable. The particular analyses employed have attempted to (1) describe the qualitative nature of the corrosive attack, (2) give a quantitative estimate of the attack and (3) describe the chemical and metallurgical correlations to the corrosive attack.

##### A. Visual Inspection

The waste package was first removed for inspection from its storage and transfer container on September 14, 1976. For the prior forty-five days since retrieval, the waste package was stored in a dry argon atmosphere. (A dry argon storage atmosphere was also utilized for subsequent intervals between sampling for corrosion studies.) A photographic survey of the waste container outer surface was performed at this time. The photographs included alphabetic labels whose coordinates were recorded, in terms of  $x$ ,  $r$ , and  $\theta$ . The coordinates ( $x$ ,  $r$  and  $\theta$ ) have as their ordinate a point defined by the intersection of the cylindrical axis and the plane of the rim at the concrete-exposed end of the container. The coordinate,  $x$ , is the distance parallel to the cylindrical axis running into the container. Looking at the concrete end,  $\theta$ , is defined as degrees of clockwise rotation about the cylindrical axis. This coordinate system is shown schematically in Figure 18. A map of the container surface is illustrated in Figure 37. In this figure, the container is shown rolled out into a plane after cutting along the  $180^\circ$  longitudinal axis. Figure 38 is a photograph of the waste package while Figure 39 is a schematic illustrating specific features of the waste container. The sediment line lies along FK in Figure 39. The container was constructed from two cylindrical carbon steel drums welded at  $x = 15\text{-}1/2"$ , the weld line being along CD. The container has three chimes, AB, GH, and IJ.

The upper portion of the container, between  $x = 0$  and  $x = 17\text{-}1/3"$  (EF) appears, from visual examination, to be attacked more severely than the remaining portion of the container. At the time of examination, much of this upper region contained loosely adhering material covering a dark red to black



scale directly adhering to the metal. Figures 40 and 41 show the severe attack as it appears on this upper portion of the container. The sediment side of this upper container region appears in Figure 40. Here much of the loosely adherent material is absent, thereby exposing the red-black substrate scale. On the sea-facing side of the container, Figure 41, more of the loose material had remained upon the surface. As shown in Figures 3(a) and 38, the rim located on this portion of the container is nearly severed as a result of the adjacent corrosive attack.

In contrast to the upper portion of the container, the mid-section exhibits relatively little general attack. The mid-section is that region bounded by CD and IJ as labelled in Figure 39. Much of an original surface coating on this portion has remained. In this area, however, severe local attack has occurred. As seen in Figure 42, the attack in this region is characterized by local pitting within the coated region, and general attack adjacent to the chimes. Figure 43 illustrates the attack specific to the neighborhood of the chimes. In fact, complete perforation was observed in some areas adjacent to the chimes, where corrosion product had deposited.

Further examination of the corrosion adjacent to the chimes, observed when the container was cut open and the inner surface viewed, indicated points of perforation. Some of these points are specific to the region immediately adjacent to the chimes, as viewed from the interior of the container. Figure 44 shows this chime specific attack perforating the sediment-facing side of the container, while Figure 45 shows a similar attack located on the sea-side of the container.

Figure 46 shows the entire inner surface of the carbon steel sheath. The upper portion in Figure 46 has retained much concrete which adheres to a rough red scale on the container. The lower portion of the container contains less adhering concrete. The metal interior surface in this region is black and appears to be smooth. The relative adherence of the concrete to these two portions of the container sheath correlates with the increased spalling of the waste form where it contacted these regions. Figure 47 shows the concrete waste form denuded of the carbon steel sheath. Clearly, the

region contacting the upper portion of the sheath (and closer to the end exposed to the sea-water) is more severely degraded.

Some further observations can be made from the inside view of the sheath. Figure 48 shows attack which has perforated a region adjacent to a longitudinal weld in the upper portion of the container. Similarly, though not severely enough to produce perforation, the corrosion has also selectively attacked the region adjacent to the longitudinal weld in the lower container, Figure 49.

At the lower portion of the cylinder, corrosion has produced more extensive and typically deeper pits than those formed within the midsection. This is shown in Figure 50.

The metal cap on the lower end of the container is shown in Figures 51 and 52. Although there is little attack on this surface of the container, specific pitting has occurred on the rim and in the center. An interesting instance of coated steel corrosion, namely "filiform" corrosion is observed in this section, shown in Figure 52. This is a form of under coating tunneling attack which forms thread-like traces under the coating. Its active corrosion cell maintains dissolution within the dark head, producing ferrous ions and ferrous hydroxide, while the tail contains the oxidized ferric ion and hydrous ferric oxides and hydroxides.<sup>(6)</sup>

#### B. Corrosion Rates as a Function of Position

Metallographic examination of a selected number of trepanned metal specimens was performed to allow a more selective and quantitative assessment of the corrosive attack. Metal samples were trepanned from the carbon steel sheath along two longitudinal lines, one at  $25^{\circ} \pm 5^{\circ}$ , and one at  $220^{\circ} \pm 5^{\circ}$ . This selection of sampling sites allowed a uniform sampling to be made from the portions of the container exposed to the sediment and the sea environment respectively. In order to minimize contamination of the samples, neither lubricant nor water was used for the trepanning operation. The trepanning was accomplished with a 1-1/2" i.d. hole saw and an air chisel. Prior to examination, the trepanned samples were stored in glass vials in a desiccator over anhydrous  $\text{MgSO}_4$ .

Characteristic  $0.05 \text{ in}^2$  ( $0.3 \text{ cm}^2$ ) to  $0.08 \text{ in}^2$  ( $0.5 \text{ cm}^2$ ) sections from the trepanned specimens were selected for an analysis of their cross section dimension. These samples were selected uniformly from over the container surface. Selected samples were cut from the trepanned metal specimens and cold mounted in a metallographic epoxy as cross sections. The mounted specimens were coarsely ground by several tenths of a millimeter, followed by a finer abrasion with 240 grit cloth. Cross sections prepared in this manner were then photographed at a calibrated 50x magnification. While this preparation does not allow observation of metallurgical microstructure, it does provide a means of rapidly determining the average cross section dimension of a rough surfaced specimen. Corrosion free specimens from within rimfolds provided reference dimensions. From these data the corrosive attack as a function of container location was quantitatively determined, as well as the average metal thinning due to corrosion.

Metal thickness as a function of position on the container is presented in Figure 53. The error bars show the magnitude of the standard deviation of this measurement. Their magnitude is a measure of the surface roughness at the observed 50x magnification used in the microscopic measurement. Approximately 0.1" of cross-section length was sampled for each point in Figure 53. Figure 53a illustrates the dimension for the sea-side of the container at  $220^\circ$ , while Figure 53b presents similar data for the sediment-side of the container at  $25^\circ$ . The unattacked thickness of the container was determined from analyses of the metal in the rim folds at both ends to be 0.047 in (0.12 cm) for the upper container, and 0.039 in (0.10 cm) for the lower. The  $x = 0$  end of the container, i.e., the upper container shows significantly more general attack than that shown by the lower container. However, the lower container shows more severe local attack, even though there are several points between  $x = 20$  and  $x = 50$  where there is no measured dimension loss. Comparing now the thinning data for the sea-side to that for the sediment side, there is a small but significant difference in the thinning, the sediment side exhibiting more attack.

Since the corrosion rate of carbon steel in sea water is essentially constant,<sup>(7)</sup> an average corrosion rate for the material in this container may be estimated and compared to rates obtained under defined conditions. An observed rate is defined as  $(d_0 - d)/t$  where  $d_0$  is the initial dimension of the cross section of the container and  $d$  is the observed dimension at the time of the container recovery, 15 years,  $(t)$ , after being placed in the marine environment. Since there are points on the container where attack has completely penetrated the 0.039 in (0.1 cm) sheath, a lower limit for local corrosion can be placed at 0.0026 in/yr (0.067 mm/yr), while the average rates for the general attack on the upper container are  $0.0013 \pm 0.0002$  and  $0.0019 \pm 0.0002$  in/yr ( $0.032 \pm .006$  and  $0.049 \pm .006$  mm/yr) for the respective sea facing and sediment facing sides. As can be seen in Table 7, these values range somewhat under those observed for carbon steel in surface water. The corrosion rate for carbon steel in deep water at a site off the coast of California has been observed to be linear in oxygen concentration, following the equation:

$$\text{Corrosion Rate (microns/yr)} = 21.3 + 25.4 (O_2) + 0.356 (T)$$

where  $O_2$ , the oxygen concentration is in ml/l, and the temperature is in  $^{\circ}\text{C}$ .<sup>(8)</sup> Using this equation, the corrosion rates calculated for 1 ml/l, 2 ml/l, 4 ml/l and 6 ml/l oxygen at  $0^{\circ}$  are tabulated in Table 7. The oxygen content at this depth and location ranges between 5 and 6 ml/l.<sup>(9)</sup> The average attack observed on the upper container is slightly less than that rate calculated assuming 1 ml/l  $O_2$ . Since this is a somewhat low estimate for oxygen concentration at this depth, the apparent inhibition must be attributed to some other factor such as an initial surface finish which is clearly in existence on the lower container, or a decrease in corrosion kinetics at long times due to a uniform deposit of scale and sediment.<sup>(10)</sup>

### C. Microscopic Examination of Local Effects

While the dimension analysis provides quantitative information on general corrosion, the more specific forms of attack and the metallic microstructure have been observed by microscopic techniques, primarily by metallographic analysis of selected sheath cross sections. The salient features of the local attack and metal structure of this container shown by these observations

are discussed in this section. The micrographs in Figures 54 and 55 show the metallic grain structures developed by nital etch of the respective upper drum and the lower drum cross section.

The metallurgies of these two portions of the container clearly differ with respect to grain size; the grain size of the upper container is larger.

While it is difficult to attribute any of the enhanced general corrosion rate of the upper container to this particular microstructure, an influence upon local corrosion of the grain structure within a metal fold of the lower container is seen in Figure 56. Here the attack prefers the ends of the grains which are elongated by the cold work of the fold.

The chimes within the lower portion of the container, although exhibiting enhanced attack, show no apparent microstructural features which differ from the rest of the lower container. As can be seen in Figure 57, the attack at the chime surface appears more or less general, but with some shallow pitting.

Although the midsection of the container has escaped from severe general attack, it has exhibited severe pitting even to the point of perforation. Therefore, the initiation of pitting at points where much of the coating has remained was investigated.

The coating surface consists of a 55  $\mu\text{m}$  lamina over a 3-5  $\mu\text{m}$  interfacial scale lying on the metal substrate. Figure 58 shows a photograph of the coating, scale, and metal. Non-dispersive x-ray fluorescence analysis of the interfacial region shows the coating to contain Ti, Cr, Zn, and Si, while the only element apparent within the scale interface is iron. Carefully removing a portion of the coating by abrasion reveals a black surface similar to the  $\text{Fe}_3\text{O}_4$  observed upon the inside of the carbon steel sheath. It can be concluded that this scale interface is not the conceivable result of a zinc phosphate or chromate conversion coating, but is, in fact, a  $\text{Fe}_3\text{O}_4$  scale.

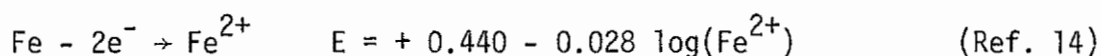
Figure 59 shows the cross section of a typical pit formed under the coating within the midsection. The microphotograph was made so as to highlight the coating and corrosion product. The coating and the interfacial

scale is elevated above the pitted region. Remaining within the pitted region is a corrosion product which appears to be wedged under the edge of the delaminating coating. The delamination structure is better illustrated in the scanning electron micrograph appearing in Figure 60. Pictured here is the coating at the top of the photograph. Failure took place to the left, where the interfacial oxide and coating had lifted.

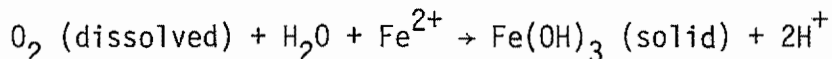
The significant point concerning this interface rests in the observation that in the neighborhood of a pit the adhesion of the coating system to the substrate fails at the interface of the scale to the metal, rather than that of the coating to the scale. This is illustrated in Figure 61. Here adhesion of the oxide to the coating remains while the oxide has lifted from the metal substrate.

Although lifting of the coating and scale appears to be influenced by the wedge of corrosion product formed within the crevice under the coating, disbonding of the metal/oxide interface appears even at a distance away from the actual lifting of the coating. This suggests an electrochemical mechanism in addition to a purely mechanically enhanced disbonding.

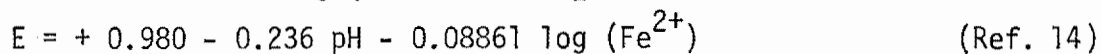
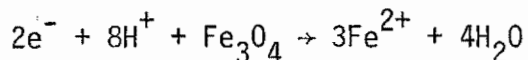
An  $\text{Fe}_3\text{O}_4$  reduction mechanism for the propagation of the coating failure by disbonding similar to that proposed<sup>(11)</sup> for coatings over thinner ferric oxides is not inconsistent with these results. By this mechanism, the anodic dissolution proceeds by the following reaction:



and subsequent oxidation:



within an occluded region of a coating break. This provides a driving force and  $\text{H}^+$  activity for the reduction of the interfacial  $\text{Fe}_3\text{O}_4$ :



to the extent sufficient to destroy the adhesion of the interfacial  $\text{Fe}_3\text{O}_4$  oxide.

Whether the interfacial oxide was initially present, or whether it had formed during the immersion period is a significant question. There is evidence that the interfacial oxide formed during the immersion period. The lack of a similar interfacial oxide within the rim fold where the coated surface was sealed from the environment suggests that the interfacial oxide was formed after immersion. Indeed, coatings are not complete barriers to the flow of corrosion reactants,<sup>(12)</sup> but serve to slow the oxygen and electrolyte penetration.<sup>(13)</sup> Therefore, a formation due to slow oxidation of the metal to  $\text{Fe}_3\text{O}_4$  at the interface is consistent with previously observed corrosion processes at coating interfaces. To take this hypothesis a step further, the stresses formed within the coating, due to the oxide formation, particularly at the chimes, could lead to coating rupture, thus initiating the more rapid pitting or general attack adjacent to the chimes.

Although neither coating nor remnant of a coating was observed upon the upper portion of the container, several aspects of the surface morphology must be noted. Figure 62 illustrates a typical cross section showing the attack which appears at the surface of the upper container. The surface appearing at the top of the photograph is the sea-facing surface. The lower portion of the photograph shows the surface morphology of the metal at the concrete/metal interface. The sea-facing surface exhibits general attack characterized by quite shallow pits. The corrosion product adhering to this surface was very loose and did not survive the sample preparation. The morphology of attack at the sea surface is to be contrasted with that observed at the concrete side. On the concrete side of the carbon steel a more adherent and compact oxide has formed and remained within pits. These pits have greater curvatures than those observed on the sea-side of the container. This oxide appears black and presumably is the  $\text{Fe}_3\text{O}_4$  as characterized by XRD for the black appearing surface oxide (Table 8). As seen in Figure 62, this oxide takes on a laminated structure where the attack leads to perforation. The formation of this compact, adherent  $\text{Fe}_3\text{O}_4$  is significant to the deterioration of concrete at concrete/metal interfaces since the volume expansion due to the density ratio of  $\text{Fe}_3\text{O}_4/\text{Fe}$  of 2 will compress the concrete causing it to spall.

#### D. Chemical Analysis

Table 8 presents the results of the x-ray diffraction of samples of loosely adhering corrosion product, scale and surface films. Correlation of predominant lines to corrosion products was done with reference to the ASTM cards. In Table 8, the species correlated by the observed XRD lines are presented in order of their predominance in the specimen whose position and description is also tabulated.

Several observations can be made from this qualitative data. On the upper, more rapidly corroding surface, a loose mixture of the ferric oxides is formed above the substrate with the hydrated  $\alpha$  form predominating, while adhering directly to the metal is the  $\gamma$  -  $\text{Fe}_2\text{O}_3$ . (In the lower portion of the container the  $\gamma$  -  $\text{Fe}_2\text{O}_3$  predominates in the loose product.) The adherent dark scale described in preceding sections and found on the interior of the sheath at the container midsection shows a well defined  $\text{Fe}_3\text{O}_4$  diffraction.

The hydrated alpha-ferric oxide is the more stable corrosion product; however, it is more slowly formed from the initially precipitated iron complexes.<sup>(16)</sup> The loose material clinging to the rusted metal on the upper container is primarily the  $\alpha$ - $\text{FeOOH}$ , while the  $\gamma$ - $\text{Fe}_2\text{O}_3$  and  $\gamma$ - $\text{Fe}_2\text{O}_3 \cdot \text{H}_2\text{O}$  predominate within the scale adhering directly to the surface of the upper container, and loosely at points of local attack upon the lower container. This suggests that corrosion on the lower portion of the container may be a more recent event, its initiation resulting from a relatively late coating breakdown.

The ferric compounds exist at sites where the subsequent oxidation of the primary ferrous species is rapid,<sup>(16)</sup> while at sites between the sheath and the concrete the  $\text{Fe}_3\text{O}_4$  is formed due to the slower oxidation of the primary ferrous ions or metal surface.

The compositions of the two parts of the container are shown in Table 9. The differences in the compositions cannot sufficiently explain the different corrosion rates exhibited by the two containers.<sup>(7)</sup> Differences in corrosion rates must be attributed to the surface finish of the respective portions of the container sheath.



## V. CONCLUSIONS

(1) Little dissolution of the concrete waste form in the ocean environment occurred as evidenced by a maximum waste package weight loss of approximately 5%. Measurement error at the time of disposal is the most satisfactory explanation for the apparent weight loss. A conservative estimate that assumes a constant 0.33%/yr weight loss due to cement phase dissolution predicts that it would require a minimum of 300 years in this environment before the concrete waste form would lose its integrity and provide no barrier to activity release.

(2) The measured compression strength of the concrete waste form is in the range expected for comparable concrete formulations. This indicates the absence of appreciable sulfate attack which is also supported by the observation that negligible deterioration of the waste form surface has occurred.

(3) The concrete waste form contained Cs-137, Cs-134 and Co-60. Based on the Cs-137 distribution in the waste form, a bulk leach rate for this radionuclide of  $2.4 \times 10^{-3}$  g/(cm<sup>2</sup>-day) was calculated. This corresponds to an average cesium-137 release rate of 3.7% per year.

(4) While the inner container which enclosed three wound filter elements imploded due to the pressure differential during or after descent, water analysis indicated that the container did not leak and hence radionuclides were contained.

(5) Corrosion rates for general attack on the upper portion of the steel drum (assuming a constant rate with no induction period) were 0.0013-0.0019 in/yr (0.032-0/0.049 mm/yr). A lower limit for the rate of local pitting corrosion of 0.0026 in/yr (0.067 mm/yr) was determined. Based upon observations after 15 years in ocean disposal, general thinning attack appears to be the most important process. Using these rates of general attack, an 18 gauge (nominal 0.0476 in thickness) mild steel drum would require 25-37 years before corrosion would cause the container to lose its effectiveness as a barrier to activity migration.

(6) Variations in the corrosion attack between the upper and lower portions of the drum are ascribed to differences in surface finishes on the respective portions of the drum. While the coating on the lower portion of the drum successfully inhibited the initiation of general attack, instances

of severe local attack leading to pitting and perforation adjacent to the drum chimes were observed.

(7) The waste container limits seawater exposure and movement through the waste form in disposal. As a result, the rate of activity loss through leaching and the rate of cement phase dissolution are decreased.

## References

1. Dyer, R.S., "Environmental Surveys of Two Deep Sea Radioactive Waste Disposal Sites using Submersibles". Proceedings of an International Symposium on Management of Radioactive Wastes from the Nuclear Fuel Cycle. International Atomic Energy Agency, Vienna, (1976) p. 317-338.
2. Dexter, Stephen C., Cruise Report on R.V. Cape Henlopen 1976 Atlantic Radioactive Waste Dumpsite Survey, December 1976.
3. Hunt, M.M., W.M. Marquet, D.A. Moller, K.R. Peal, W.K. Smith, and R.C. Spindell, 1974, "An Acoustic Navigation System", Woods Hole Oceanographic Institution Technical Report, WHOI 74-6, unpublished manuscript.
4. U.S. Department of the Interior, Bureau of Reclamation, Concrete Manual, 7th Edition, (1966), p. 148.
5. National Association of Corrosion Engineers, Technical Practices Committee, "Recommended Practice, Collection and Identification of Corrosion Products", NACE Standard RP-01-73, February 1973, Houston, Texas.
6. Fontana, M.G. and N.D. Greene, Corrosion Engineering, 47-48, McGraw-Hill, New York, (1967).
7. Tamada, A., M. Tammura and G. Tenny, "Corrosion Behavior of Low Alloy Steels in Sea Water" Fifth Int. Congress on Metallic Corrosion, 1972, 786, NACE, Houston, Texas, 1974.
8. Reinhart, F.M. and J.R. Jenkins, "The Relationship Between the Concentration of Oxygen in Seawater Corrosion of Metals" Proc. 3rd Congr. on Marine Corrosion and Fouling, p. 562, et. seq. 1972.
9. National Science Foundation, GEOSECS Atlas, to be published.
10. LaQue, F.S., Marine Corrosion, p. 97.
11. Gonzalez, O.P., P.H. Josephic and R.A. Oriani, J. Electrochem. Soc., 121, 29 (1974).
12. Mayne, J.E.O., Research (London), 5, 278 (1952).
13. Kendig, M.W. and H. Leidheiser, Jr. "The Electrical Properties of Protective Polymer Coatings as Related to Corrosion of the Substrate", J. Electrochem Soc., 123 (7), 986 (1976).
14. Pourbaix, Atlas of Electrochemical Equilibria.

15. Kakehi, T. and H. Yoshino, "Corrosion of Steel in Polluted Sea Waters", Proc. 5th Int. Cong. on Metallic Corrosion, 1972, NACE, (1974), p. 76.
16. Misawa, T., K. Hashimoto and S. Shumodiara, Corrosion Science, 14, 131 (1974).

TABLE 1

Major U. S. Radioactive Waste Disposal Sites<sup>(1)</sup>

<u>Site</u>	<u>Coordinates</u>	<u>Depth (m)</u>	<u>Distance from Land (km)</u>	<u>Years Dumpsite Used</u>	<u>Estimated No. of 55-Gallon Drums Dumped</u>	<u>Estimated Activity in Drums at Time of Packaging (Ci)</u>
Atlantic	38°30'N 72°06'W	2800	190	1951-56 1959-62	14,300	41,400
Atlantic	37°50'N 70°35'W	3800	320	1957-59	14,500	2,100
Pacific Farallon Island (Subsite A)	37°38'N 123°08'W	900	60	1951-53	3,500	1,100
Farallon Island (Subsite B)	37°37'N 123°17'W	1700	77	1946-50 1954-65	44,000	13,400

TABLE 2  
Analysis of Liquid found in the Inner  
Steel Container and Bottom Seawater

<u>Constituent</u>	Composition, ppm	
	<u>Inner Container Liquid</u>	<u>Bottom Seawater</u>
Sodium	1,250	7,350
Magnesium	2.6	500
Sulfate	245	2,100
Na/Mg ratio	480	15
Na/SO <sub>4</sub> ratio	2.6	3.5

TABLE 3

Core Specific Activity - Curies/Gram  $\pm \sigma$  (%)

<u>Core</u>	<u>Core Mass (Grams)</u>	<u>Cs-137</u>	<u>Cs-134</u>	<u>Co-60</u>
OA4	52.08	1.28E - 09 $\pm$ 0.4%	2.02E - 12 $\pm$ 51.3%	8.74E - 12 $\pm$ 12.8%
OA6	189.37	1.61E - 09 $\pm$ 0.4%	5.31E - 12 $\pm$ 13.7%	7.56E - 12 $\pm$ 10.4%
OB2	139.50	3.26E - 11 $\pm$ 4.0%	--	4.26E - 12 $\pm$ 15.0%
OB4	129.76	3.64E - 10 $\pm$ 1.1%	--	--
OB6	119.05	3.91E - 09 $\pm$ 0.4%	1.65E - 11 $\pm$ 9.0%	4.56E - 12 $\pm$ 25.2%
OC2	179.48	8.30E - 12 $\pm$ 11.1%	--	2.70E - 12 $\pm$ 13.5%
OC4	169.20	1.73E - 11 $\pm$ 5.3%	--	2.30E - 12 $\pm$ 22.2%
OC6	151.66	6.87E - 12 $\pm$ 2.6%	--	2.44E - 12 $\pm$ 19.7%
OC7.5	63.75	3.02E - 10 $\pm$ 1.1%	--	4.46E - 12 $\pm$ 15.7%
OD2	157.33	3.11E - 11 $\pm$ 4.5%	--	--
OD4	153.39	2.65E - 10 $\pm$ 1.2%	--	1.61E - 12 $\pm$ 50.0%
OD6	57.13	6.38E - 10 $\pm$ 0.9%	--	3.43E - 12 $\pm$ 39.3%
OD7.5	92.65	5.39E - 10 $\pm$ 1.1%	--	3.81E - 12 $\pm$ 39.2%
OE2	197.80	2.44E - 11 $\pm$ 5.0%	--	--
OE4	126.67	1.14E - 10 $\pm$ 2.2%	--	1.95E - 12 $\pm$ 50.0%
OE6	117.16	8.66E - 10 $\pm$ 0.8%	1.96E - 12 $\pm$ 44.1%	1.39E - 12 $\pm$ 50.0%
OE7.5	92.31	1.14E - 09 $\pm$ 0.7%	--	1.44E - 12 $\pm$ 28.8%
OF4	171.79	1.72E - 10 $\pm$ 1.4%	--	2.11E - 12 $\pm$ 34.3%
OF6	110.03	5.87E - 10 $\pm$ 1.0%	3.68E - 12 $\pm$ 28.3%	4.62E - 12 $\pm$ 29.6%
OG2	133.45	7.42E - 12 $\pm$ 11.7%	--	1.85E - 12 $\pm$ 50.0%

TABLE 3 (Cont'd)

Core Specific Activity - Curies/Gram  $\pm \sigma$  (%)

Core	Core Mass (Grams)	Cs-137	Cs-134	Co-60
OG4	158.37	1.17E - 11 $\pm$ 8.1%	--	1.91E - 12 $\pm$ 36.1%
OG6	169.88	5.52E - 11 $\pm$ 2.7%	--	1.45E - 12 $\pm$ 50.0%
OG7.5	100.86	4.53E - 10 $\pm$ 1.1%	--	3.71E - 12 $\pm$ 33.9%
OH4	92.58	1.31E - 10 $\pm$ 2.4%	--	4.82E - 12 $\pm$ 31.8%
OH6	150.72	5.96E - 10 $\pm$ 0.8%	--	2.28E - 12 $\pm$ 28.8%
OH7.5	54.56	2.26E - 10 $\pm$ 0.6%	--	1.81E - 12 $\pm$ 50.0%
90C4	133.22	2.46E - 12 $\pm$ 12.2%	--	2.30E - 11 $\pm$ 13.4%
90C6	103.53	7.84E - 12 $\pm$ 7.1%	--	--
90E2	173.08	6.07E - 12 $\pm$ 9.4%	--	--
90E4	120.36	4.37E - 12 $\pm$ 12.6%	--	3.41E - 12 $\pm$ 14.8%
90E6	91.24	3.18E - 12 $\pm$ 20.0%	--	1.49E - 12 $\pm$ 35.9%
90G2	120.41	1.59E - 12 $\pm$ 16.8%	--	4.73E - 12 $\pm$ 10.1%
90G4	114.59	6.43E - 12 $\pm$ 18.7%	--	6.61E - 12 $\pm$ 15.6%
90G6	100.81	7.75E - 12 $\pm$ 8.5%	--	6.76E - 12 $\pm$ 11.0%
180A2	179.96	1.06E - 11 $\pm$ 6.9%	--	--
180A4	129.57	3.82E - 12 $\pm$ 6.2%	--	3.21E - 12 $\pm$ 13.7%
180A6	149.06	1.05E - 10 $\pm$ 1.9%	--	5.07E - 12 $\pm$ 13.8%
180D3.5	107.34	5.51E - 12 $\pm$ 9.8%	--	2.79E - 12 $\pm$ 15.6%
180F4	99.81	2.14E - 11 $\pm$ 7.0%	--	6.71E - 12 $\pm$ 16.8%
180F6	54.80	1.98E - 11 $\pm$ 6.3%	--	4.74E - 12 $\pm$ 31.3%
270C2	148.92	2.75E - 12 $\pm$ 14.8%	--	1.96E - 12 $\pm$ 19.9%
270C4	125.31	1.02E - 10 $\pm$ 1.5%	--	--



TABLE 3 (Cont'd)

Core Specific Activity - Curies/Gram  $\pm \sigma$  (%)

<u>Core</u>	<u>Core Mass (Grams)</u>	<u>Cs-137</u>	<u>Cs-134</u>	<u>Co-60</u>
270C6	114.59	1.40E - 10 $\pm$ 0.6%	2.12E - 12 $\pm$ 22.2%	--
270E2	151.06	4.48E - 12 $\pm$ 20.5%	--	--
270E4	152.92	2.82E - 11 $\pm$ 4.2%	--	2.67E - 12 $\pm$ 35.0%
270E6	85.99	3.71E - 10 $\pm$ 1.0%	1.49E - 12 $\pm$ 50.0%	--
270G2	121.86	7.30E - 11 $\pm$ 2.8%	--	4.74E - 12 $\pm$ 31.4%
270G4	113.23	3.47E - 11 $\pm$ 3.0%	--	2.30E - 12 $\pm$ 20.2%
270G6	135.41	4.09E - 10 $\pm$ 0.7%	4.25E - 13 $\pm$ 88.3%	2.57E - 12 $\pm$ 16.2%

TABLE 4

Cement Specific Activity - Curies/Gram  $\pm \sigma$  (%)

<u>Core</u>	<u>Cement Mass (Grams)</u>	<u>Cs-137</u>	<u>Cs-134</u>	<u>Co-60</u>
0A4	17.08	3.90E - 09 $\pm$ 0.4%	6.17E - 12 $\pm$ 51.3%	2.66E - 11 $\pm$ 12.8%
0A6	60.52	5.05E - 09 $\pm$ 0.4%	1.61E - 11 $\pm$ 13.7%	2.37E - 11 $\pm$ 10.4%
0B2	46.75	9.73E - 11 $\pm$ 4.0%	--	1.27E - 11 $\pm$ 15.0%
0B4	38.67	1.22E - 09 $\pm$ 1.1%	--	--
0B6	69.02	6.75E - 09 $\pm$ 0.4%	2.84E - 11 $\pm$ 9.0%	7.87E - 12 $\pm$ 25.2%
0C2	48.13	3.10E - 11 $\pm$ 11.1%	--	1.01E - 11 $\pm$ 13.5%
0C4	65.44	4.47E - 11 $\pm$ 5.3%	--	5.95E - 12 $\pm$ 22.2%
0C6	55.63	1.87E - 11 $\pm$ 2.6%	--	6.65E - 12 $\pm$ 19.7%
0C7.5	25.81	7.49E - 10 $\pm$ 1.1%	--	1.10E - 11 $\pm$ 15.7%
0D2	71.50	6.84E - 11 $\pm$ 4.5%	--	--
0D4	28.08	1.45E - 09 $\pm$ 1.2%	--	8.77E - 12 $\pm$ 50.0%
0D6	20.79	1.75E - 09 $\pm$ 0.9%	--	9.42E - 12 $\pm$ 39.3%
0D7.5	29.99	1.67E - 09 $\pm$ 1.1%	--	1.18E - 11 $\pm$ 39.2%
0E2	62.10	7.76E - 11 $\pm$ 5.0%	--	--
0E4	49.02	2.94E - 10 $\pm$ 2.2%	--	5.03E - 12 $\pm$ 50.0%
0E6	47.68	2.13E - 09 $\pm$ 0.8%	4.81E - 12 $\pm$ 44.1	3.43E - 12 $\pm$ 50.0%
0E7.5	25.82	4.07E - 09 $\pm$ 0.7%	--	5.15E - 12 $\pm$ 28.8%
0F4	83.22	3.55E - 10 $\pm$ 1.4%	--	4.35E - 12 $\pm$ 34.3%
0F6	31.20	2.07E - 09 $\pm$ 1.0%	1.30E - 11 $\pm$ 28.3%	2.06E - 11 $\pm$ 29.6%
0G2	24.94	3.97E - 11 $\pm$ 11.7	--	9.85E - 11 $\pm$ 50.0%

TABLE 4 (Cont'd)

Cement Specific Activity - Curies/Gram  $\pm \sigma$  (%)

Core	Cement Mass (Grams)	Cs-137	Cs-134	Co-60
OG4	42.61	4.33E - 11 $\pm$ 8.1%	--	7.09E - 12 $\pm$ 36.1%
OG6	30.77	3.05E - 10 $\pm$ 2.7%	--	8.00E - 12 $\pm$ 50.0%
OG7.5	76.62	5.96E - 10 $\pm$ 1.1%	--	4.89E - 12 $\pm$ 33.9%
OH4	16.01	7.55E - 10 $\pm$ 2.4%	--	2.79E - 11 $\pm$ 31.8%
OH6	35.03	2.56E - 09 $\pm$ 0.8%	--	1.12E - 11 $\pm$ 28.8%
OH7.5	13.30	9.27E - 10 $\pm$ 0.6%	--	7.41E - 12 $\pm$ 50.0%
90C4	35.40	9.25E - 12 $\pm$ 12.2%	--	1.28E - 10 $\pm$ 13.4%
90C6	32.57	2.49E - 11 $\pm$ 7.1%	--	--
90E2	37.44	2.81E - 11 $\pm$ 9.4%	--	--
90E4	38.03	1.38E - 11 $\pm$ 12.6%	--	1.08E - 11 $\pm$ 14.8%
90E6	33.42	8.69E - 12 $\pm$ 20.0%	--	4.13E - 12 $\pm$ 35.9%
90G2	32.56	5.87E - 12 $\pm$ 16.8%	--	1.80E - 11 $\pm$ 10.1%
90G4	32.31	2.28E - 11 $\pm$ 18.7%	--	2.34E - 11 $\pm$ 15.6%
90G6	32.90	2.37E - 11 $\pm$ 8.5%	--	2.18E - 11 $\pm$ 11.0%
180A2	33.42	5.69E - 11 $\pm$ 6.9%	--	--
180A4	22.52	2.20E - 11 $\pm$ 6.2%	--	1.85E - 11 $\pm$ 13.7%
180A6	33.87	4.61E - 10 $\pm$ 1.9%	--	2.23E - 11 $\pm$ 13.8%
1800D3.5	31.16	1.90E - 11 $\pm$ 9.8%	--	9.60E - 12 $\pm$ 15.6%
180F4	27.59	7.74E - 11 $\pm$ 7.0%	--	2.43E - 11 $\pm$ 16.8%
180F6	10.45	1.04E - 10 $\pm$ 6.3%	--	2.48E - 11 $\pm$ 31.3%
270C2	37.59	1.09E - 11 $\pm$ 14.8%	--	7.79E - 12 $\pm$ 19.9%
270C4	34.26	3.72E - 10 $\pm$ 1.5%	--	--

TABLE 4 (Cont'd)

Cement Specific Activity - Curies/Gram  $\pm \sigma$  (%)

<u>Core</u>	<u>Cement Mass (Grams)</u>	<u>Cs-137</u>	<u>Cs-134</u>	<u>Co-60</u>
270C6	25.08	6.37E - 10 $\pm$ 0.6%	9.69E - 12 $\pm$ 22.2%	--
270E2	42.52	1.59E - 11 $\pm$ 20.5%	--	--
270E4	32.52	1.32E - 10 $\pm$ 4.2%	--	1.26E - 11 $\pm$ 35.0%
270E6	20.90	1.53E - 09 $\pm$ 1.0%	6.14E - 12 $\pm$ 50.0%	--
270G2	31.81	2.80E - 10 $\pm$ 2.8%	--	1.82E - 11 $\pm$ 31.4%
270G4	29.40	1.34E - 10 $\pm$ 3.0%	--	8.85E - 12 $\pm$ 20.2%
270G6	23.30	2.38E - 09 $\pm$ 0.7%	2.47E - 12 $\pm$ 88.3%	1.49E - 11 $\pm$ 16.2%

TABLE 5

Cesium-137 Content in Annular Volumes of  
the Concrete Waste Form as a Function of Depth

<u>Annular element (core depth), in.</u>	<u>Element Volume, cm<sup>3</sup></u>	<u>Average Cesium-137 curies/gram concrete</u>	<u>Cesium-137 content, curies</u>
0-2	$1.07 \times 10^5$	$2.02 \times 10^{-11}$	$4.78 \times 10^{-6}$
2-4	$8.63 \times 10^4$	$1.54 \times 10^{-10}$	$2.94 \times 10^{-5}$
4-6	$6.60 \times 10^4$	$5.83 \times 10^{-10}$	$8.50 \times 10^{-5}$
6-7.5	$3.62 \times 10^4$	$5.32 \times 10^{-10}$	$4.26 \times 10^{-5}$
TOTAL	$2.96 \times 10^5$		$1.62 \times 10^{-4}$

Average concrete density =  $2.21 \text{ g/cm}^3$ .

TABLE 6

Concrete Core Compressive Strength

<u>Distance From Core Location, in.</u>	<u>Core Location</u>	<u>Core Diameter, in.</u>	<u>Core Length, in.</u>	<u>Comprehensive Strength psi</u>
8	180 D	1.73	2.24	1720
3	180 E	1.73	2.28	1910
4	180 F	1.73	3.15	1700
5	180 F	1.73	2.17	1680
5	180 F	1.73	3.58	1720
4	180 H	1.73	2.17	1510
Impact Hammer Method (Average)				4100

TABLE 7

Mild Steel Corrosion Rates in Ocean Environments

	<u>Corrosion Rate of Carbon Steel in/yr</u>	<u>Ref.</u>
Clean Surface Waters off Coast of Japan	0.002	(15)
Projected from Five Year Tests in Surface Waters	0.0023	(7)
Emperical Formula		
1 ml/l O <sub>2</sub> , 0°C	0.0019	(8)
2 ml/l O <sub>2</sub> , 0°C	0.0028	(8)
4 ml/l O <sub>2</sub> , 0°C	0.0048	(8)
6 ml/l O <sub>2</sub> , 0°C	0.0069	(8)
General Attack in Upper Container		
Sea Side	0.0013 ± 0.0002	
Sediment Side	0.0019 ± 0.0002	
Local Attack in Container	>0.0026	

TABLE 8

X-ray Diffraction Identification of Surface Scrapings

#	X	$\theta$	
7	44	$220^{\circ}$	$\gamma - \text{Fe}_2\text{O}_3$
10	27	$220^{\circ}$	$\gamma - \text{Fe}_2\text{O}_3 \cdot \text{H}_2\text{O}, \alpha - \text{Fe}_2\text{O}_3 \cdot \text{H}_2\text{O}$
32	17	$45^{\circ}$	$\alpha - \text{Fe}_2\text{O}_3 \cdot \text{H}_2\text{O}, \gamma - \text{Fe}_2\text{O}_3 \cdot \text{H}_2\text{O}, \gamma - \text{Fe}_2\text{O}_3$
4	13	$207^{\circ}$	$\alpha - \text{Fe}_2\text{O}_3 \cdot \text{H}_2\text{O}, \gamma - \text{Fe}_2\text{O}_3 \cdot \text{H}_2\text{O}$
40	10	$180^{\circ}$	$\alpha - \text{Fe}_2\text{O}_3 \cdot \text{H}_2\text{O}$ Loose Surface Material
M-25	0	$25^{\circ}$	$\gamma - \text{Fe}_2\text{O}_3$ Surface Scraping
M-25	0	$25^{\circ}$	$\gamma - \text{Fe}_2\text{O}_3$ Surface Diffraction
M-6	0		$\text{Fe}_3\text{O}_4$ Surface Diffraction of Black Inner Surface



TABLE 9

Trace Element Analyses of Container Materials

	Weight Percent					
	<u>C</u>	<u>Mn</u>	<u>Si</u>	<u>Cu</u>	<u>Cr</u>	<u>Ni</u>
Upper Container	0.097	0.30	0.0023	0.123	0.013	0.024
Lower Container	0.090	0.35	0.0046	0.067	0.007	0.019
Weld in Lower Container	0.096	0.33	0.0038	0.086	0.017	0.029

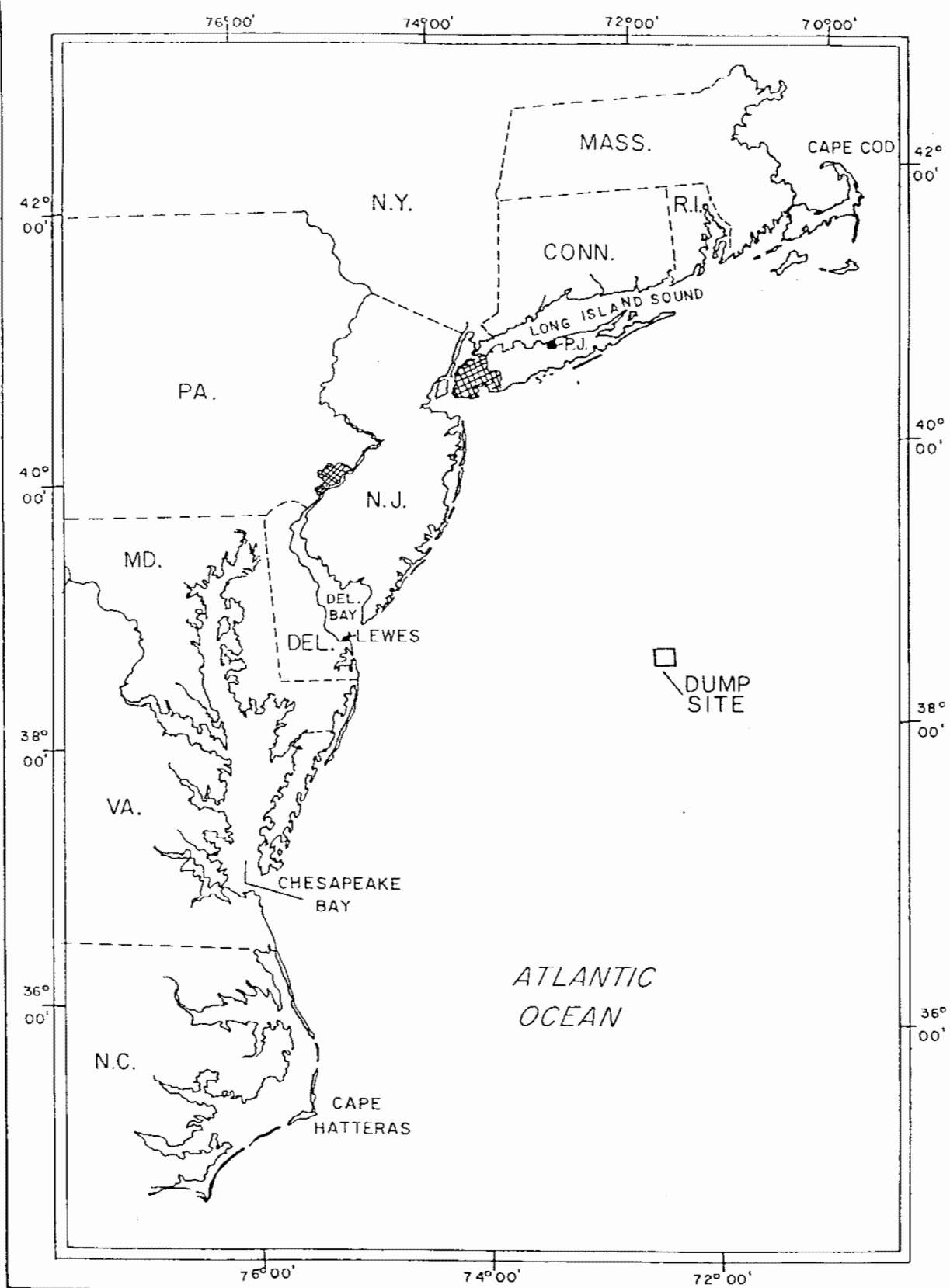


Figure 1(a). Approximate Location of the Atlantic 2800 m Radioactive Waste Disposal Site.(2)

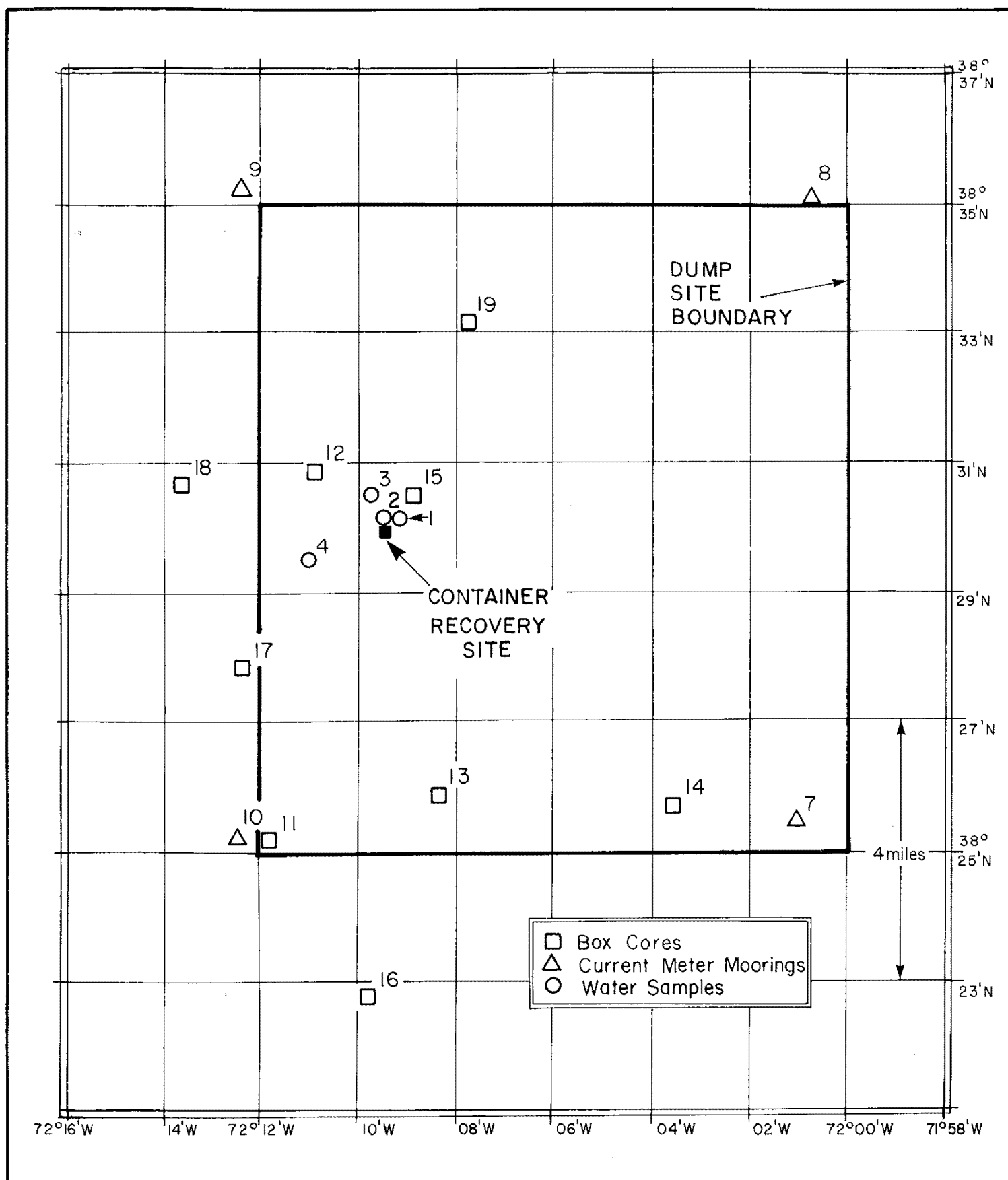


Figure 1b. Location of the Retrieved 80 - Gallon Radioactive Waste Package <sup>(2)</sup>

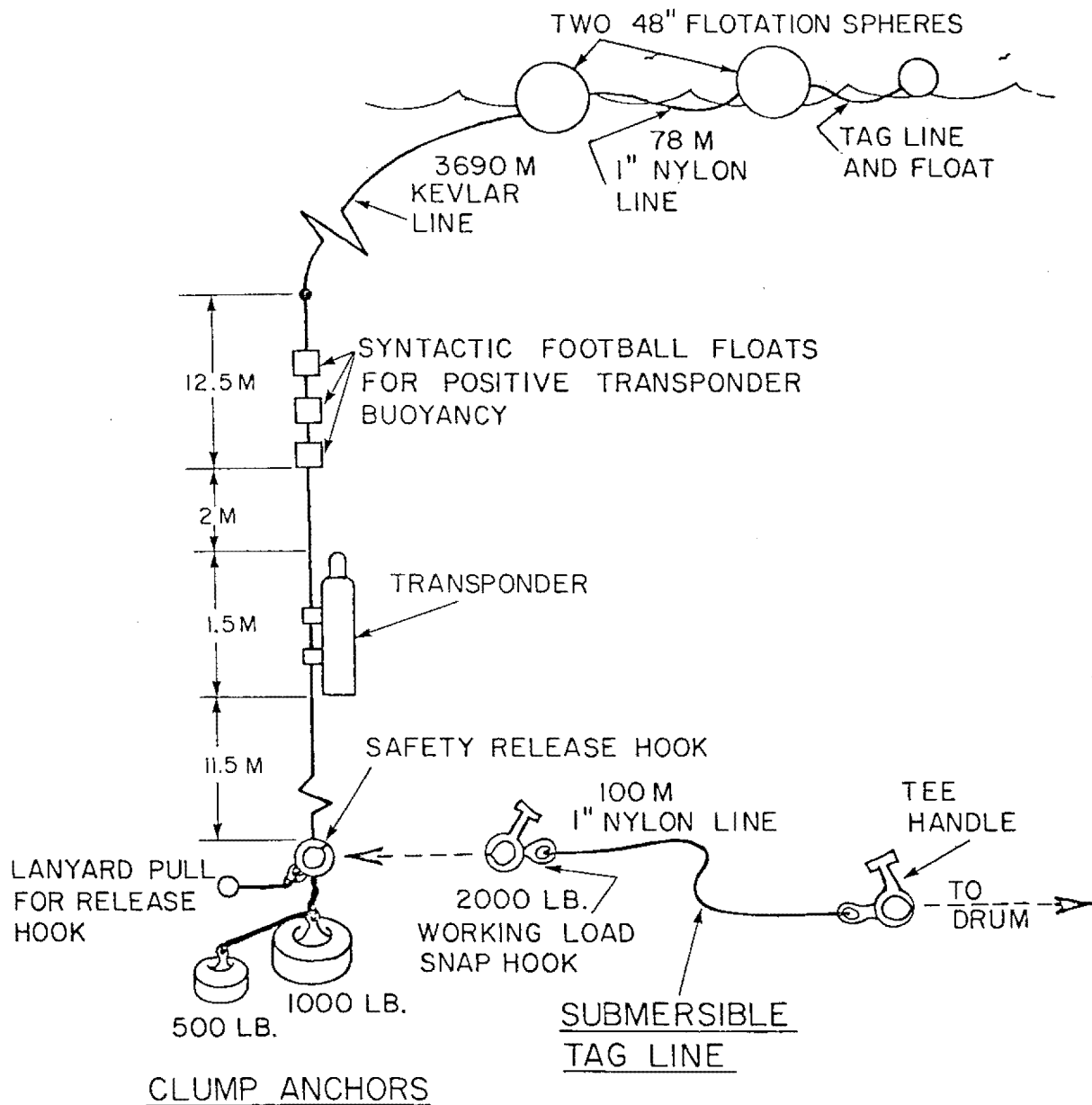


Figure 2. Schematic Diagram of the Hoist System Used for the Retrieval of the Waste Package from the Ocean Floor at a Depth of 2783 meters.<sup>(2)</sup>

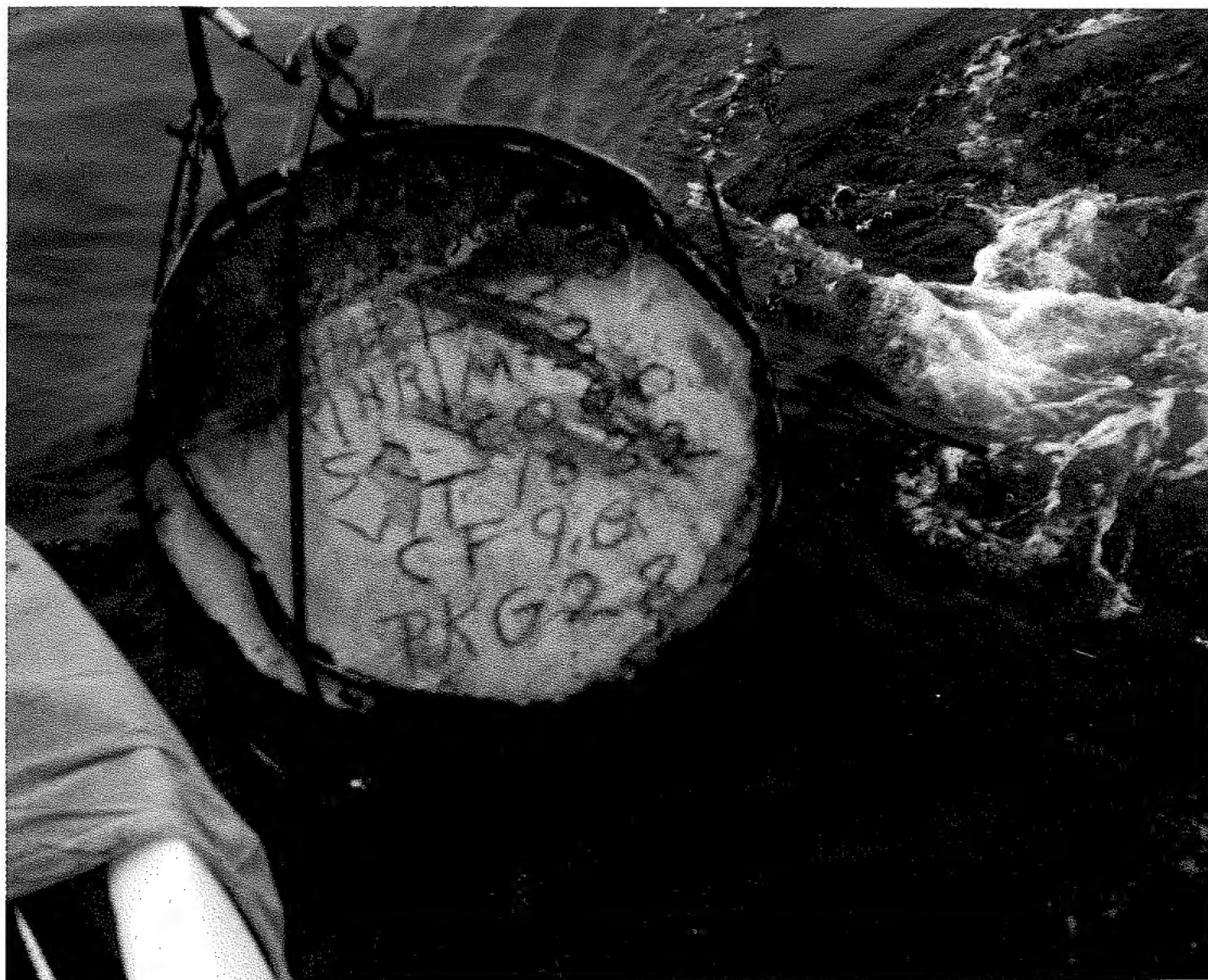


Figure 3(a). Open End of Radioactive Waste Package Immediately after Surfacing from the Atlantic 2800 m Disposal Site.

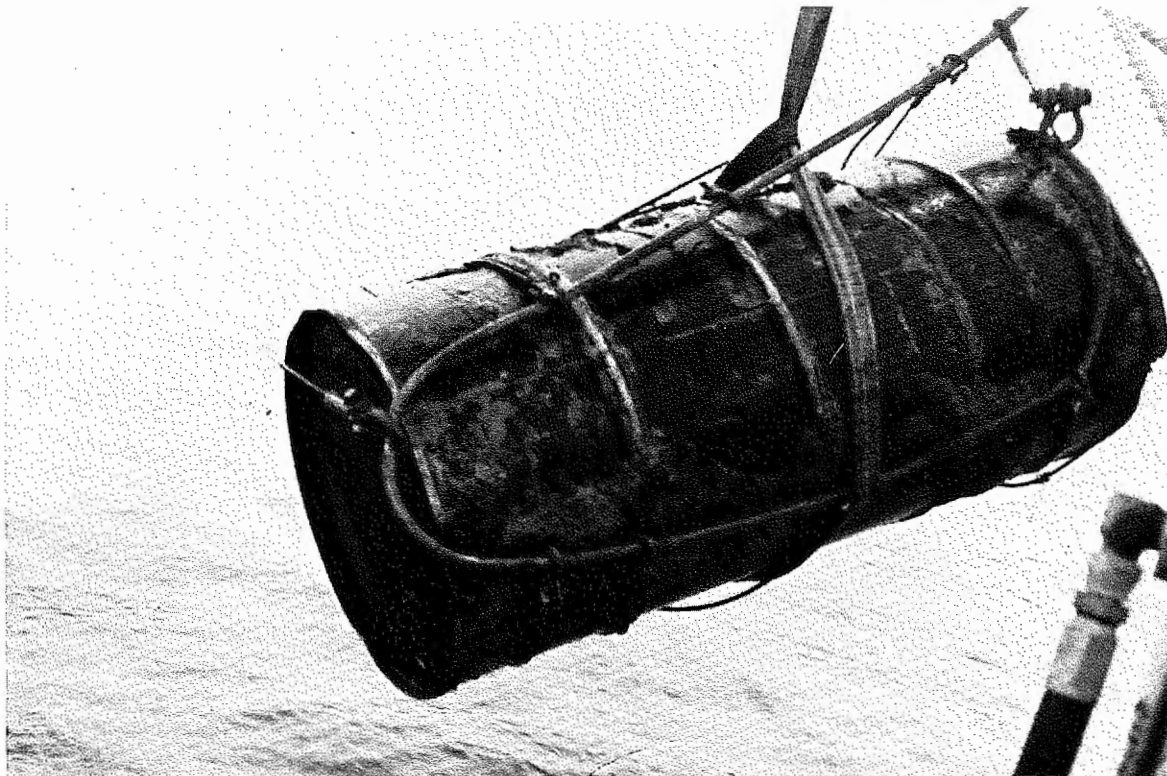


Figure 3(b). Side View of Radioactive Waste Package Prior to Being Brought Aboard.

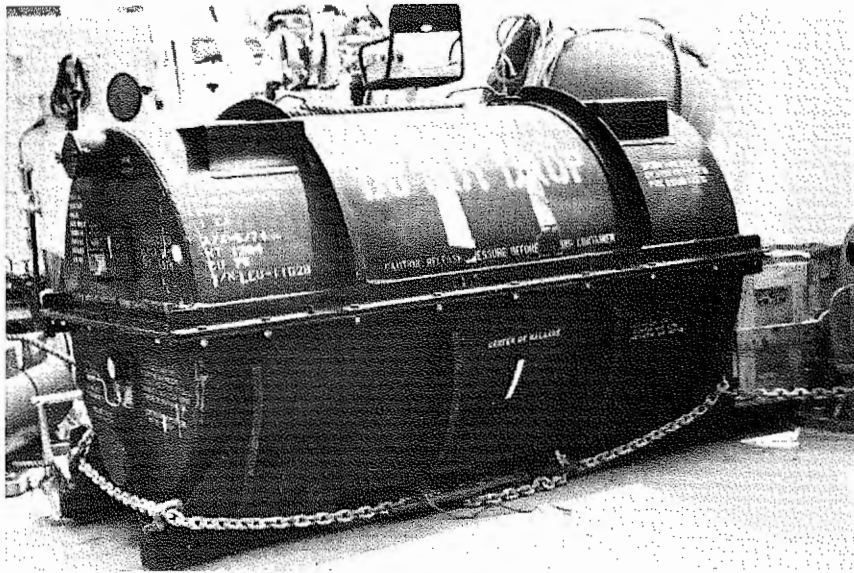


Figure 4(a). A Modified H47 Jet Engine Container Used for the Encapsulation and Shipment of the Retrieved Radioactive Waste Package.

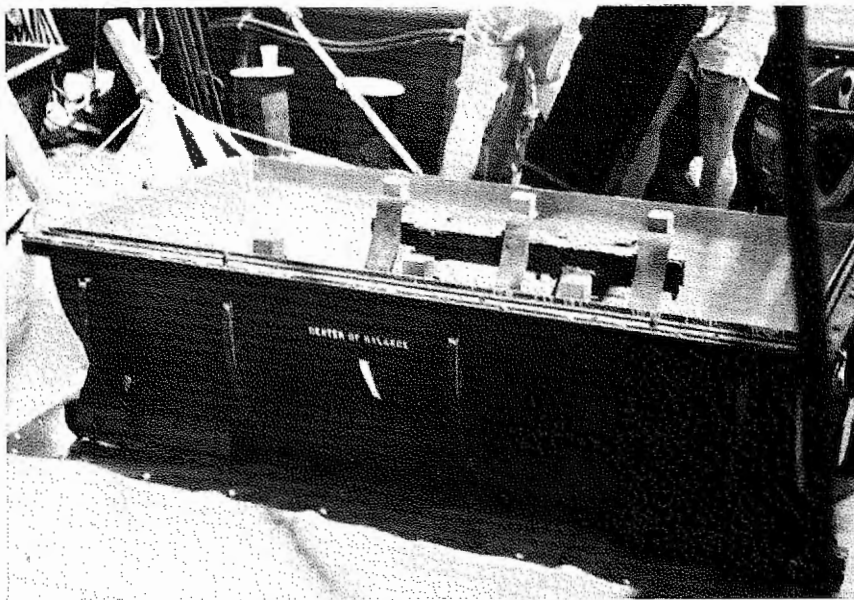
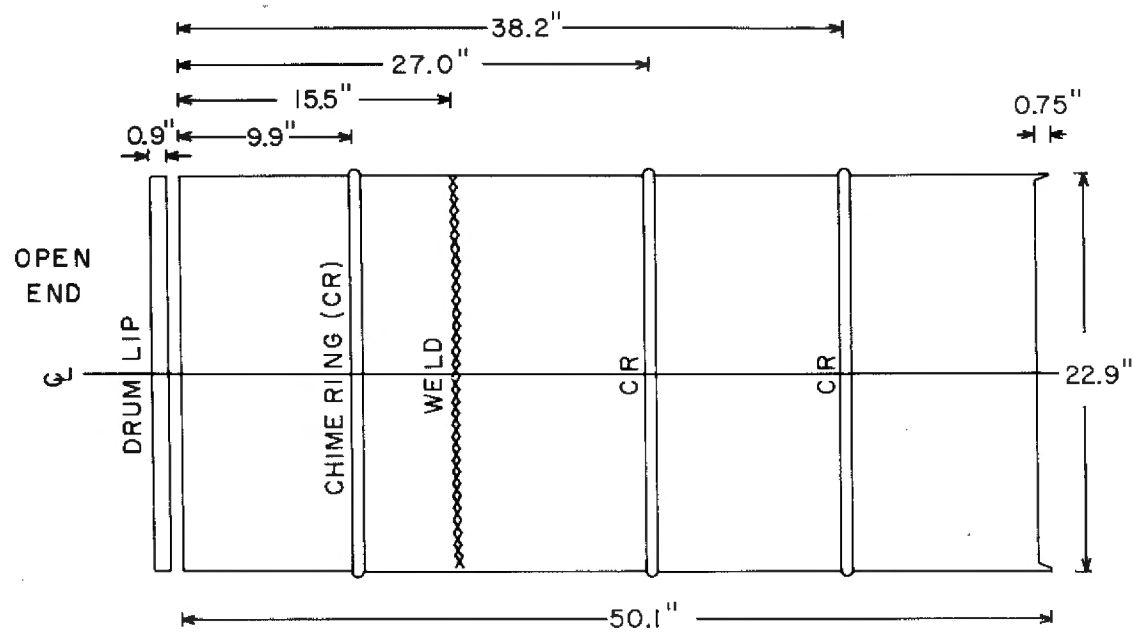


Figure 4(b). An Open H47 Jet Engine Container Showing Rubber Faced Interior Clamp Rings Provided to Hold the Radioactive Waste Package Against Shock and Vibration.



Figure 5. Surface Markings on the Exposed Concrete Face of the Waste Package.





80 GALLON RETRIEVED DRUM

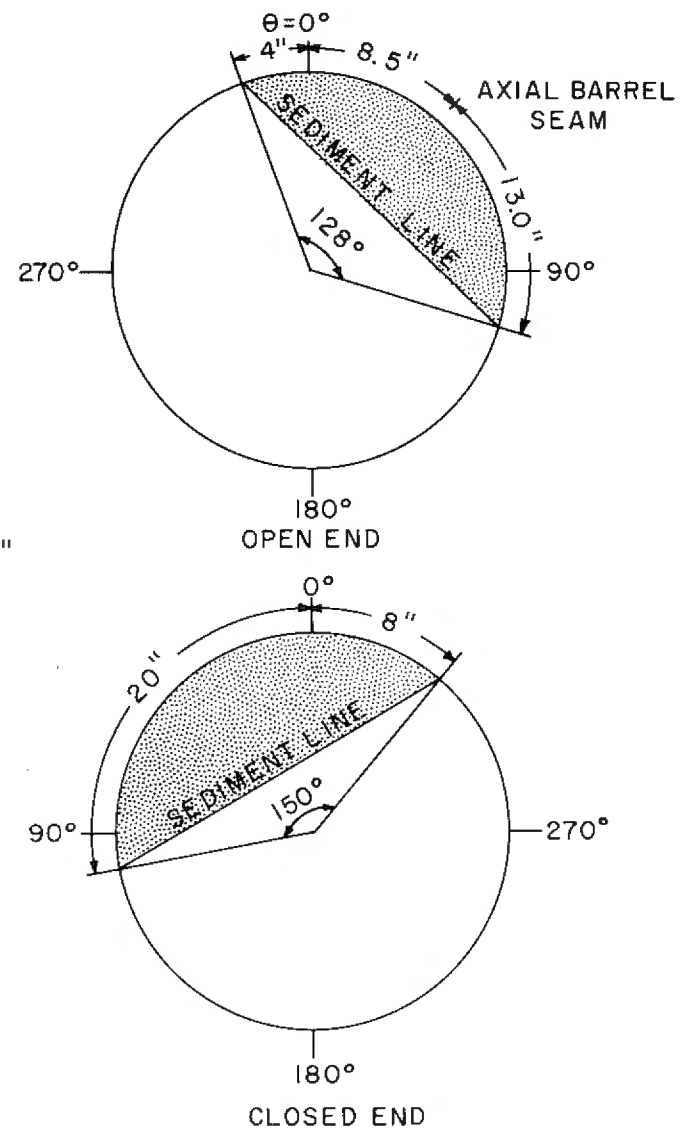


Figure 6. Orientation System Used to Describe the Waste Package.

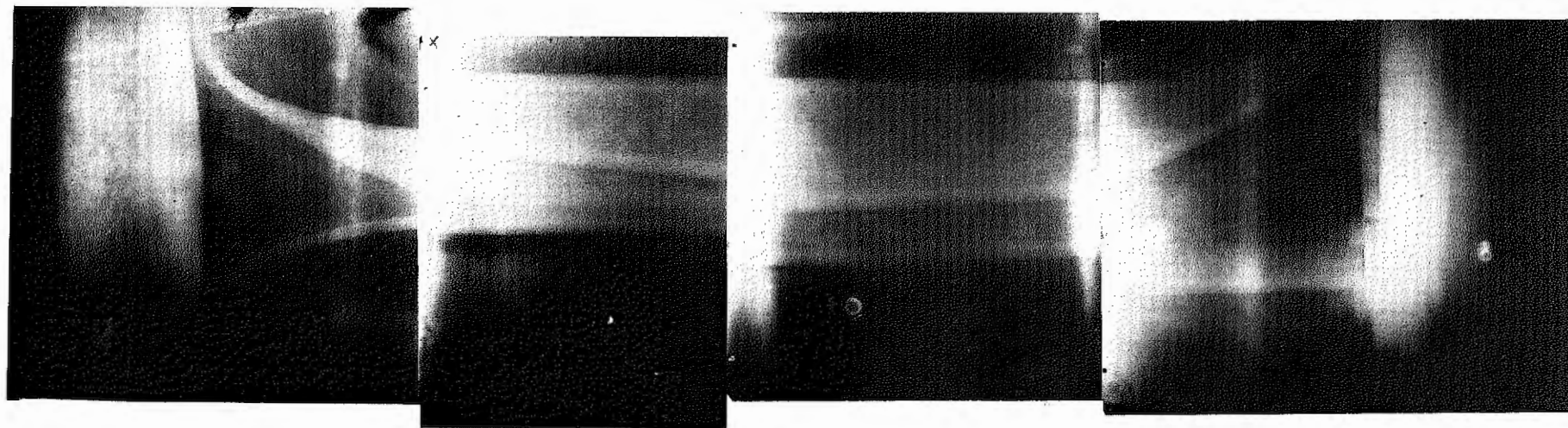


Figure 7. Montage of Waste Package Radiographs. The Top of the Figure Shows the Flanged End of the Internal Container Which Was Located Approximately 5.5 Inches from the Open End of the Waste Package. Note the Concavity along the Length of the Container (on the right edge in this figure) Which Resulted from Implosion During or After Descent to the Seafloor. Film was Positioned along 270° Axis.

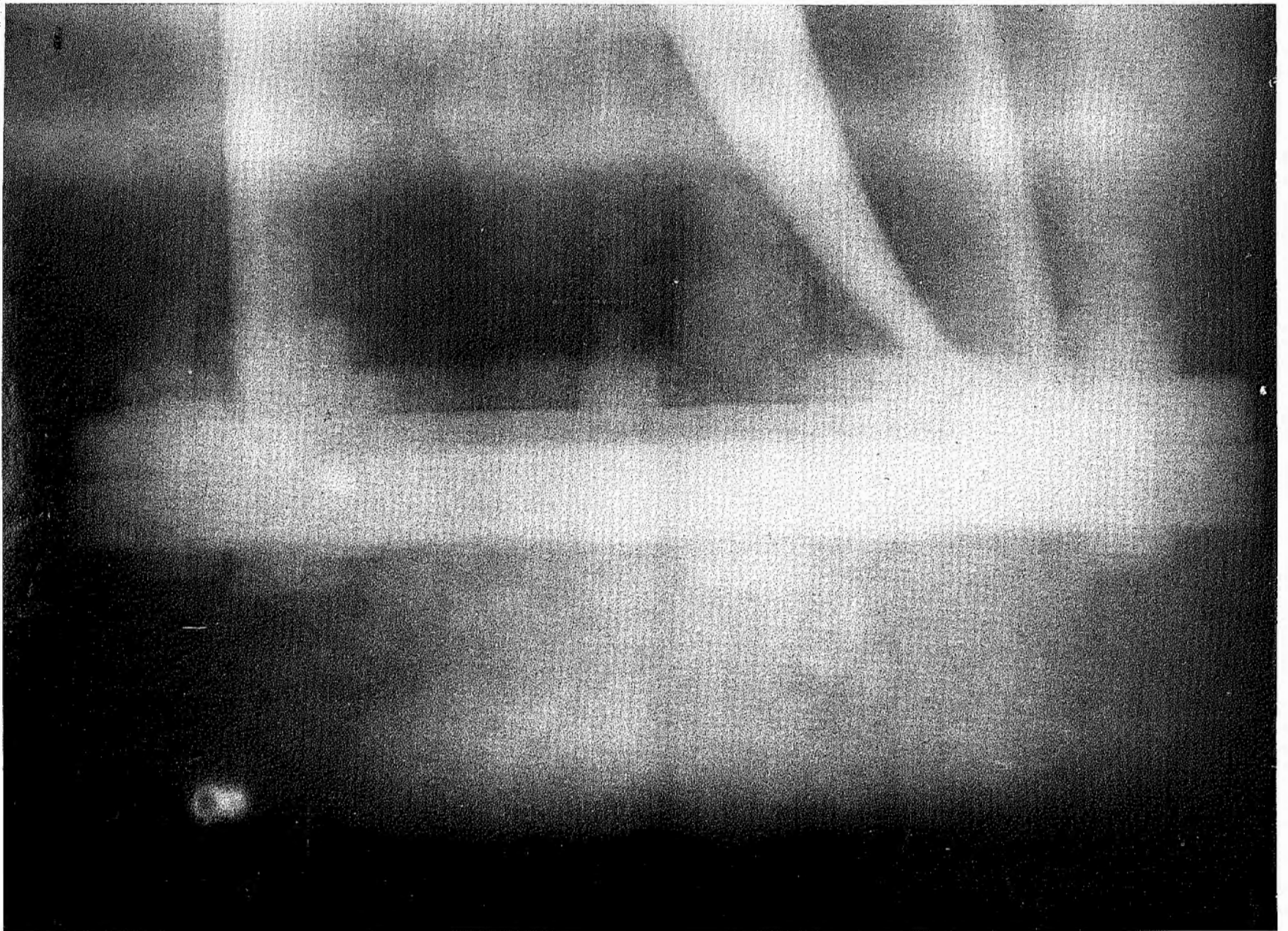


Figure 8. Radiograph of the Flanged End of the Internal Container.

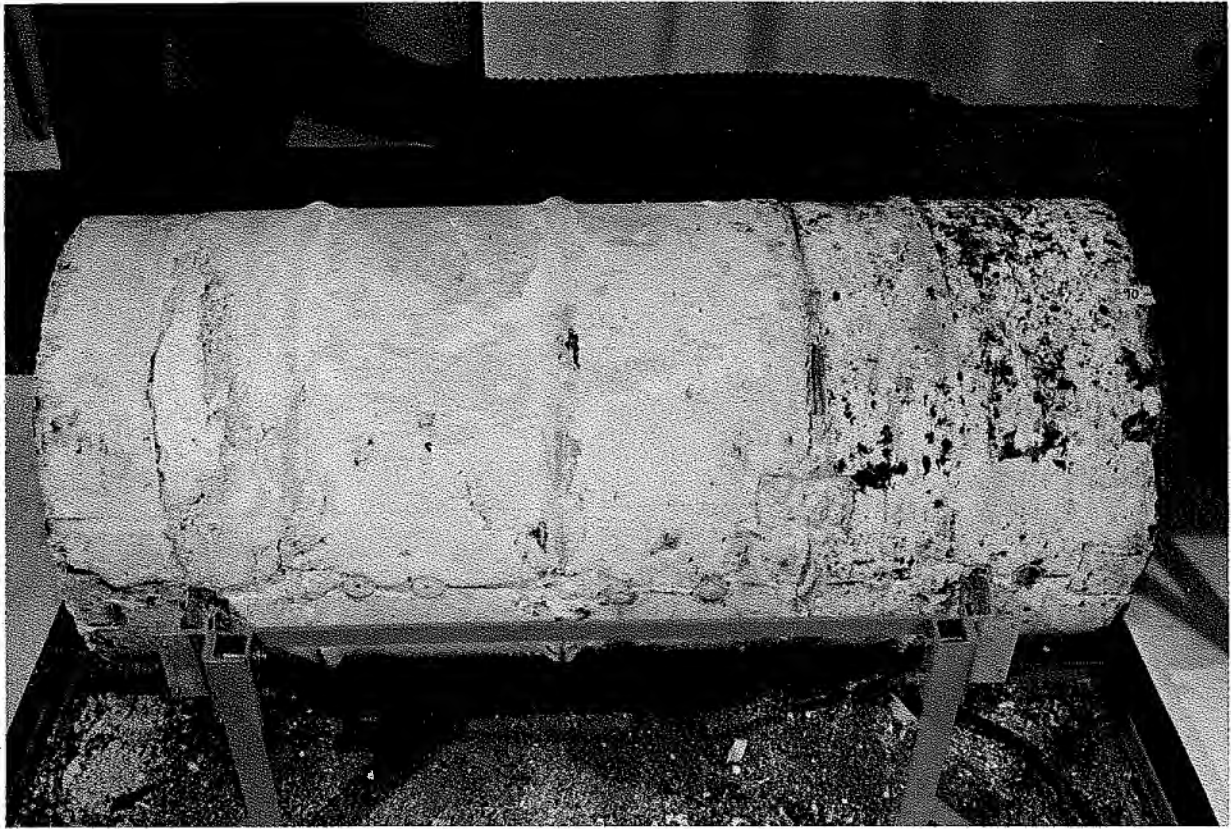


Figure 9. View of the Concrete Waste Form  
with the Steel Drum Removed  
(0° axis).

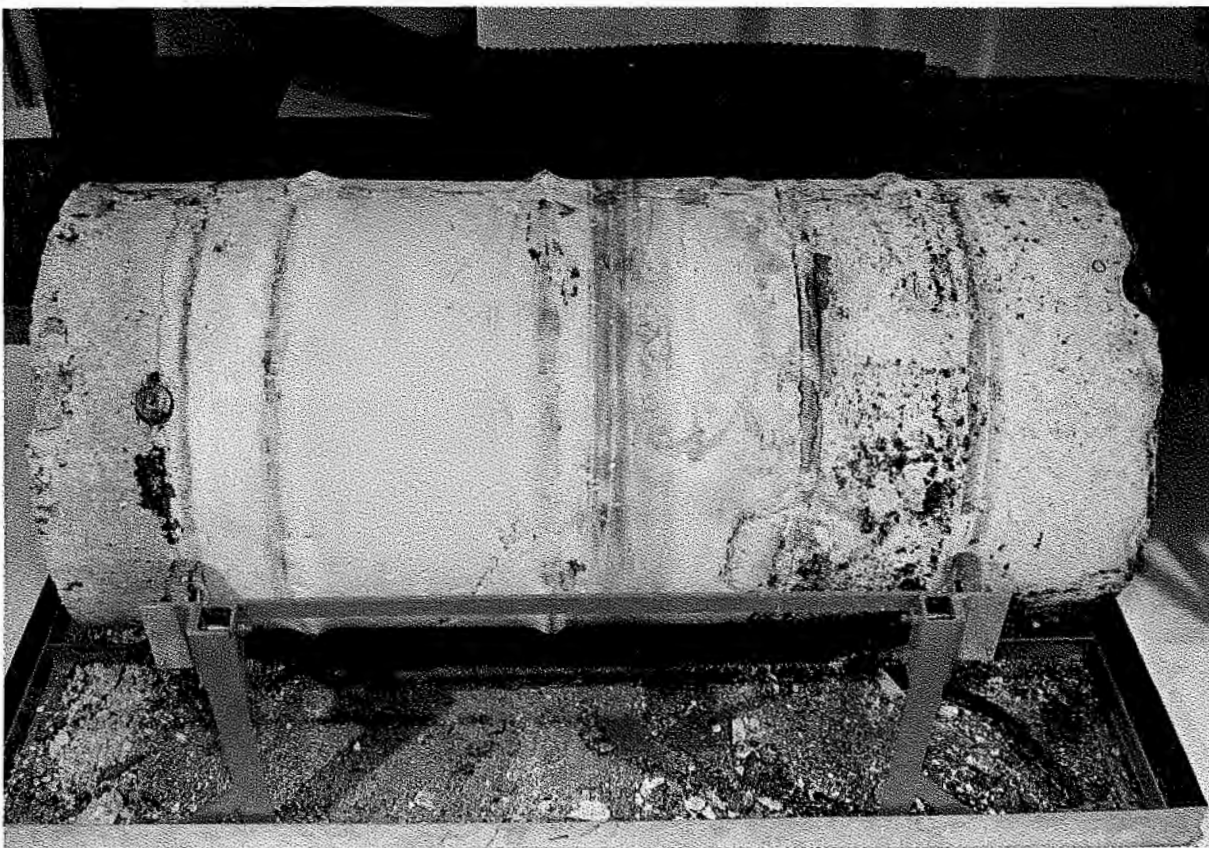


Figure 10. View of the Concrete Waste Form  
with the Steel Drum Removed  
(90° axis).



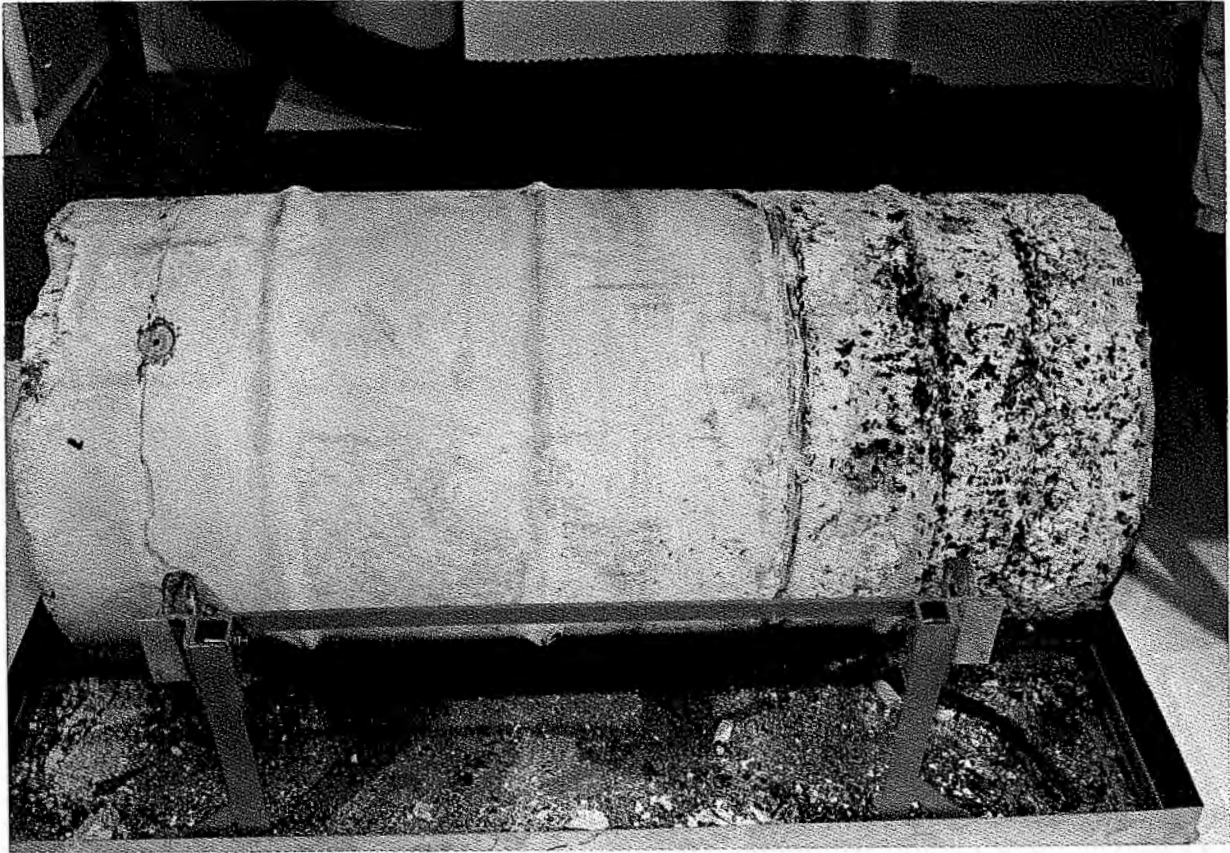


Figure 11. View of the Concrete Waste Form  
with the Steel Drum Removed  
(180° axis).

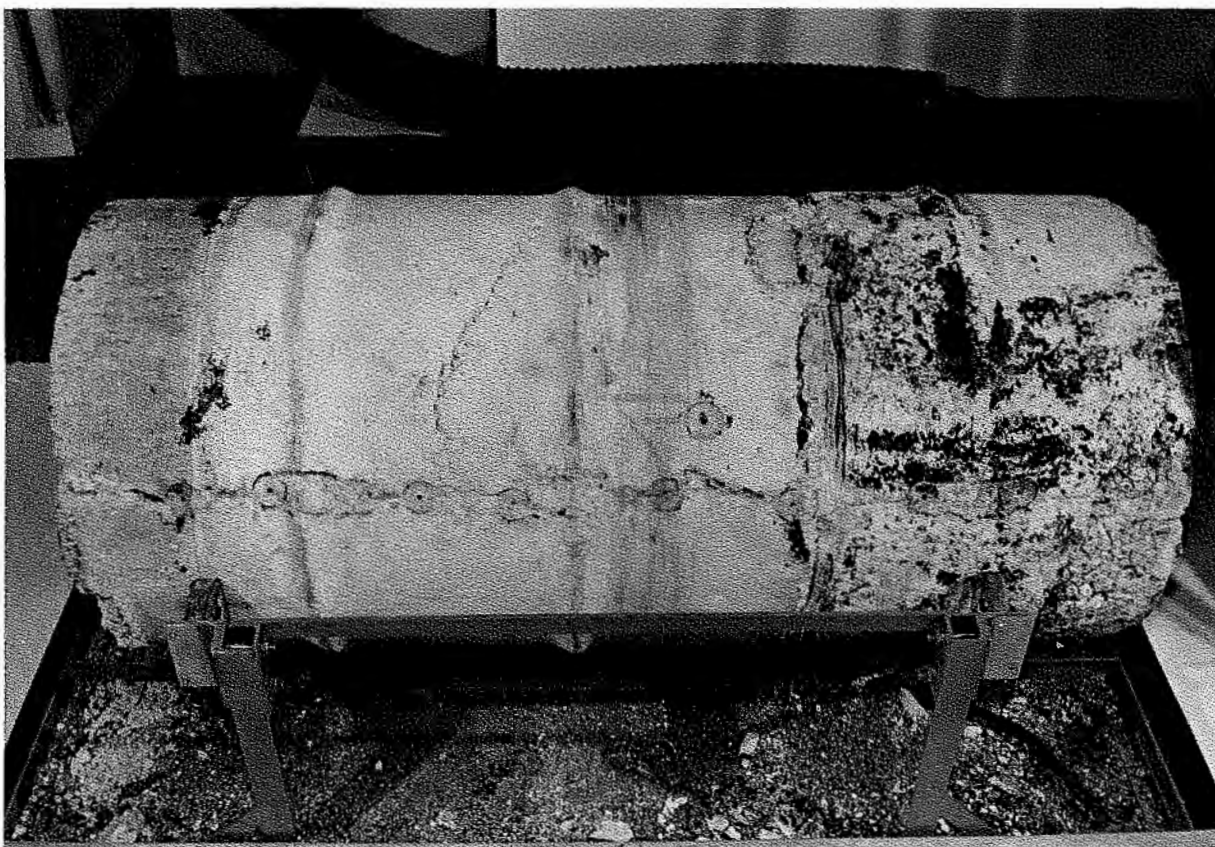


Figure 12. View of the Concrete Waste Form  
with the Steel Drum Removed  
(270° axis).

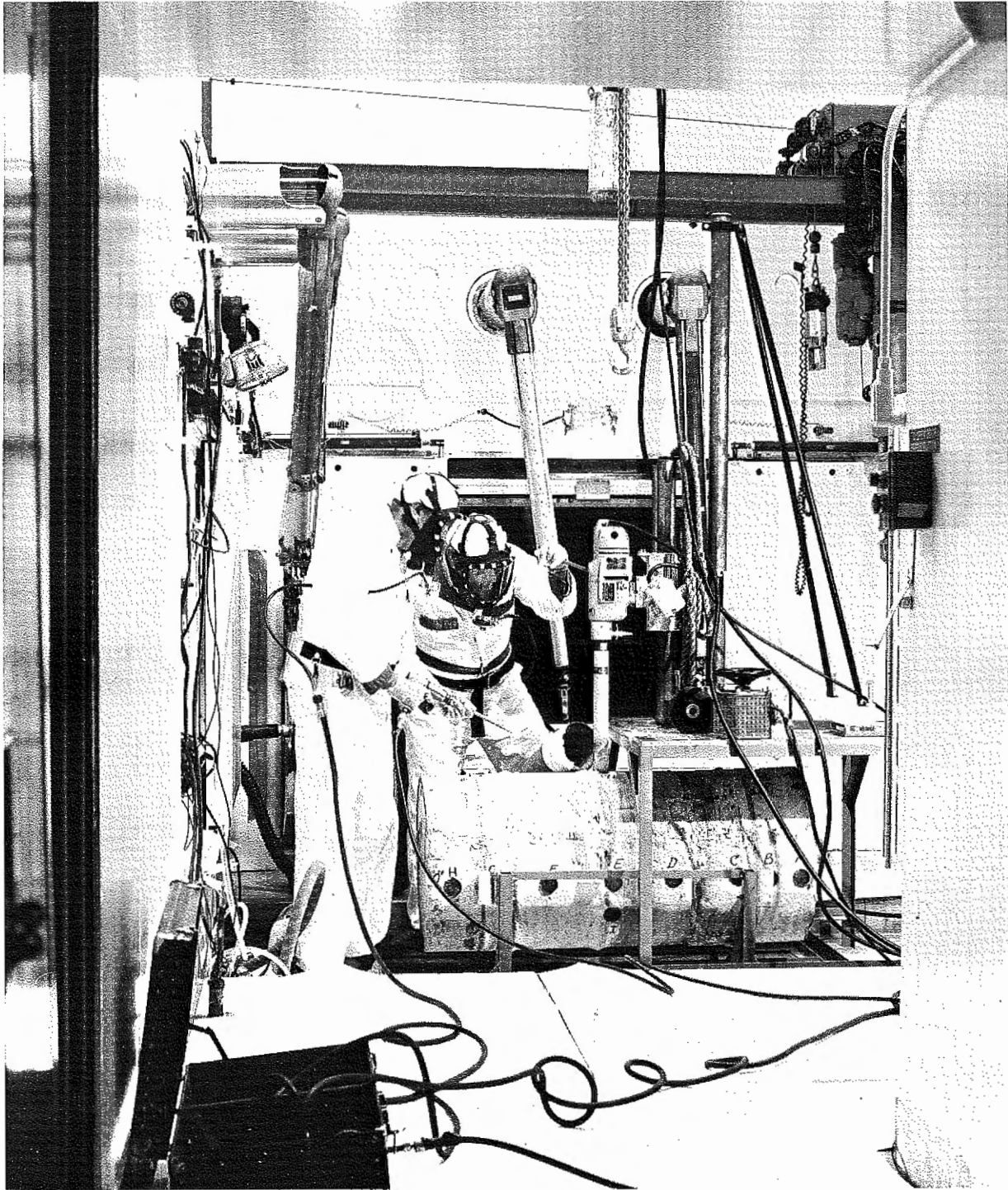


Figure 13. Core Drilling of the Concrete Waste Form. The Worker on the Right is Moving the Drill Bit into the Waste Form While the Worker on the Left Holds the Pneumatic Chisel Used to Remove the Steel Drum.



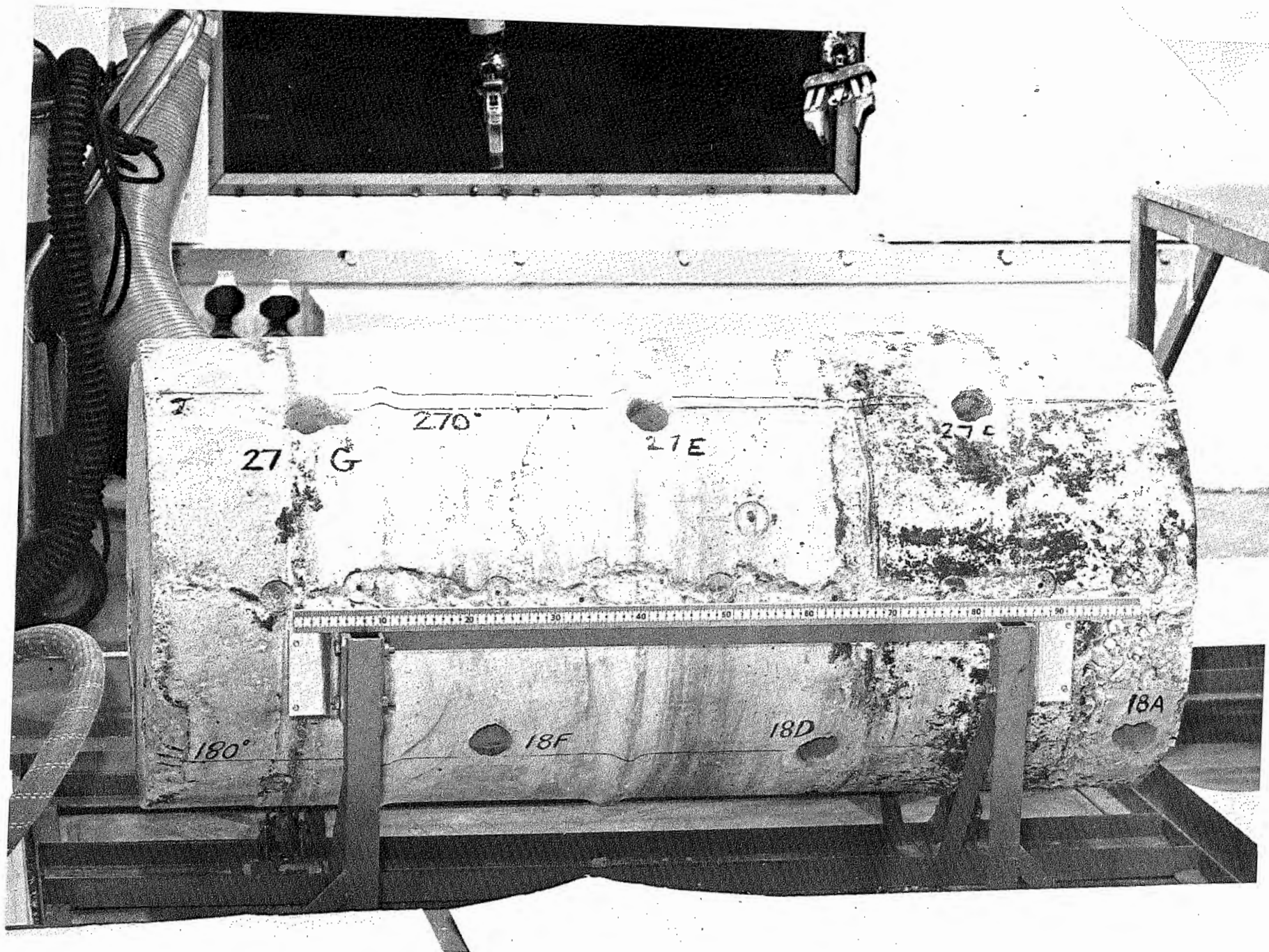


Figure 14. Letter Designation of Core Locations as Shown along the  $0^{\circ}$  and  $20^{\circ}$  Longitudinal Axis.

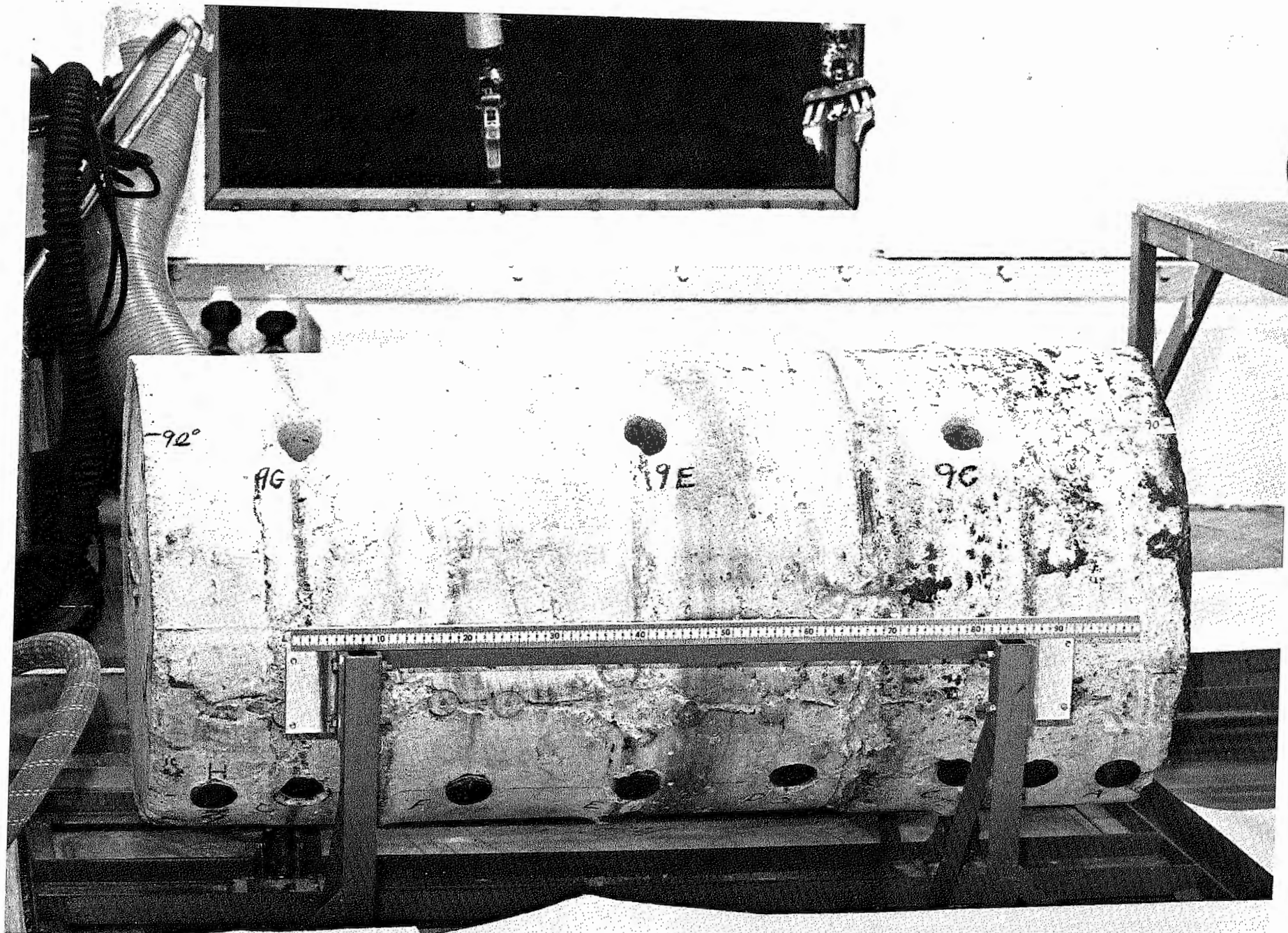


Figure 15. Letter Designation of Core Locations along the 90° Longitudinal Axis.



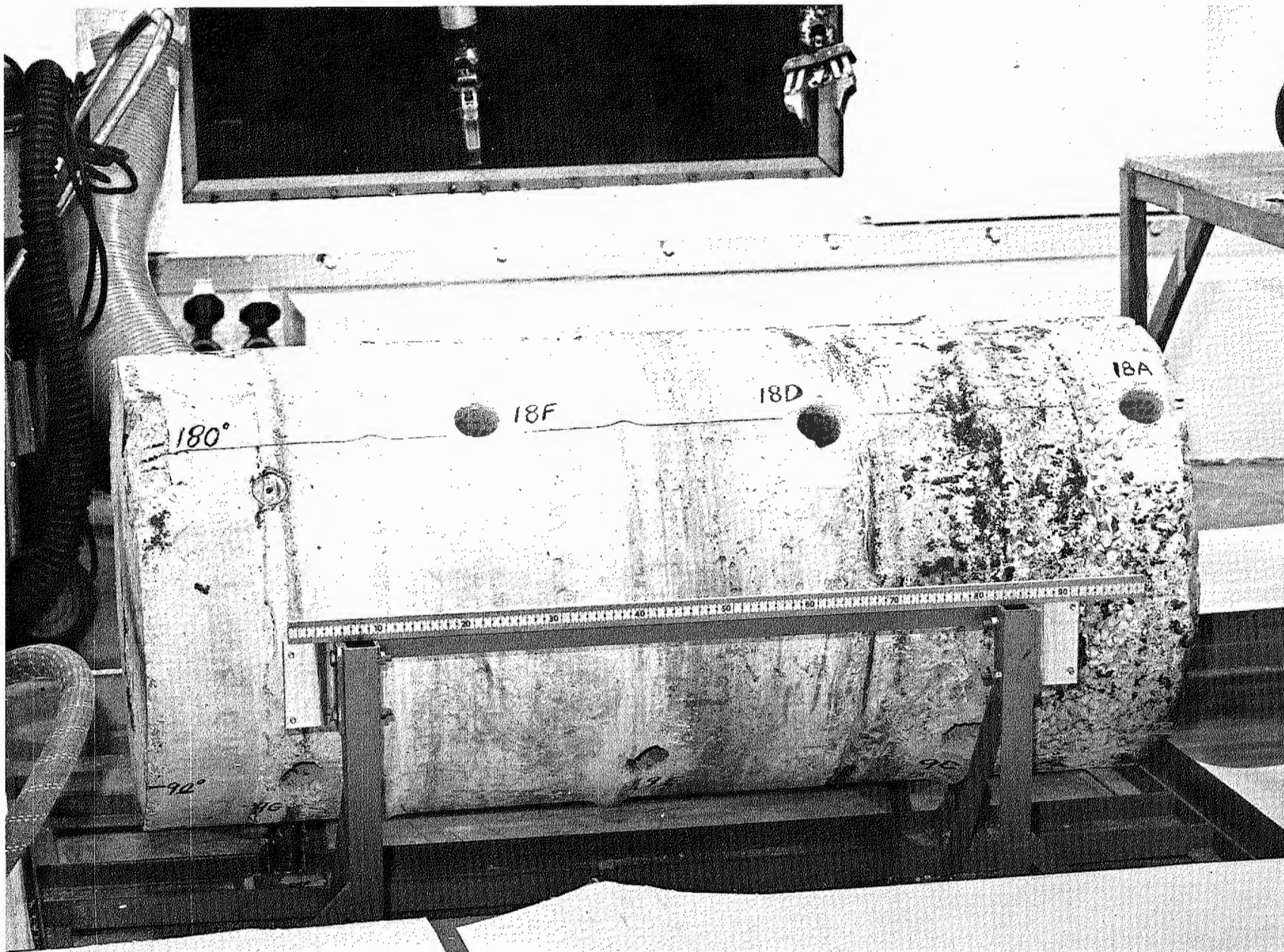


Figure 16. Letter Designation of Core Locations along the 180° Longitudinal Axis.

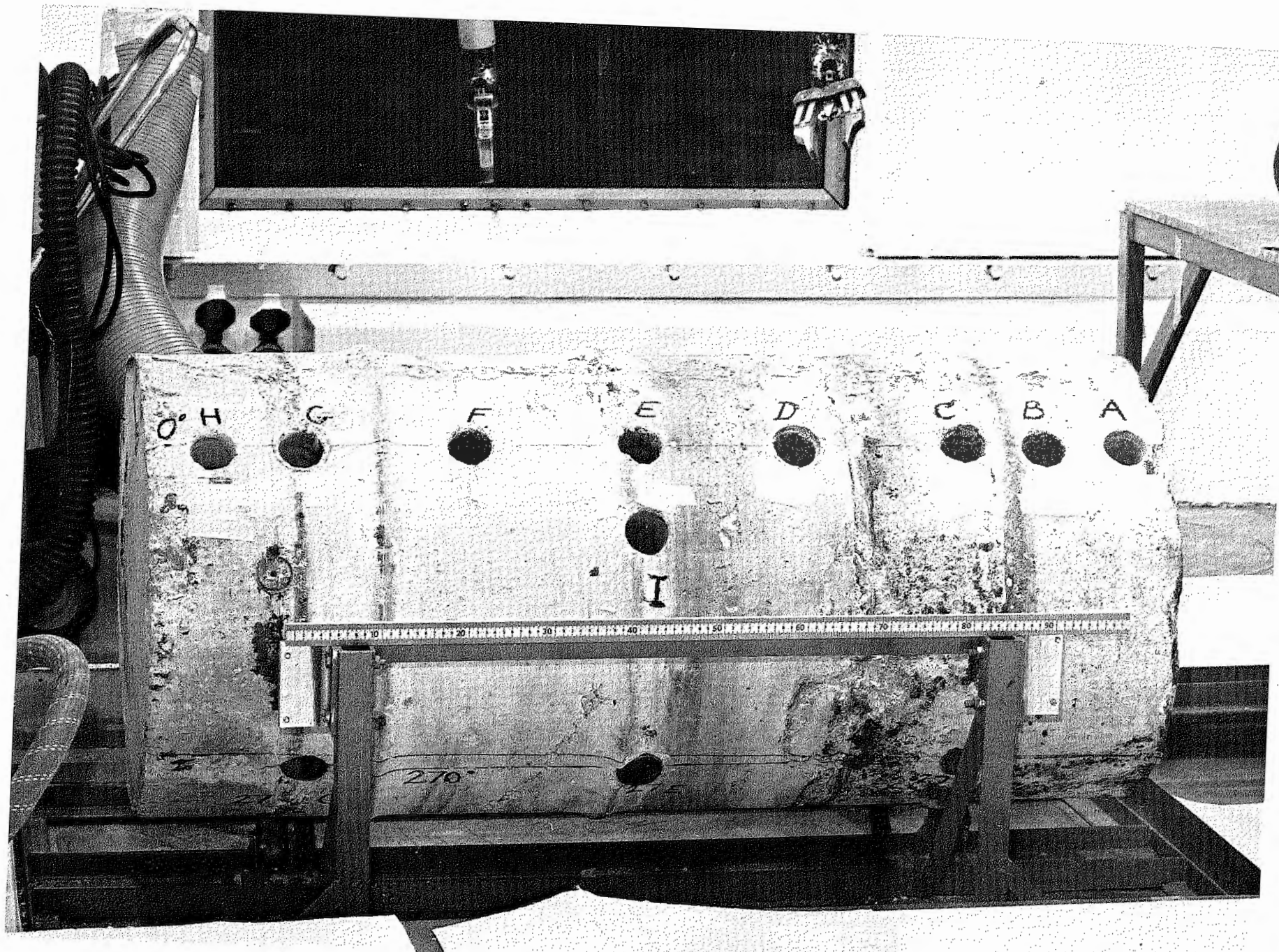


Figure 17. Letter Designation of Core Locations along the 270° Longitudinal Axis

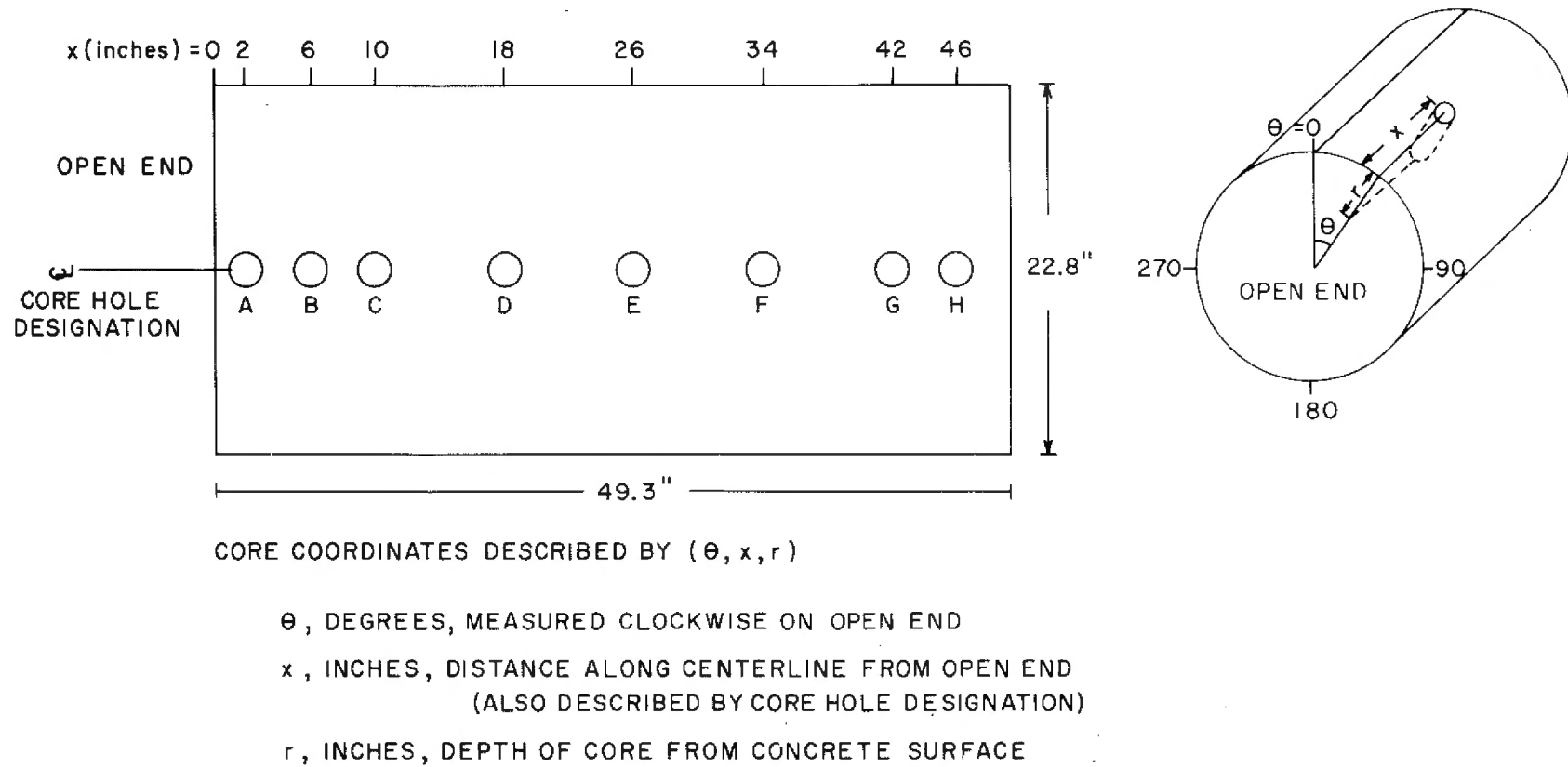


Figure 18. Schematic Showing the Letter Designation of Core Holes as Related to  $(\theta, x, r)$  Location Coordinates.



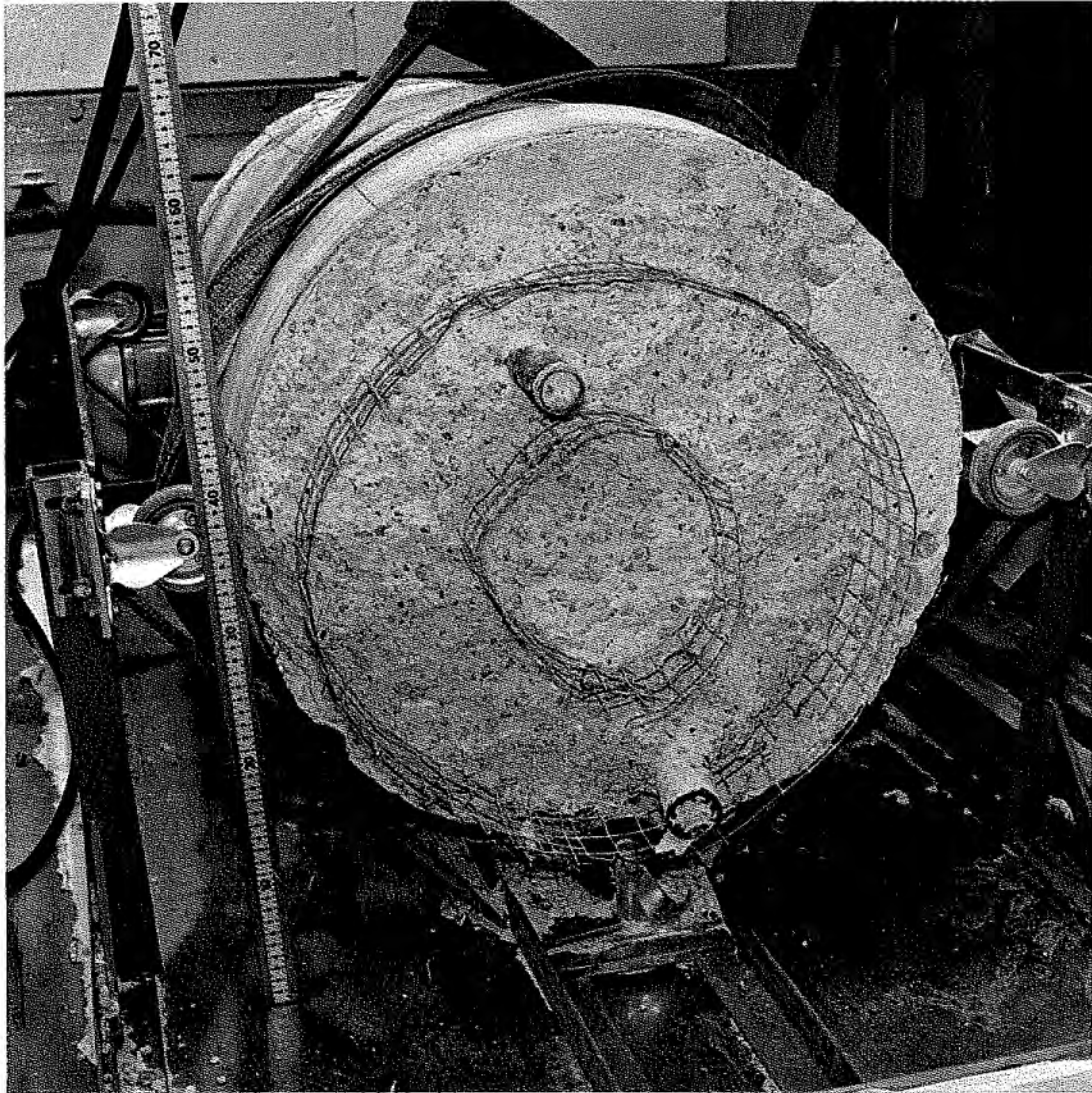


Figure 19. Closed End of the Waste Form after Removal of the Five Inch Thick Initial Concrete Pouring.

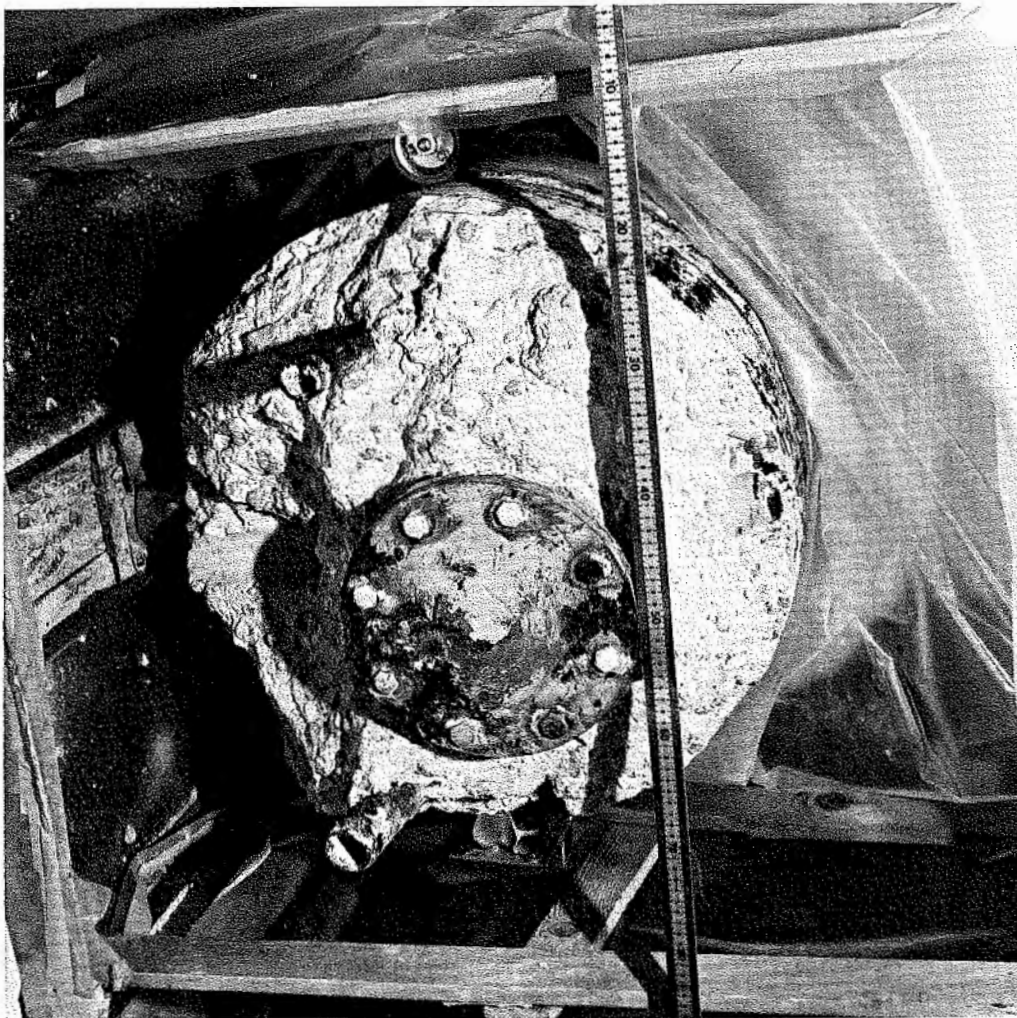


Figure 20. Waste Form after Removal of the Upper Eight Inches of Concrete from the Open End, Exposing the Flanged End of the Inner Container.

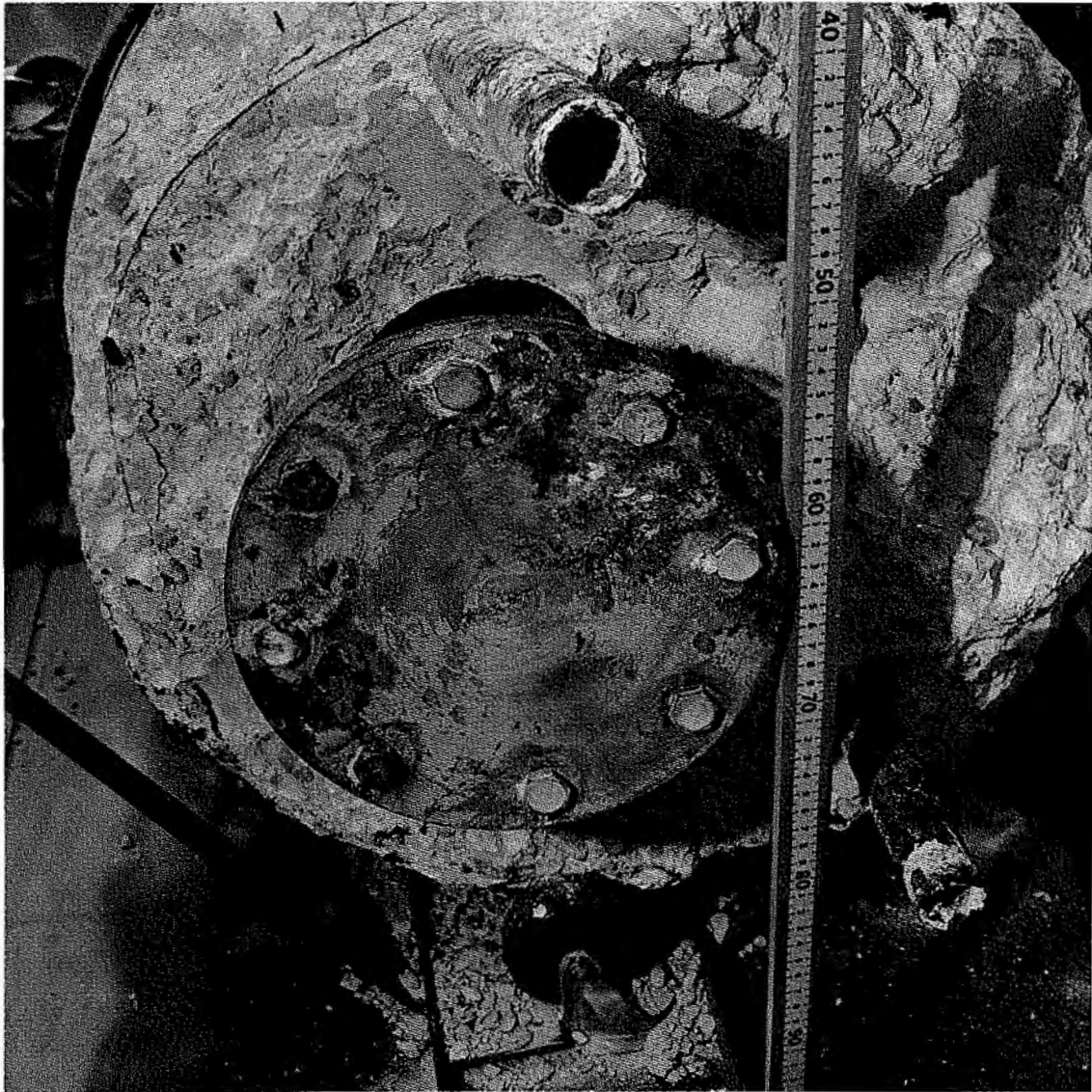


Figure 21. View of the Exposed Flange End of the Inner Container. Note the Gap between the Container and the Concrete Formed by Implosion of the Inner Container Wall during Descent.





Figure 22. Concrete Waste Form after Removal of the Inner Container.

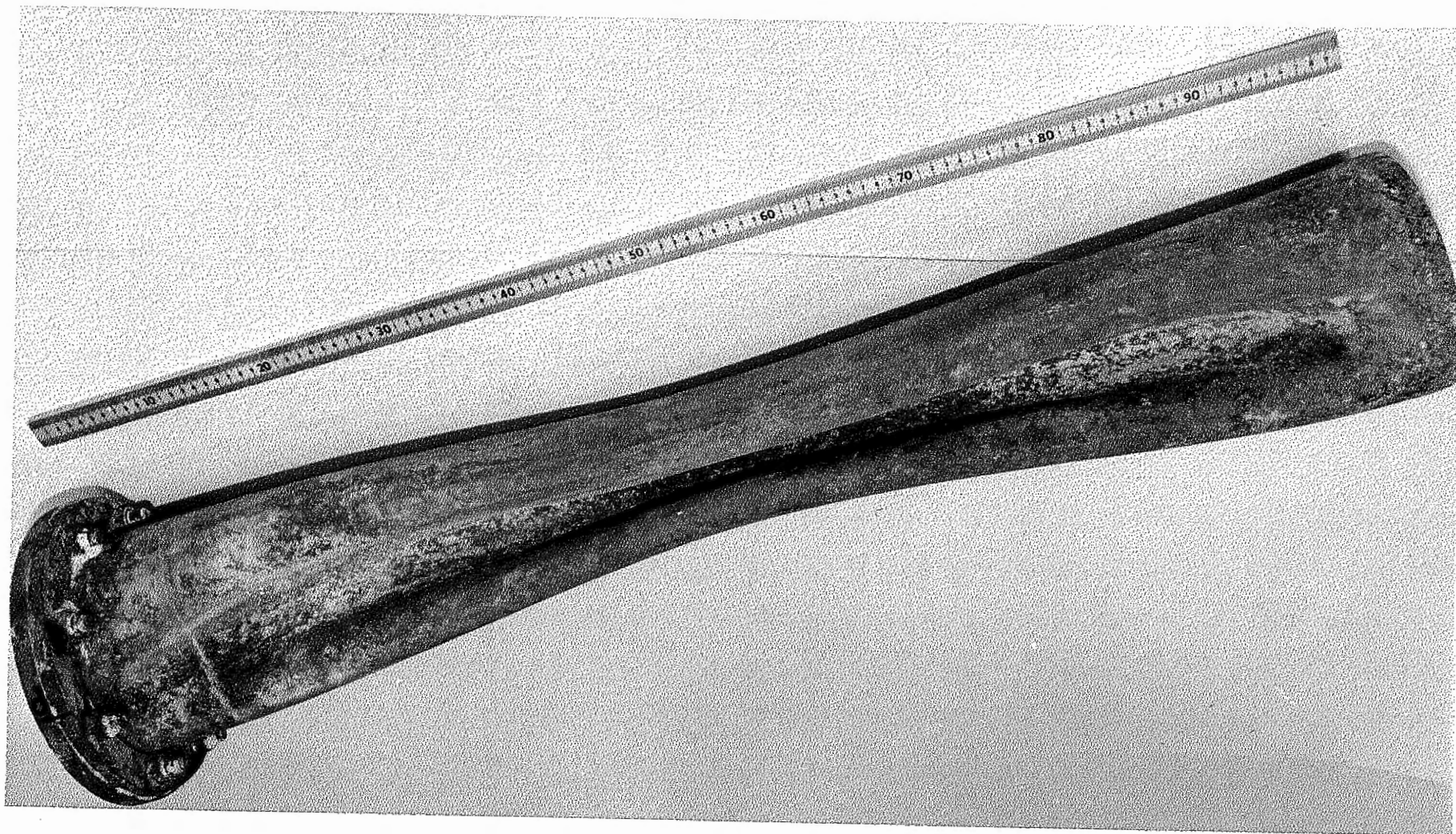


Figure 23. Inner Steel Vessel after Removal from the Waste Form. Note Implosion of the Container Walls along the 0° Longitudinal Axis.





Figure 24. Inner Steel Vessel Viewed along the  $180^{\circ}$  Longitudinal Axis.

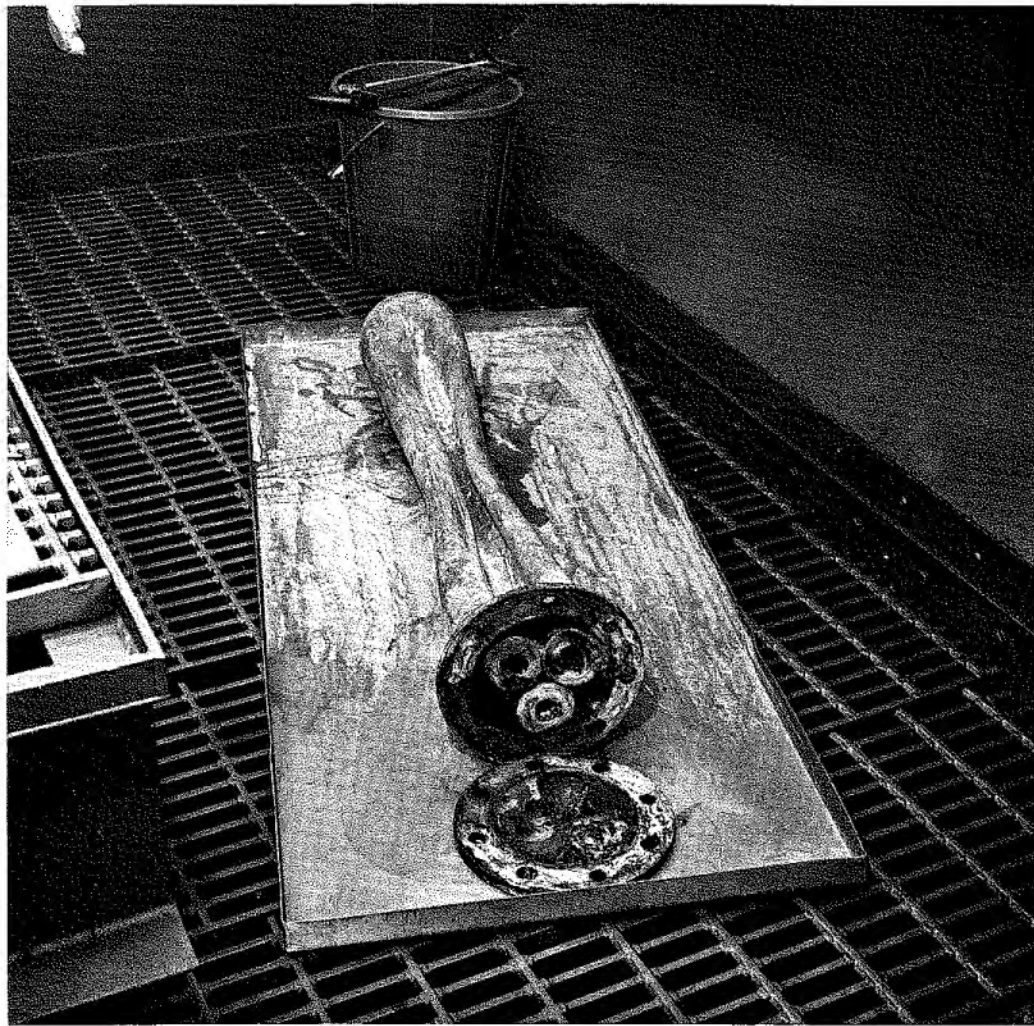


Figure 25. Inner Steel Vessel with the Cover Removed, Showing the Enclosed Wound Filter Assemblies.

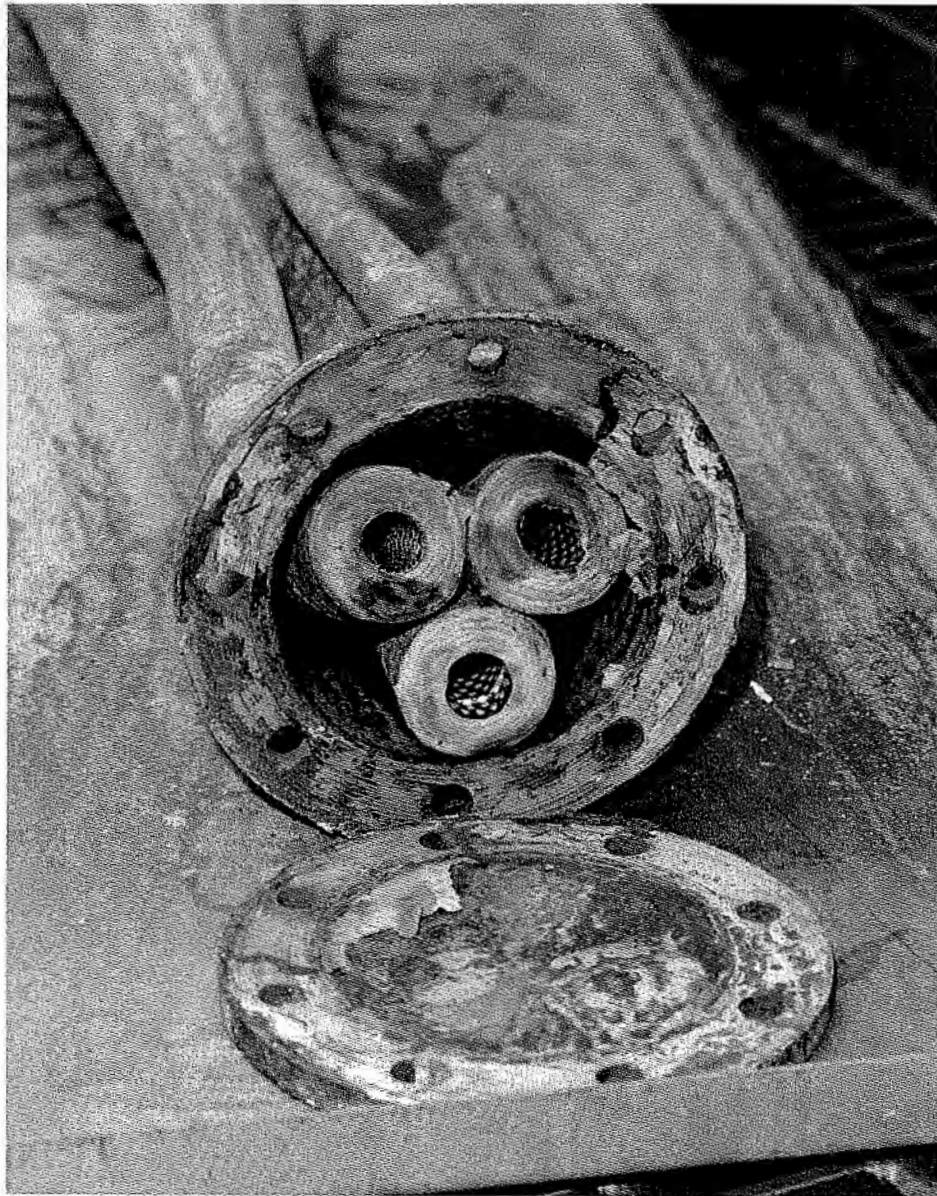


Figure 26. Close up View of the Inner Container Cover, Flange and Enclosed Filter Assemblies.

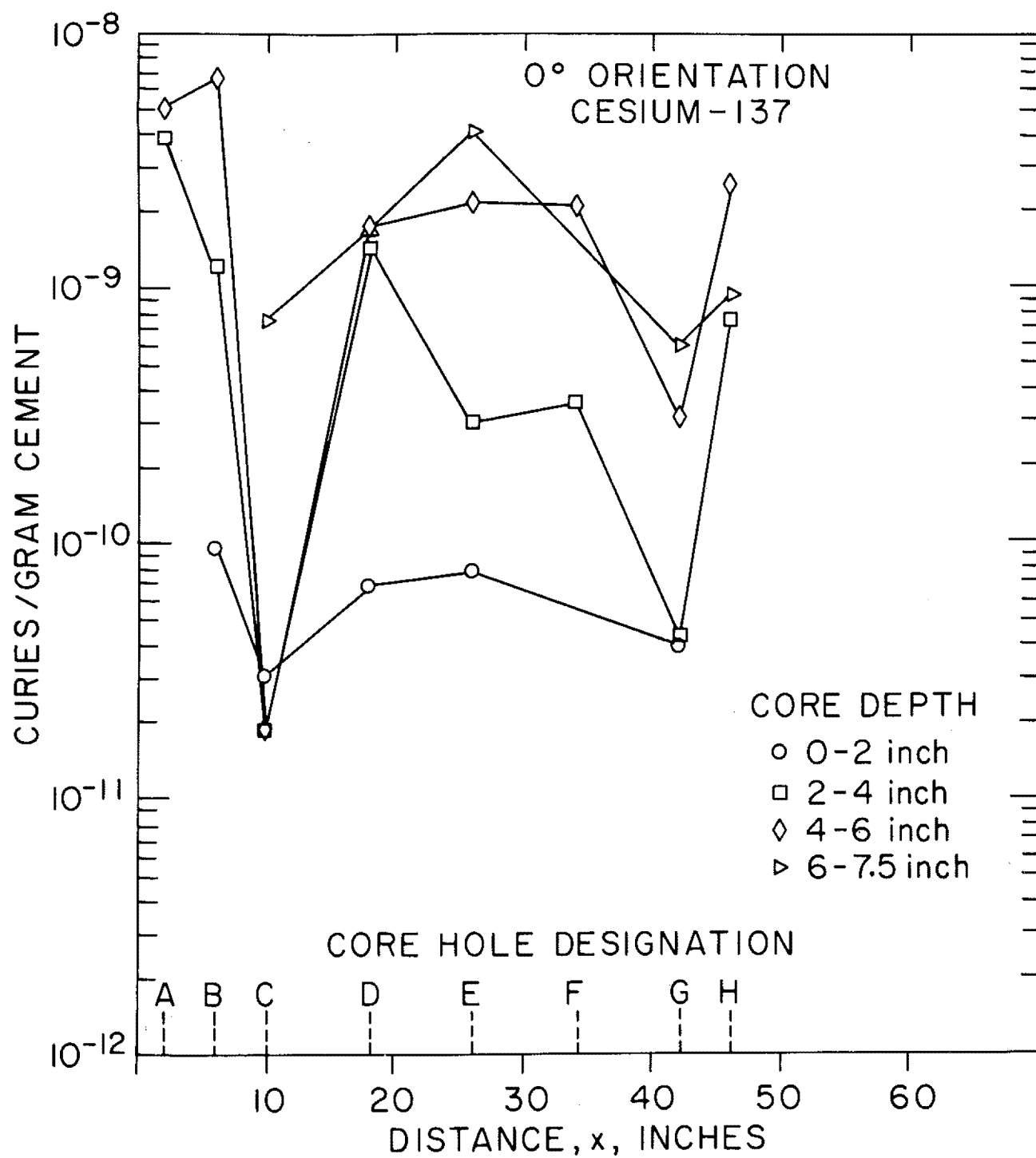


Figure 27. Cesium-137 Content in Concrete Cores along the 0° Longitudinal Axis.

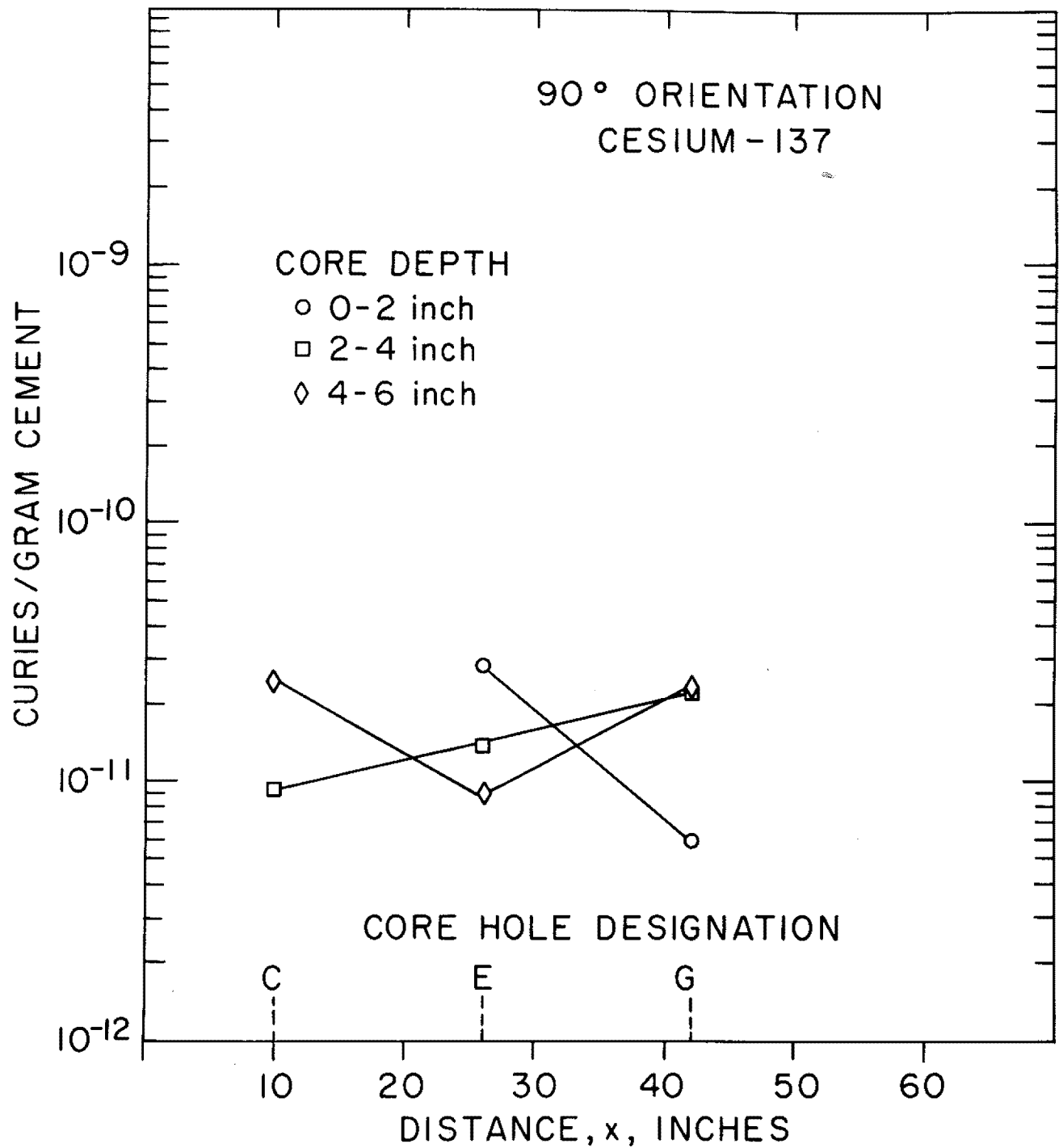


Figure 28. Cesium-137 Content in Concrete Cores along the 90° Longitudinal Axis.

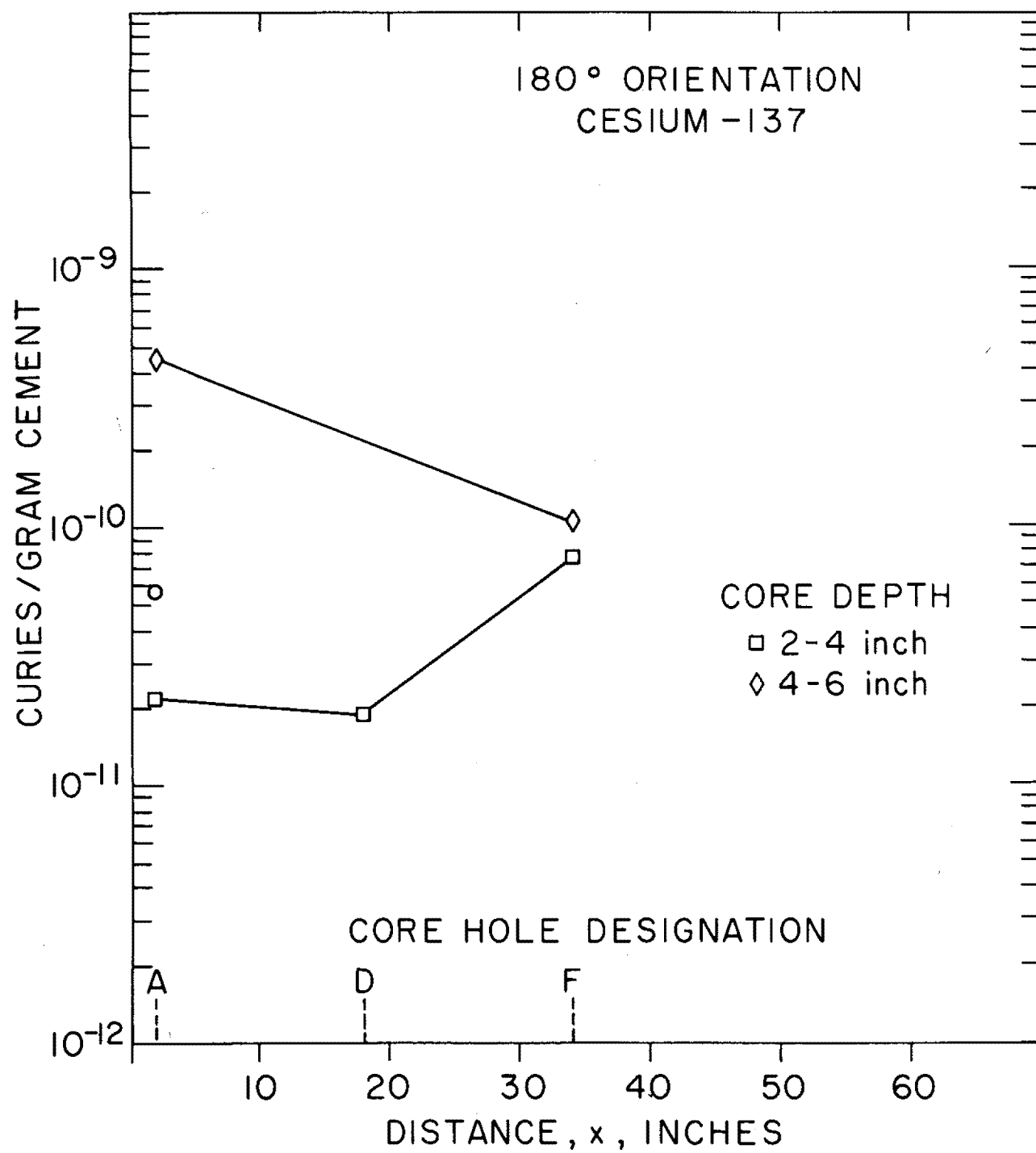


Figure 29. Cesium-137 Content in Concrete Cores along the 180° Longitudinal Axis.



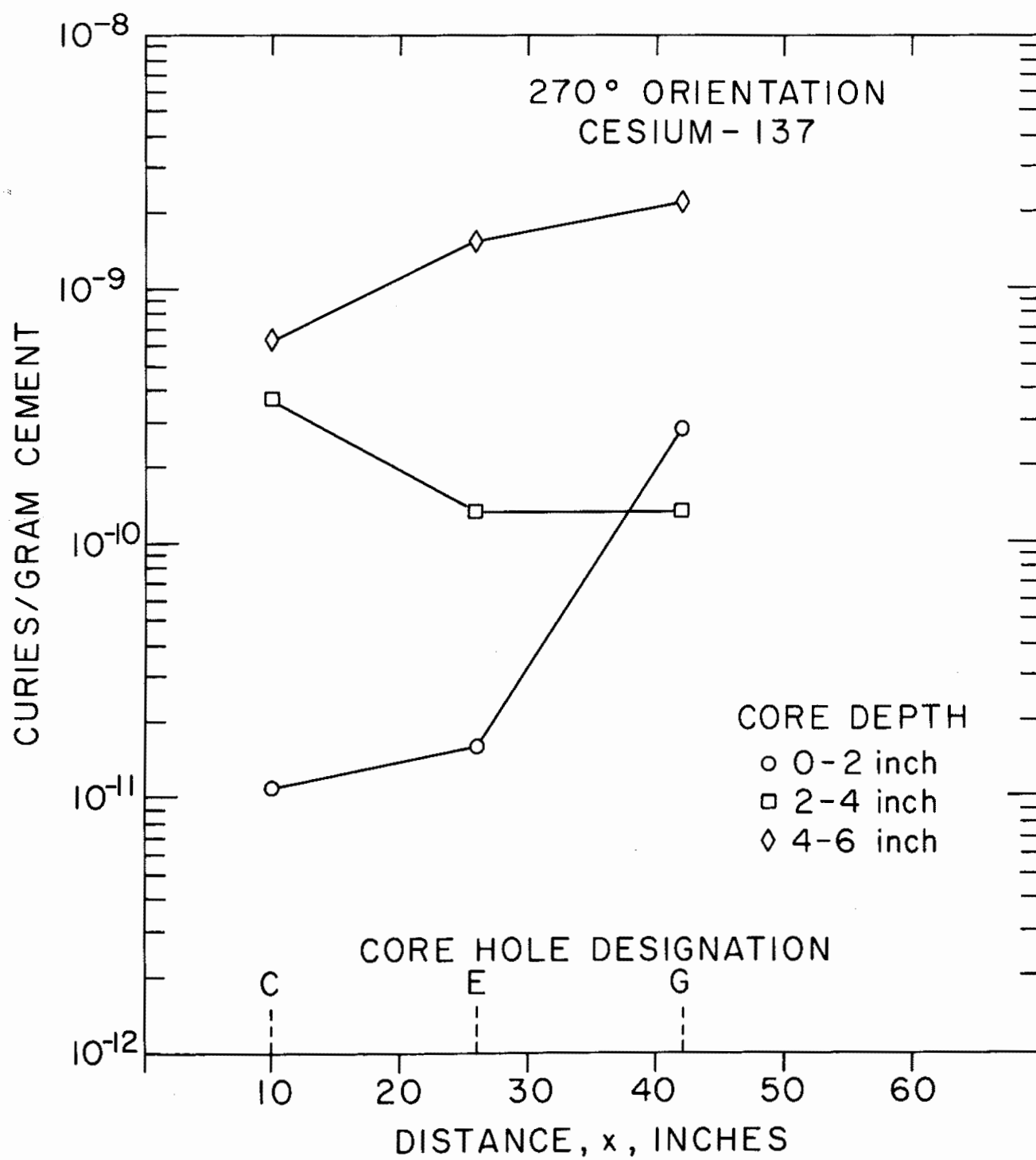


Figure 30. Cesium-137 Content in Concrete Cores along the 270° Longitudinal Axis.

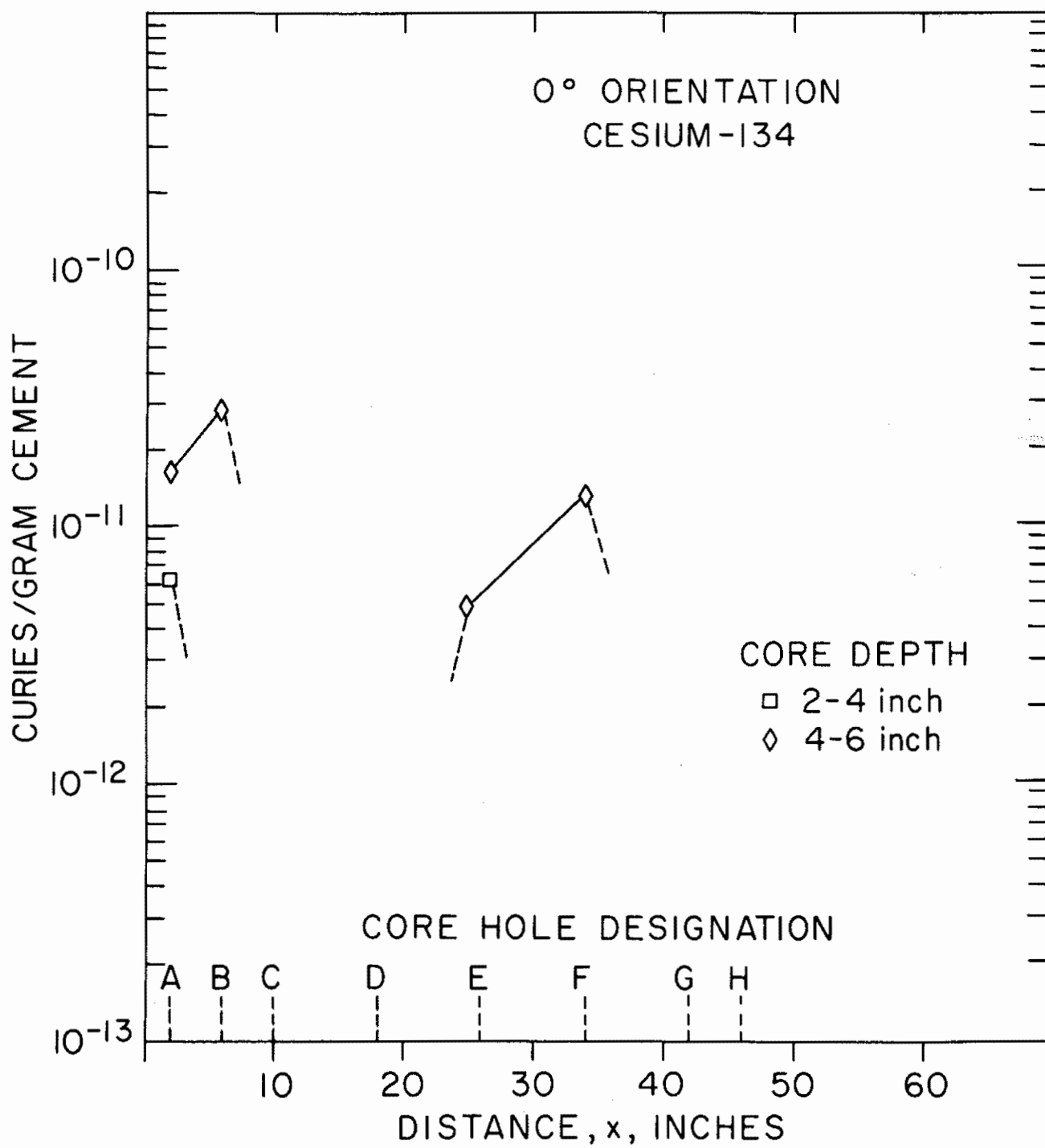


Figure 31. Cesium-134 Content in Concrete Cores along the 0° Longitudinal Axis.

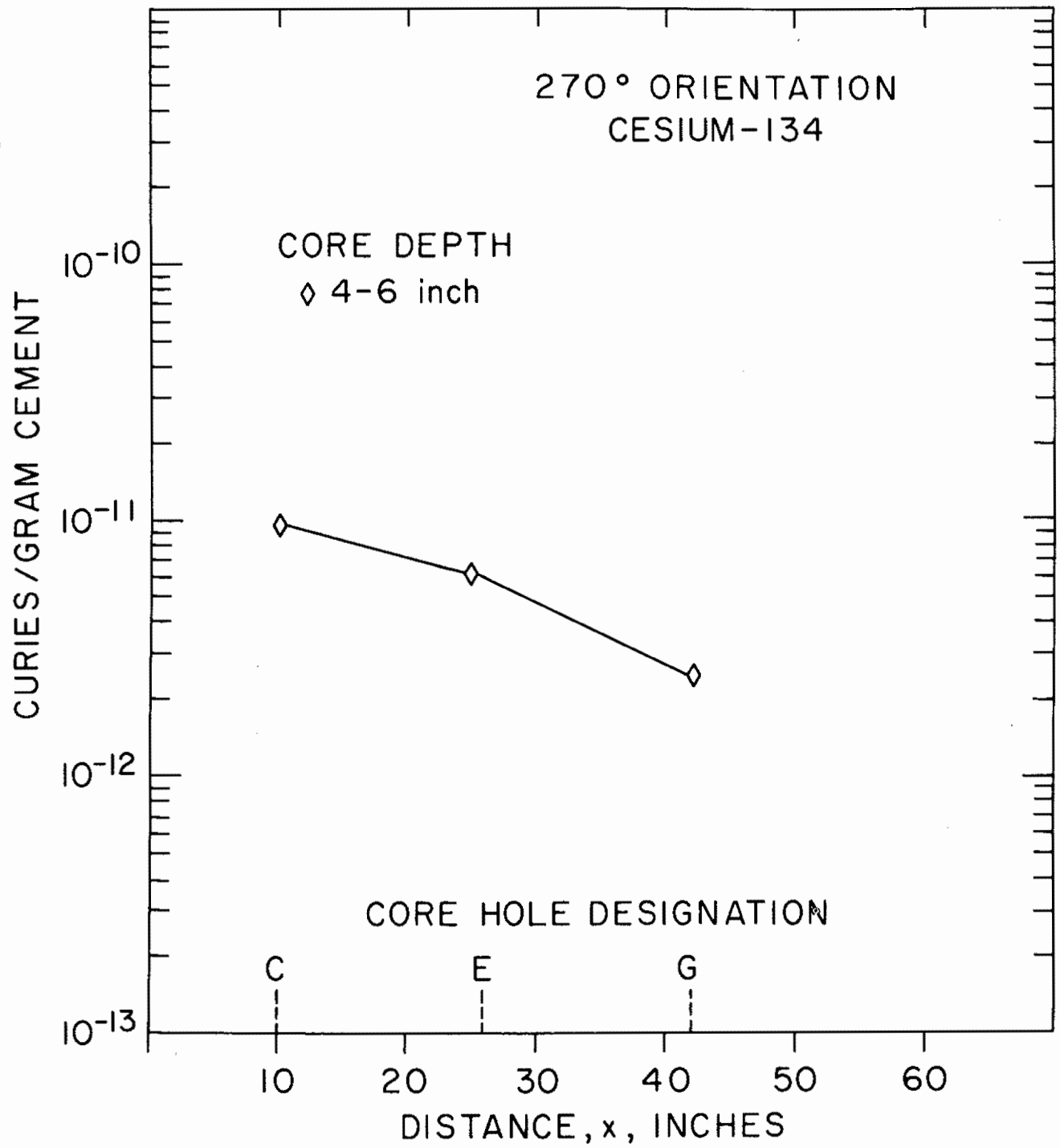


Figure 32. Cesium-134 Content in Concrete Cores along the 270° Longitudinal Axis.

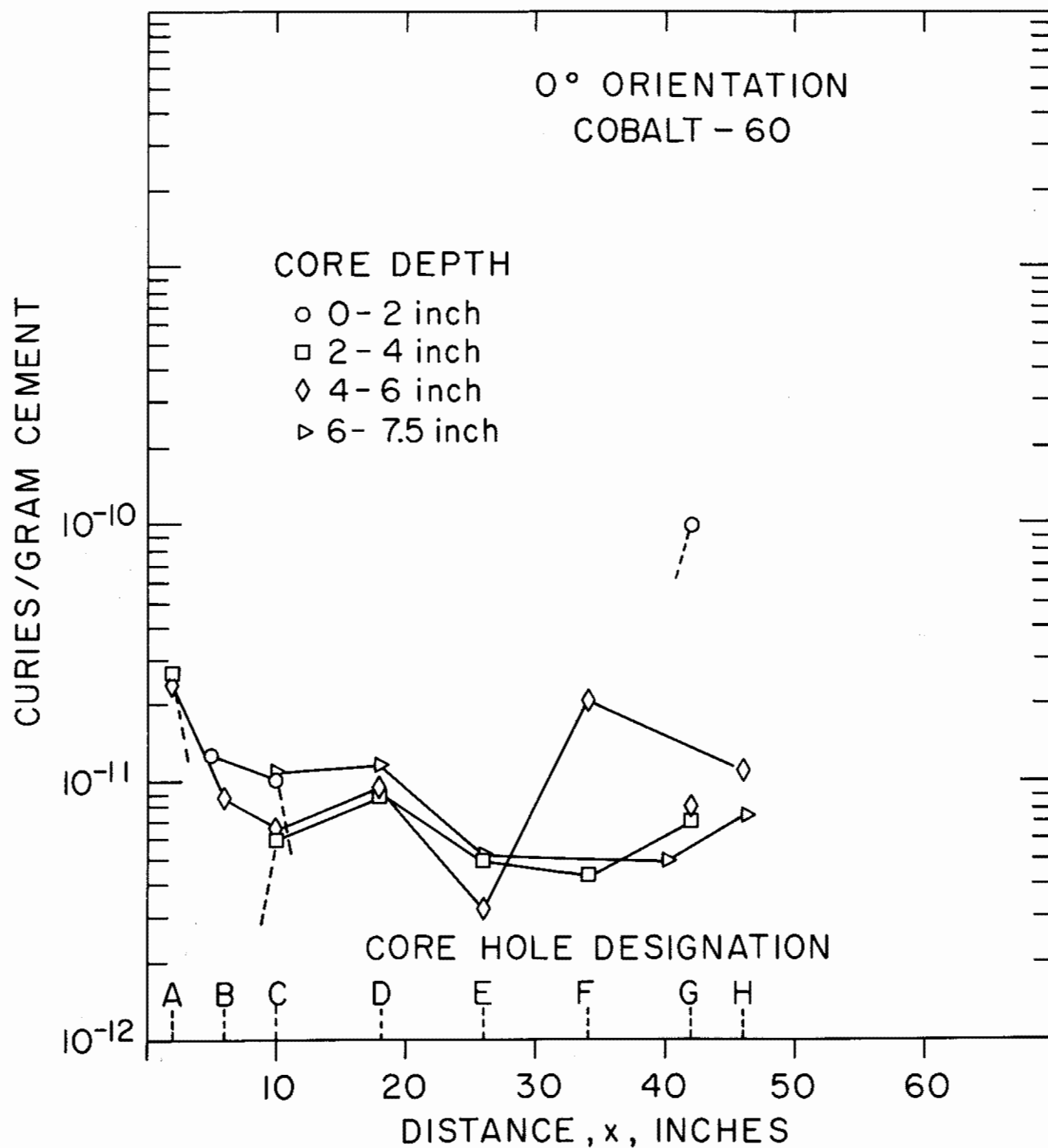


Figure 33. Cobalt-60 Content in Concrete Cores along the 0° Longitudinal Axis.

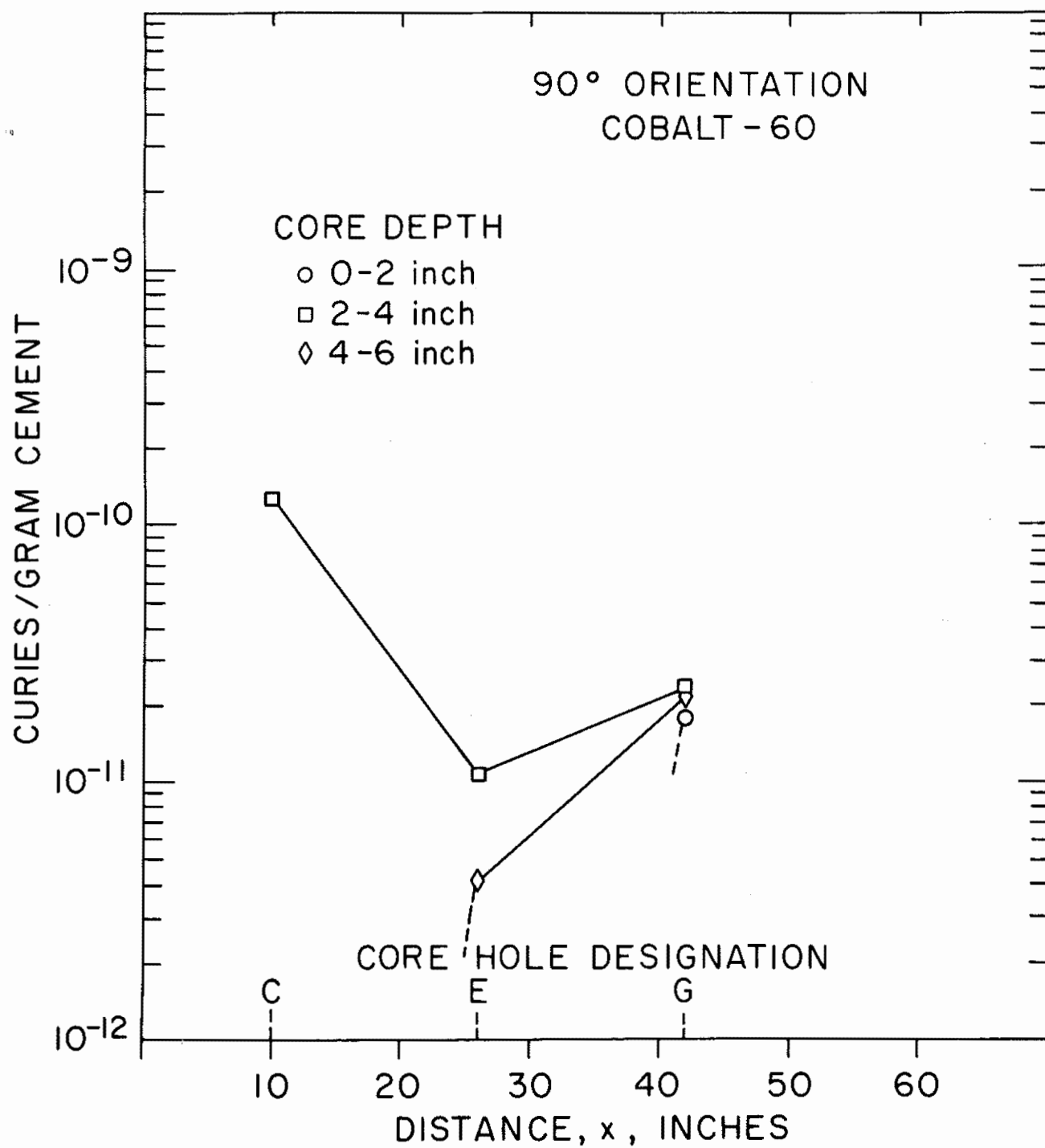


Figure 34. Cobalt-60 Content in Concrete Cores along the 90° Longitudinal Axis.

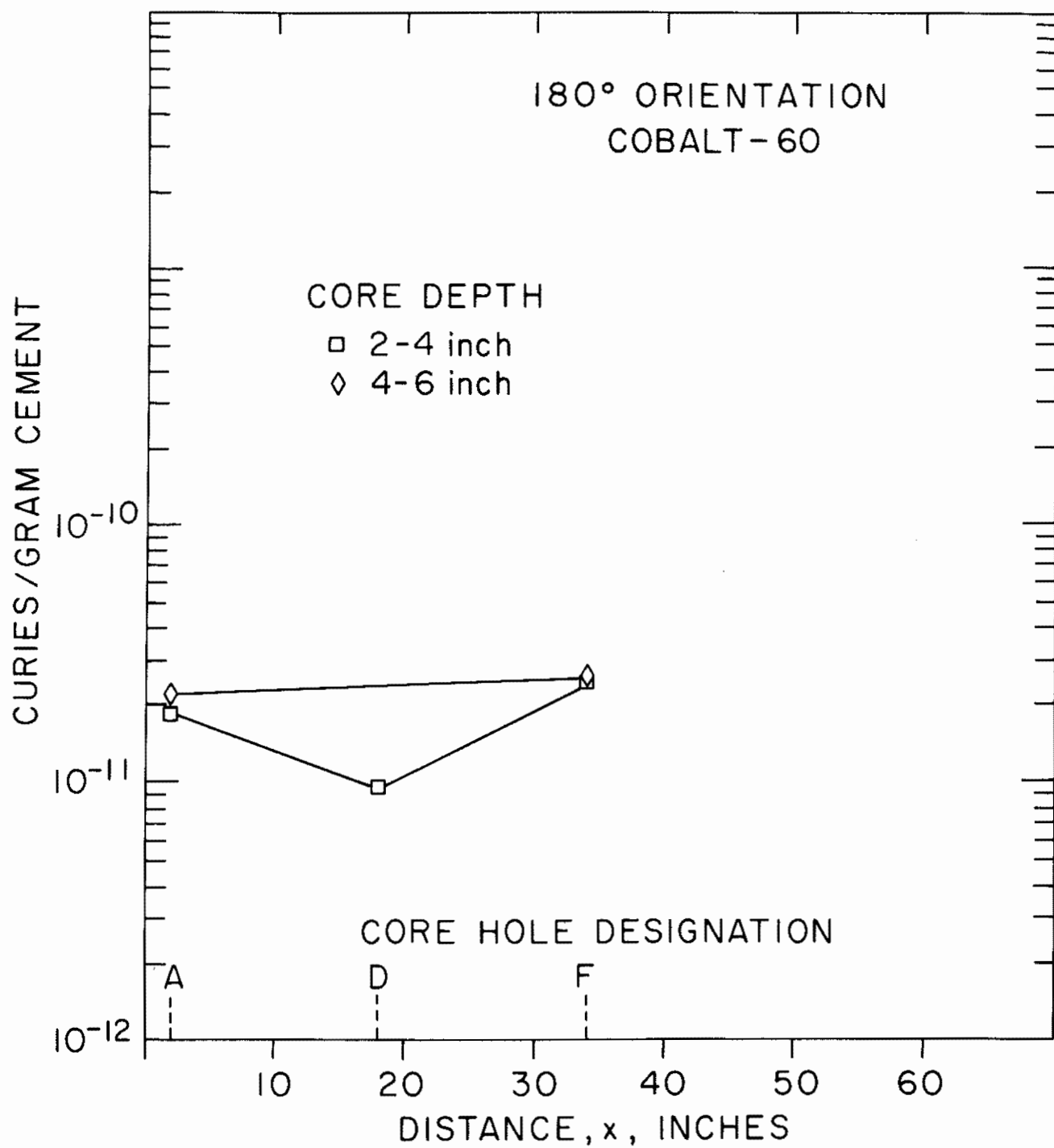


Figure 35. Cobalt-60 Content in Concrete Cores along the 180° Longitudinal Axis.

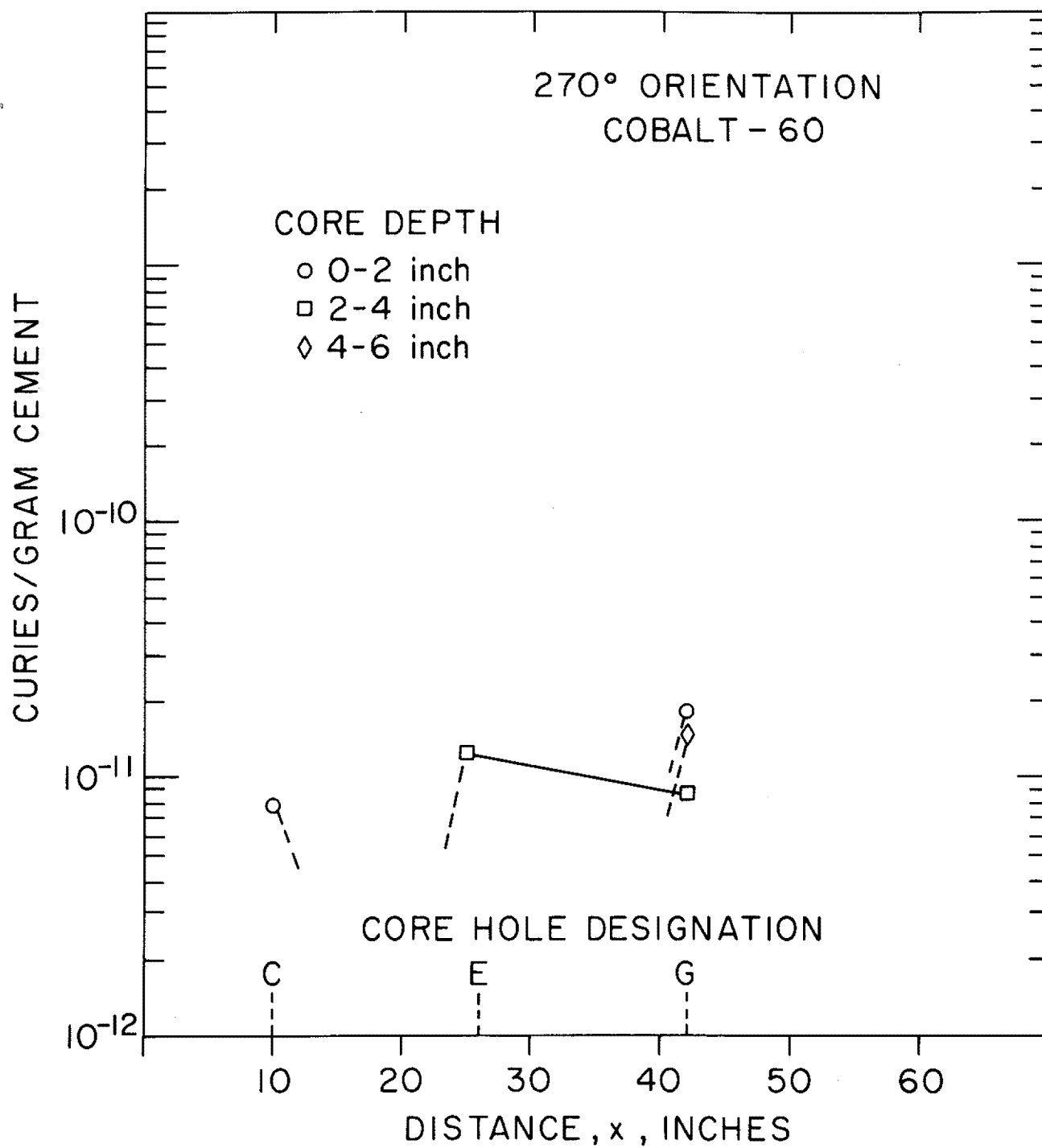


Figure 36. Cobalt-60 Content in Concrete Cores along the 270° Longitudinal Axis.

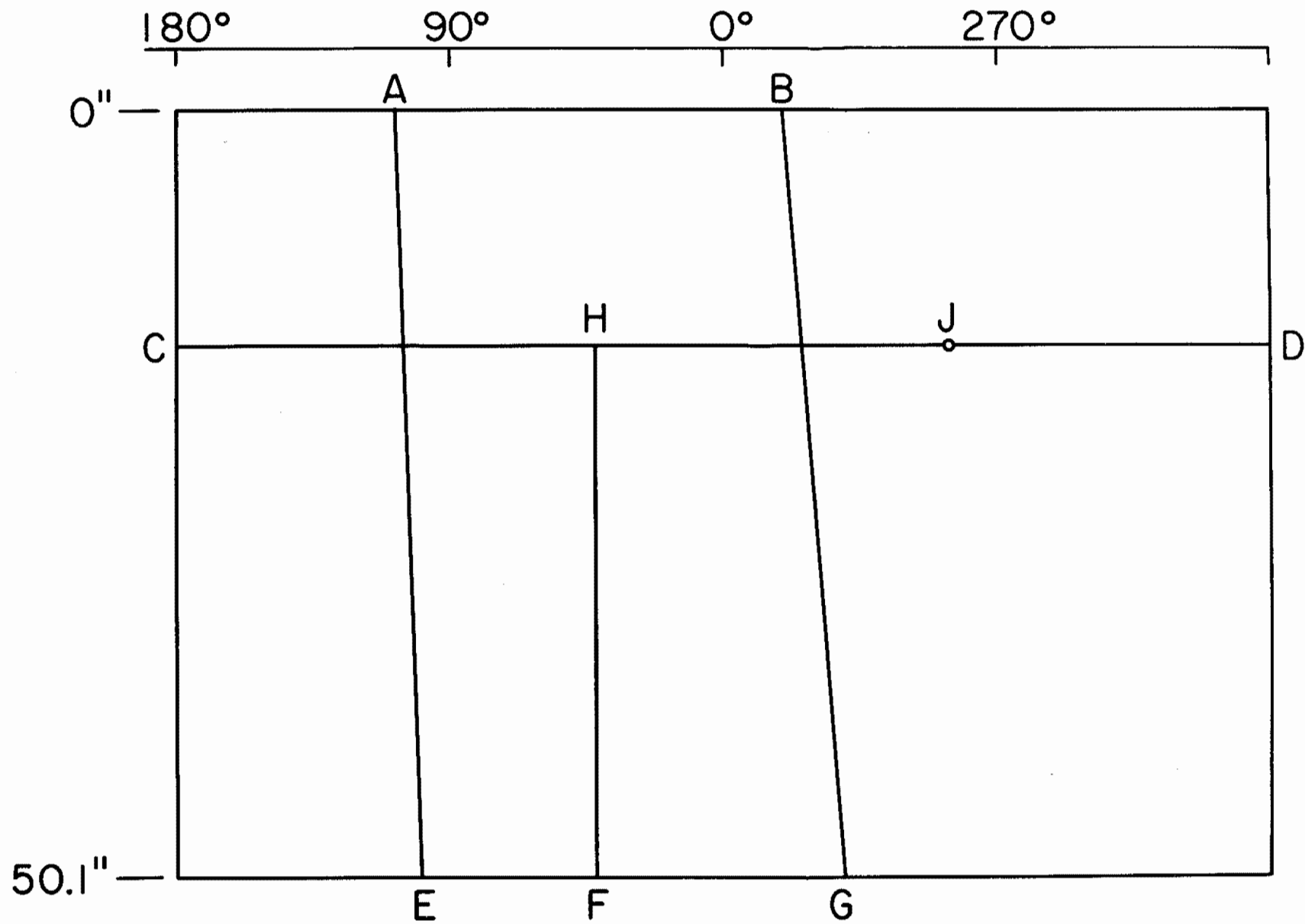


Figure 37. A Map of the Surface of the Container.



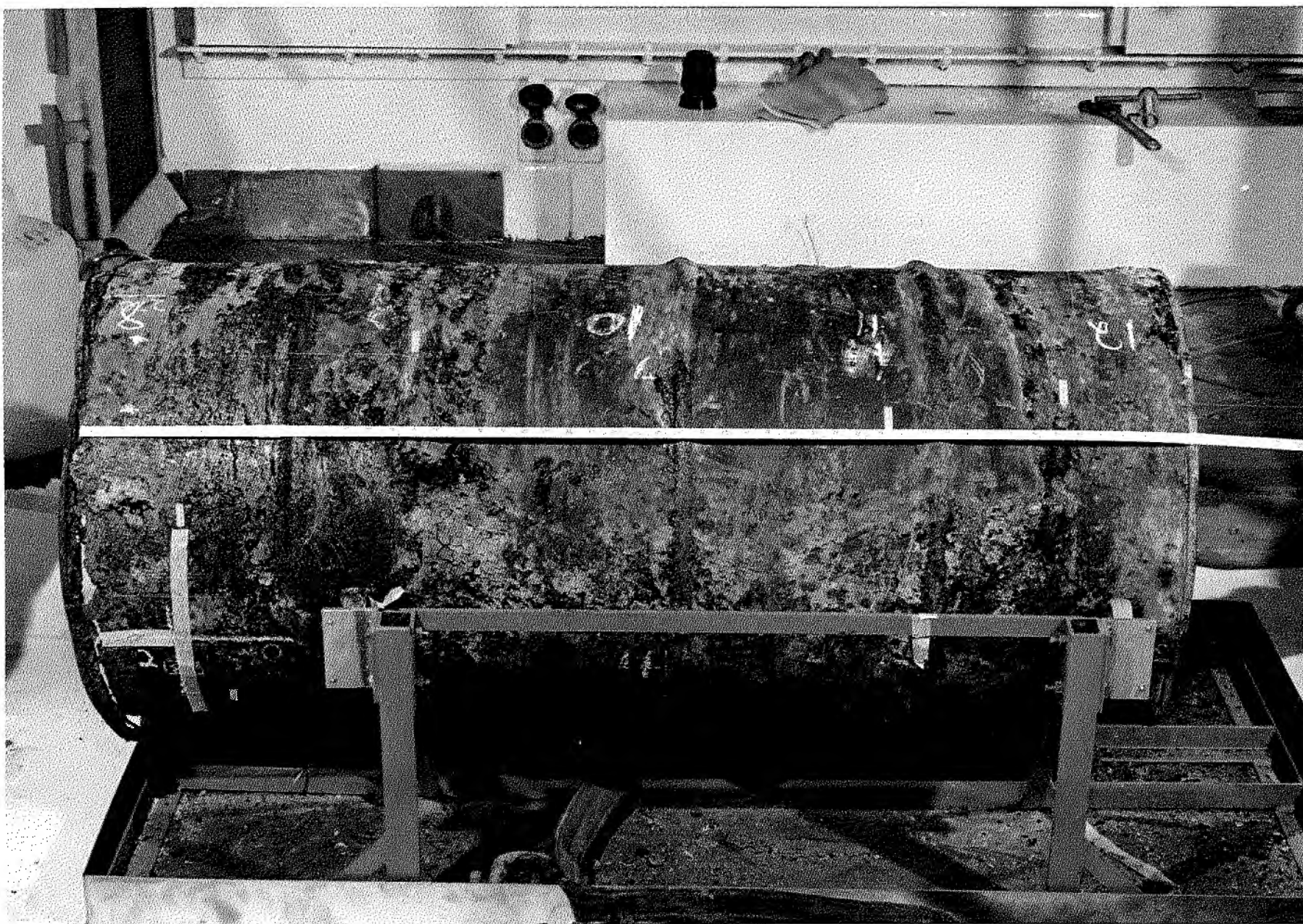
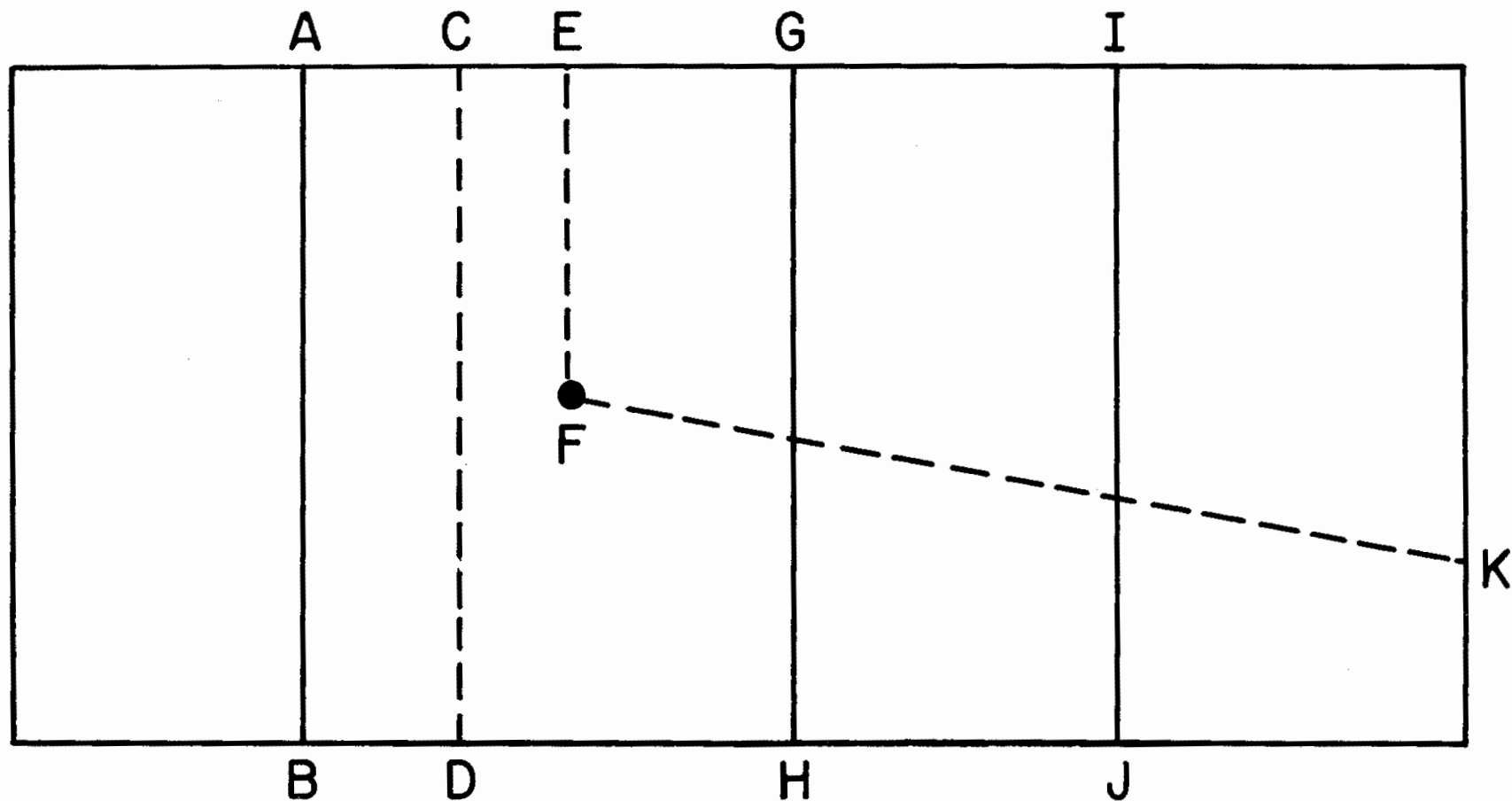


Figure 38. The Entire Length of the Container.



## CONTAINER SCHEMATIC

Figure 39. A Schematic illustrating Specific Features of the Container as Seen in Figure 38.



Figure 40. An Exterior View of the Upper Portion of the Container - Sediment Facing Side.



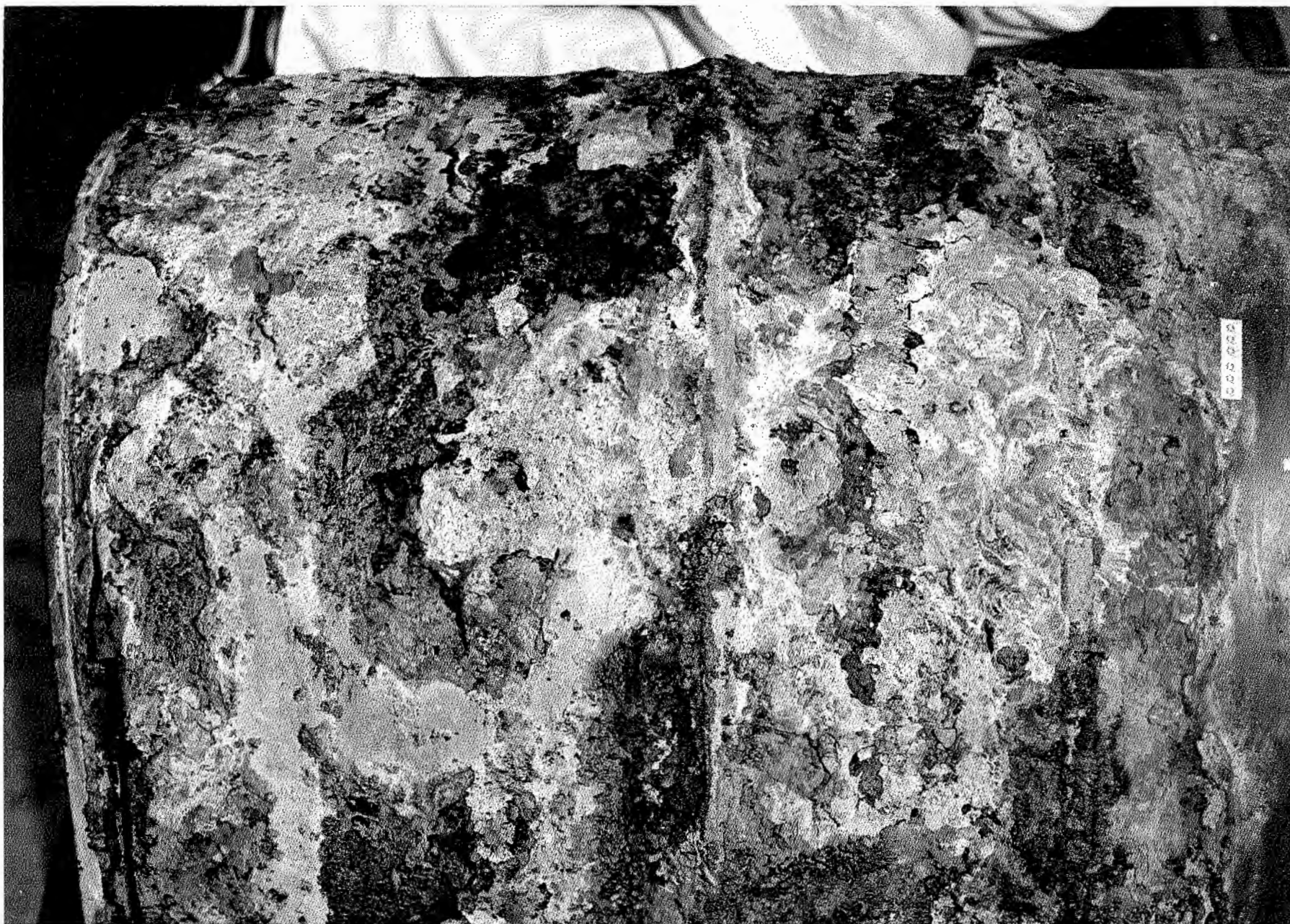


Figure 41. An Exterior View of the Upper Portion of the Container - Sea Facing Side.



1"

Figure 42. An Exterior View of the Mid-Section of the Container.



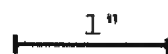


Figure 43. An Exterior View of General Attack Adjacent to a Chime within the Mid-Section.



Figure 44. Sediment Side Perforation Adjacent to a Chime as Viewed from the Inside of the Carbon Steel Sheath.

↓ Chime



Figure 45. Sea Side Perforation Adjacent to a Chime as Viewed from the Inside of the Carbon Steel Sheath.



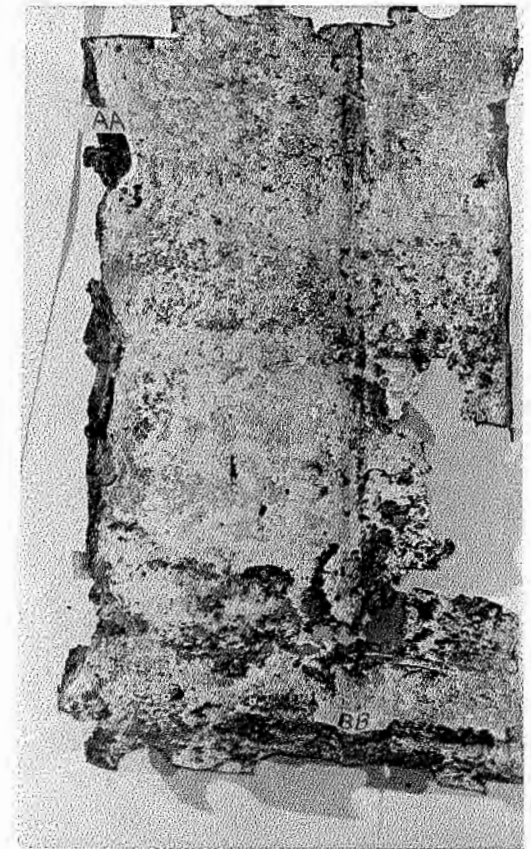
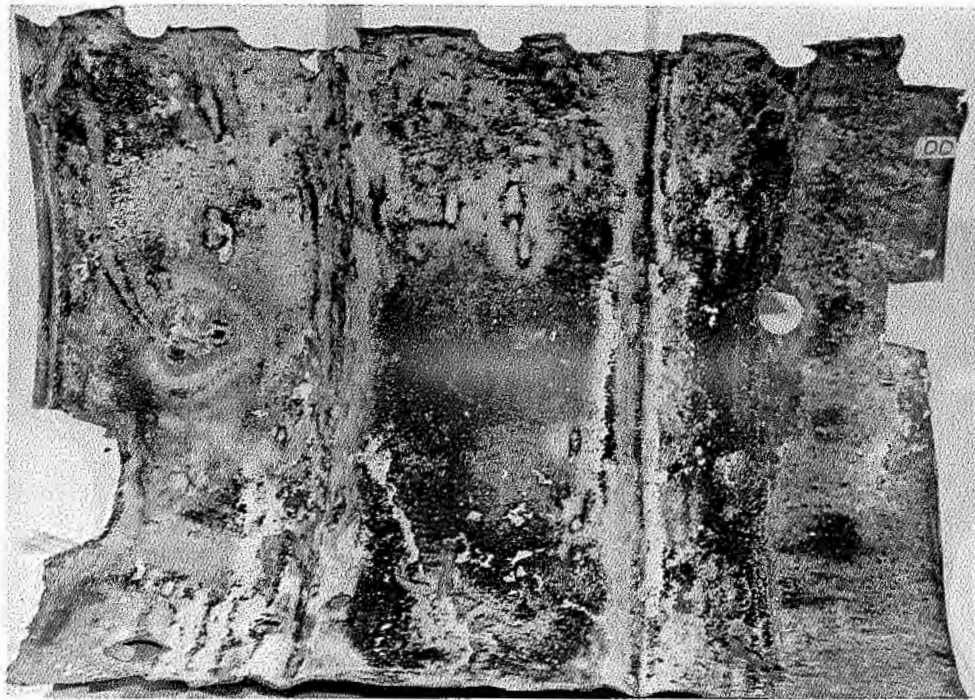


Figure 46. The Interior Surface of the Carbon Steel Sheath.

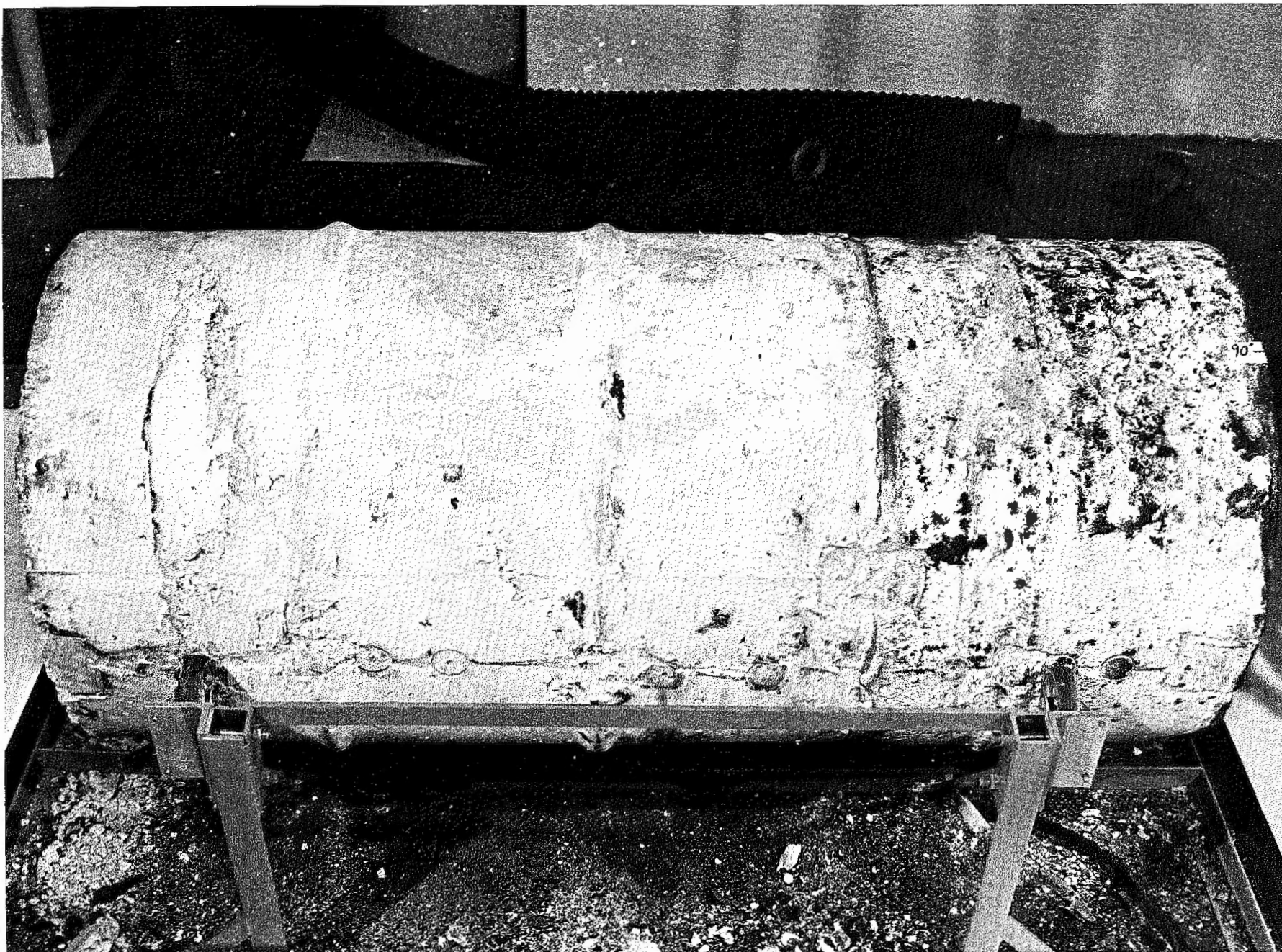
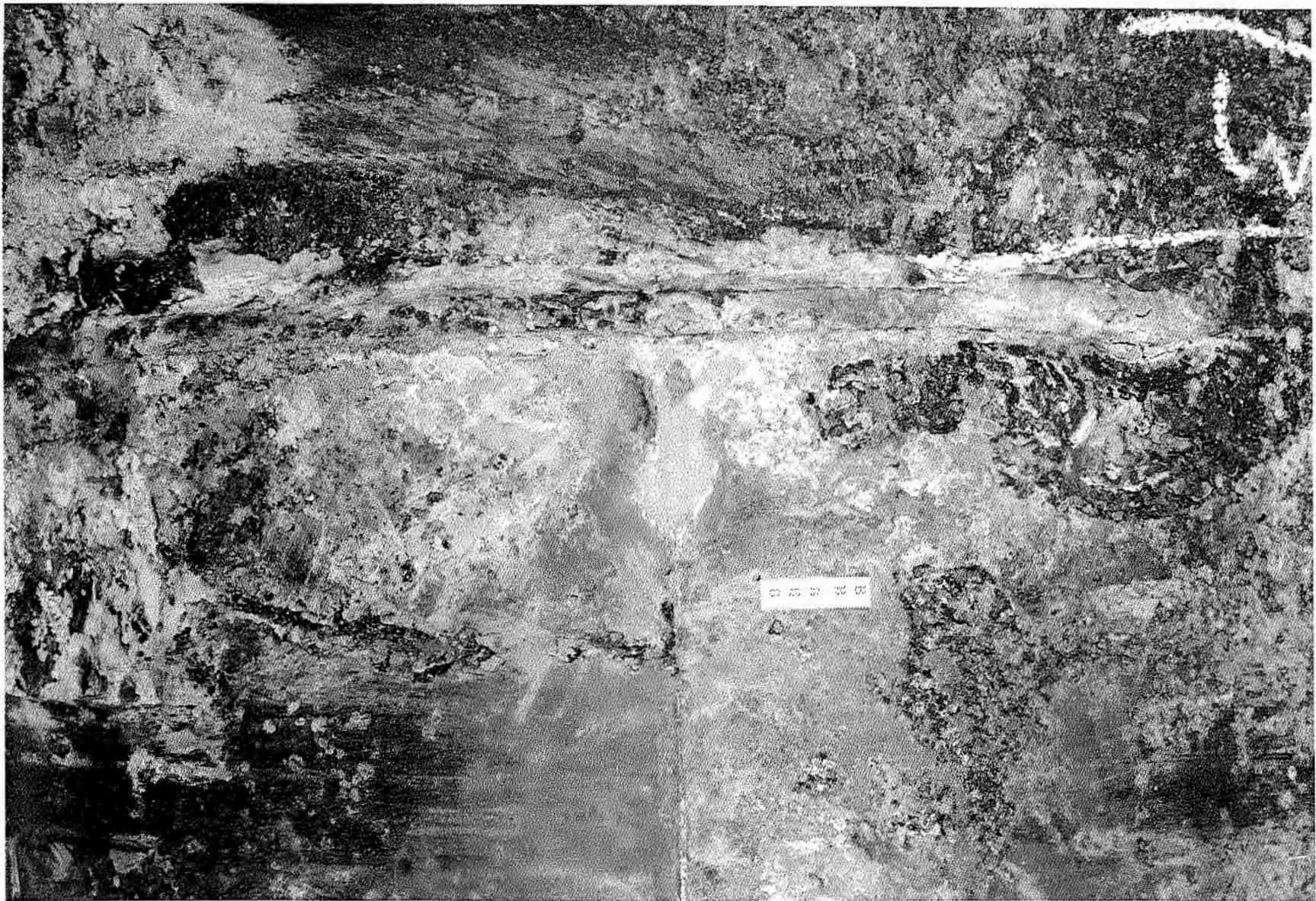


Figure 47. The Concrete Waste Form. The Upper Portion of the Form is to the Right in the Photograph.





Figure 48. Attack Adjacent to the Weld in the Upper Container.



1"

Figure 49. Attack Adjacent to the Weld in the Lower Container.





Figure 50. Macroscopic Pits Covering the Carbon S End of the Container.



Figure 51. The Metal End of the Container.





Figure 52. An Example of Filiform Corrosion.

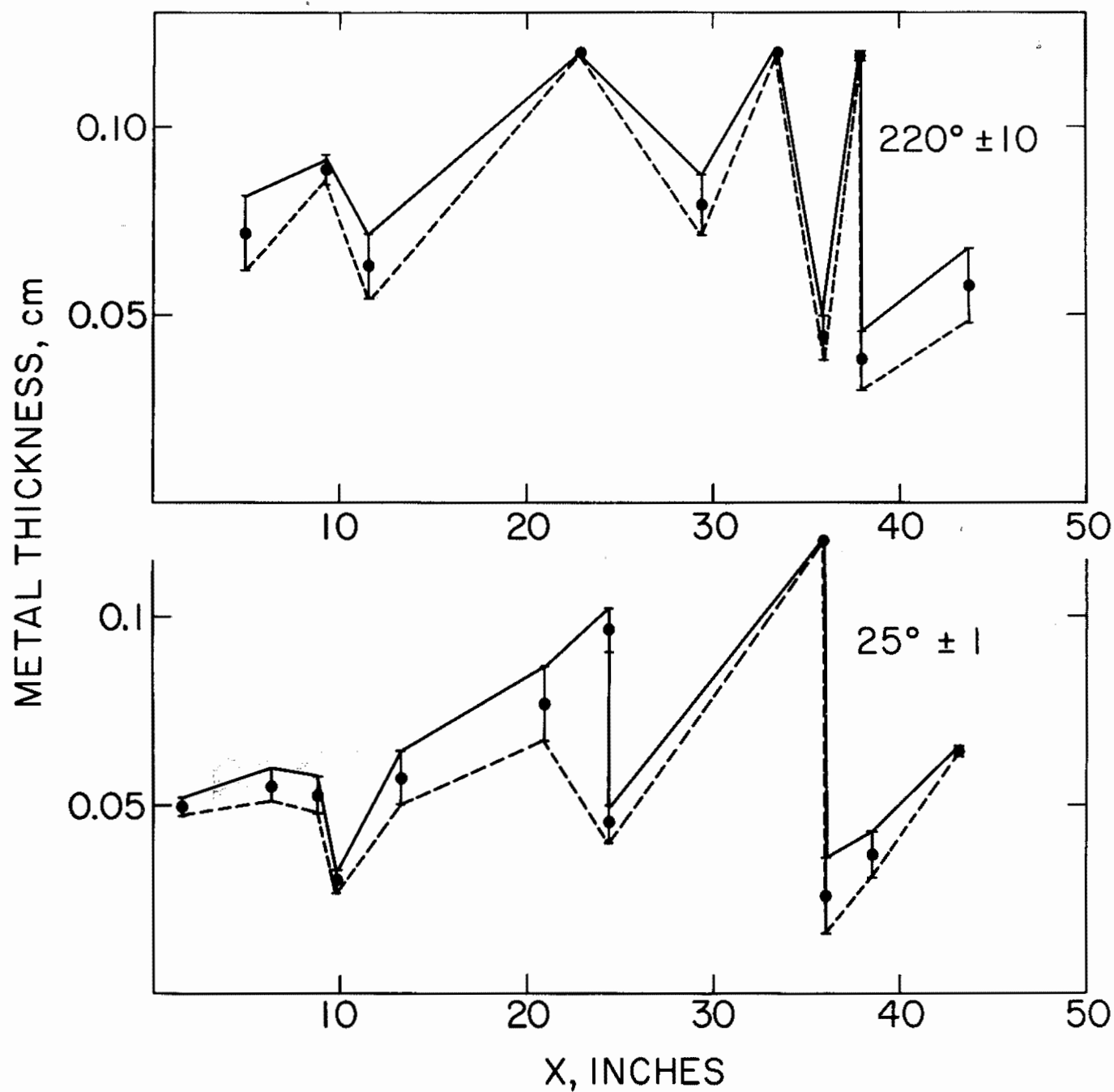


Figure 53. The Sheath Thickness vs. Container Position.



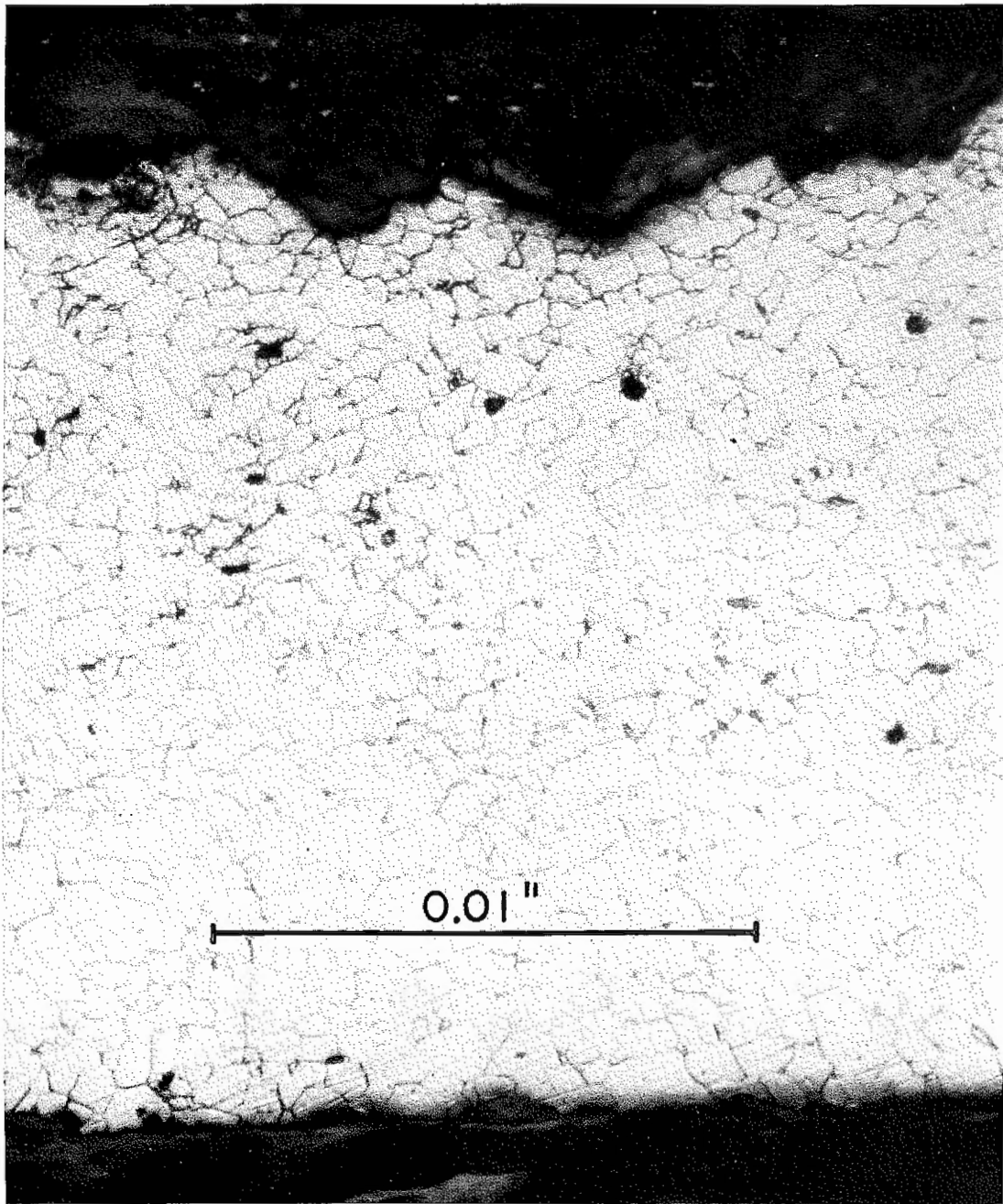


Figure 54. A Typical Metallographic Cross Section of the Upper Container.

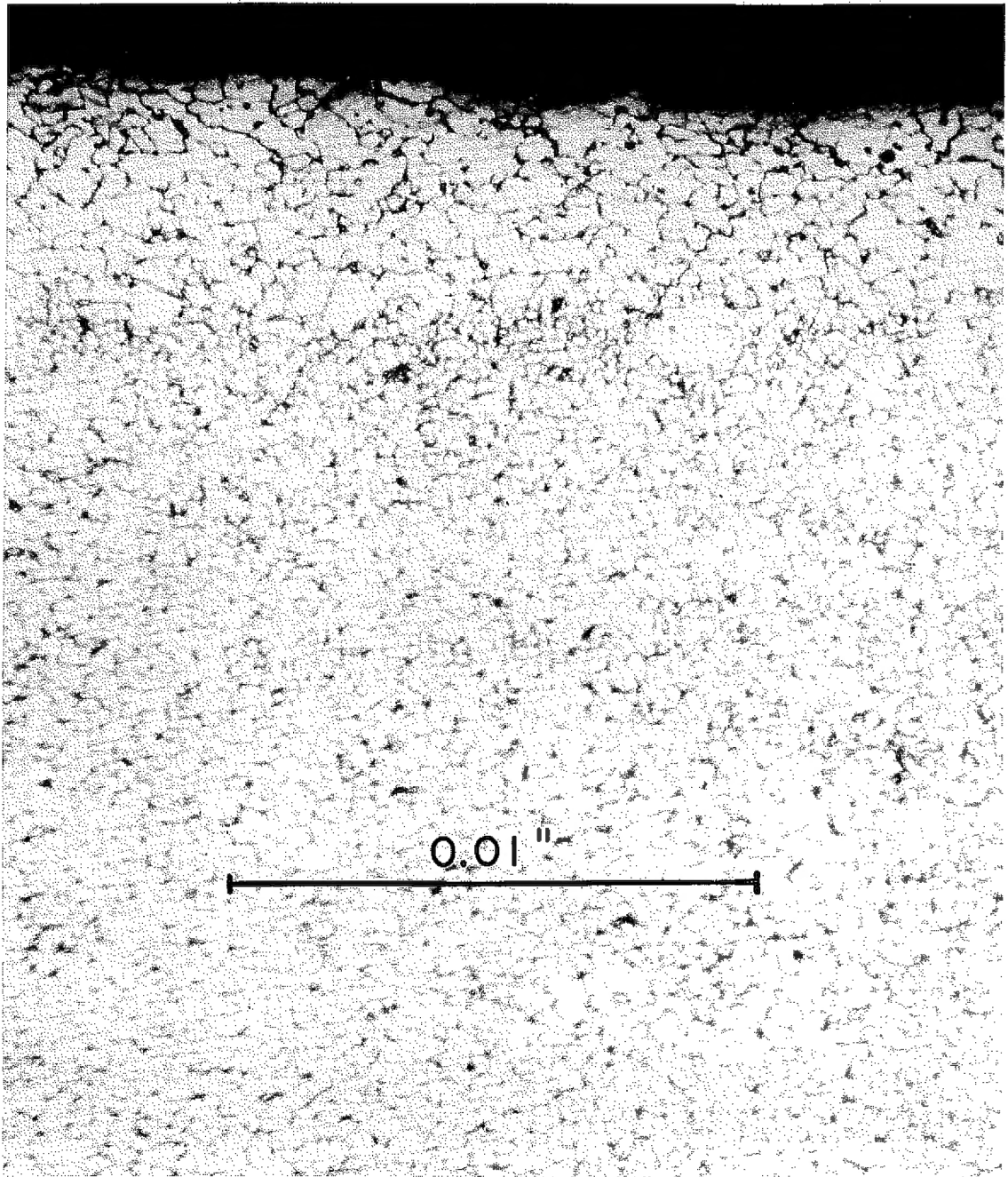


Figure 55. A Typical Metallographic Cross Section of the Lower Container.



Figure 56. Attack Within a Rim Fold.

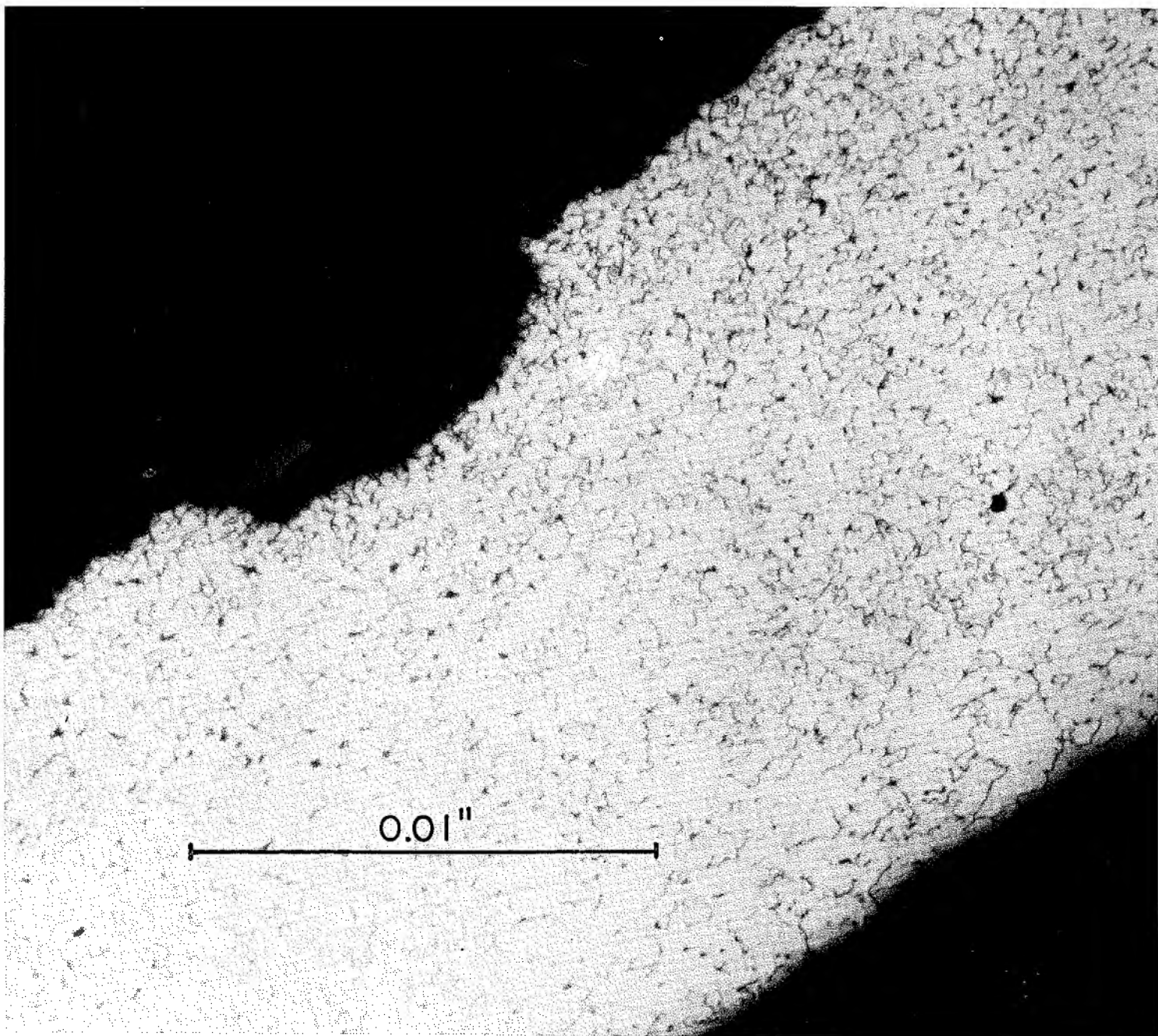


Figure 57. Attack at a Chime.



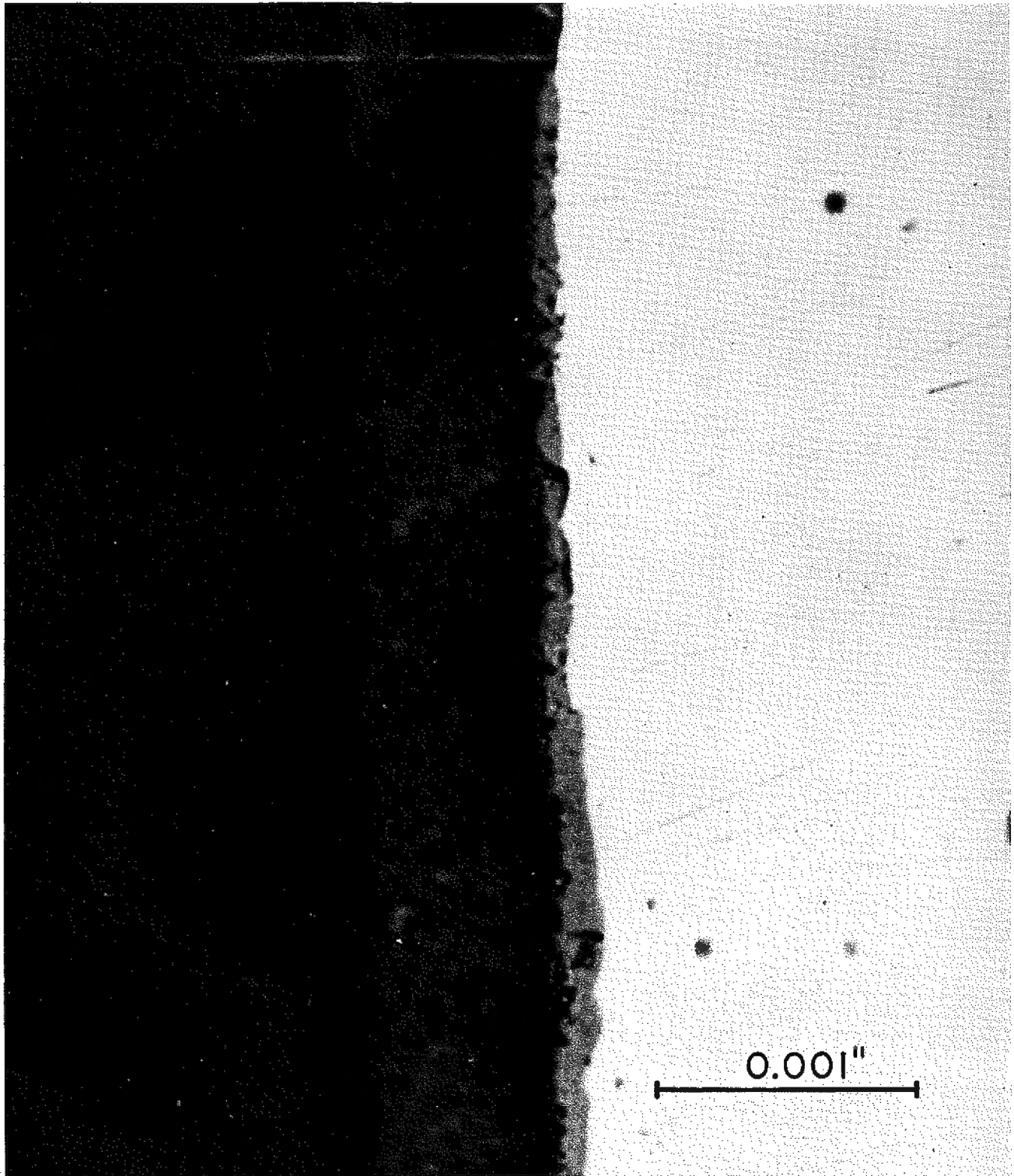


Figure 58. The Coated Interface.

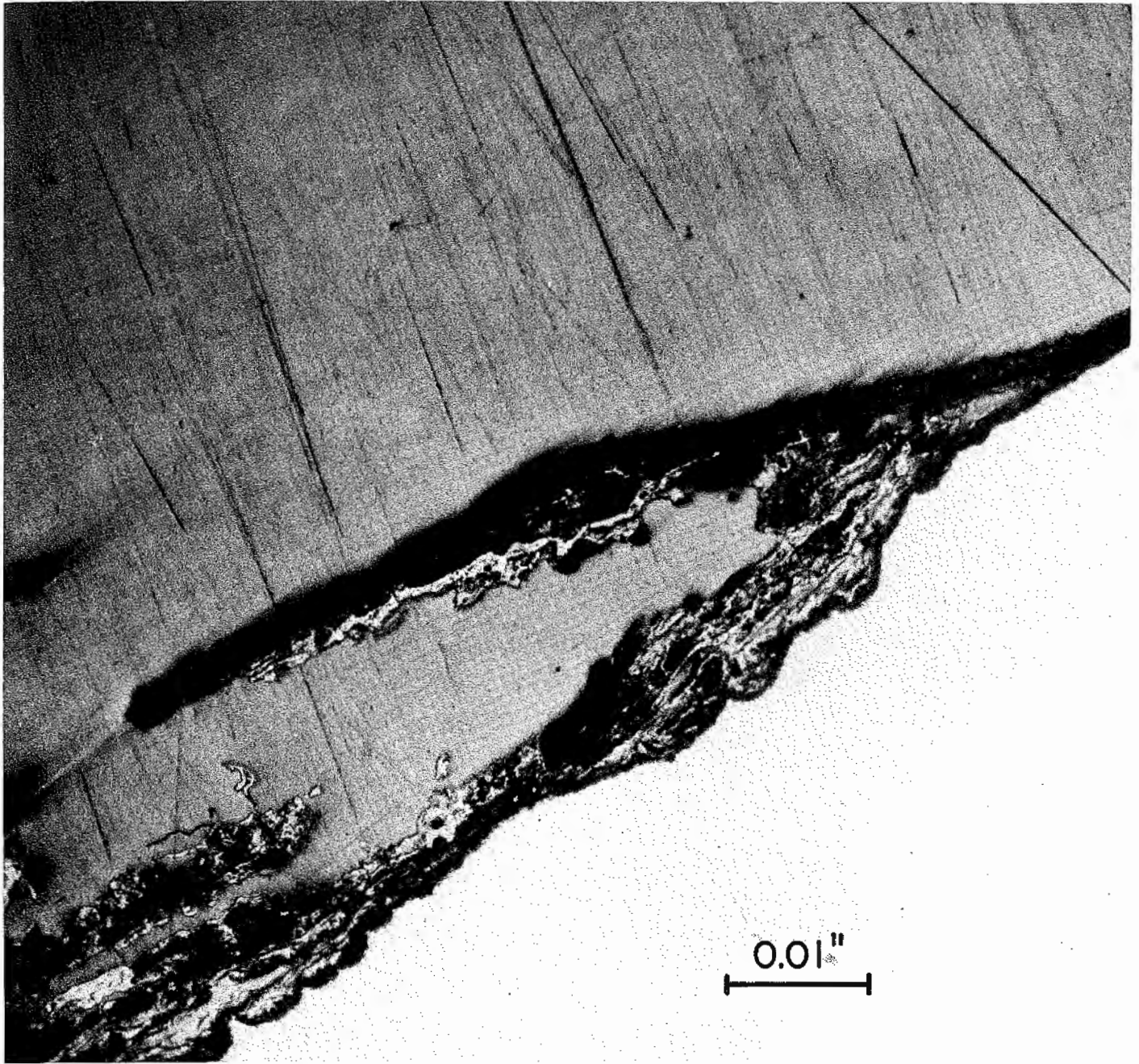


Figure 59. A Pit Formed Within the Coated Region of the Mid-Section of the Container.

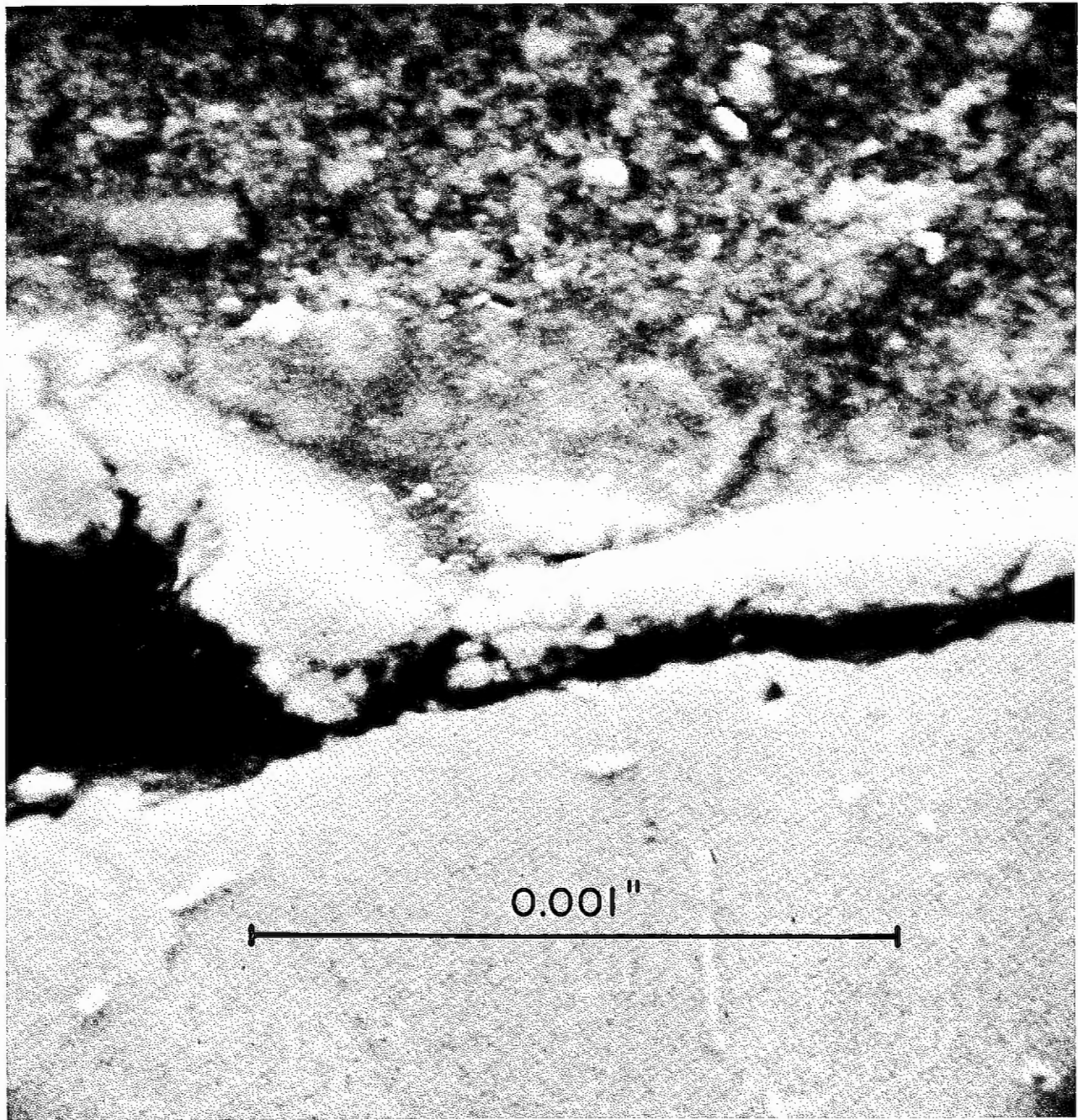


Figure 60. Scanning Electron Micrograph of  
the Disbonding of the Interfacial  
Oxide.

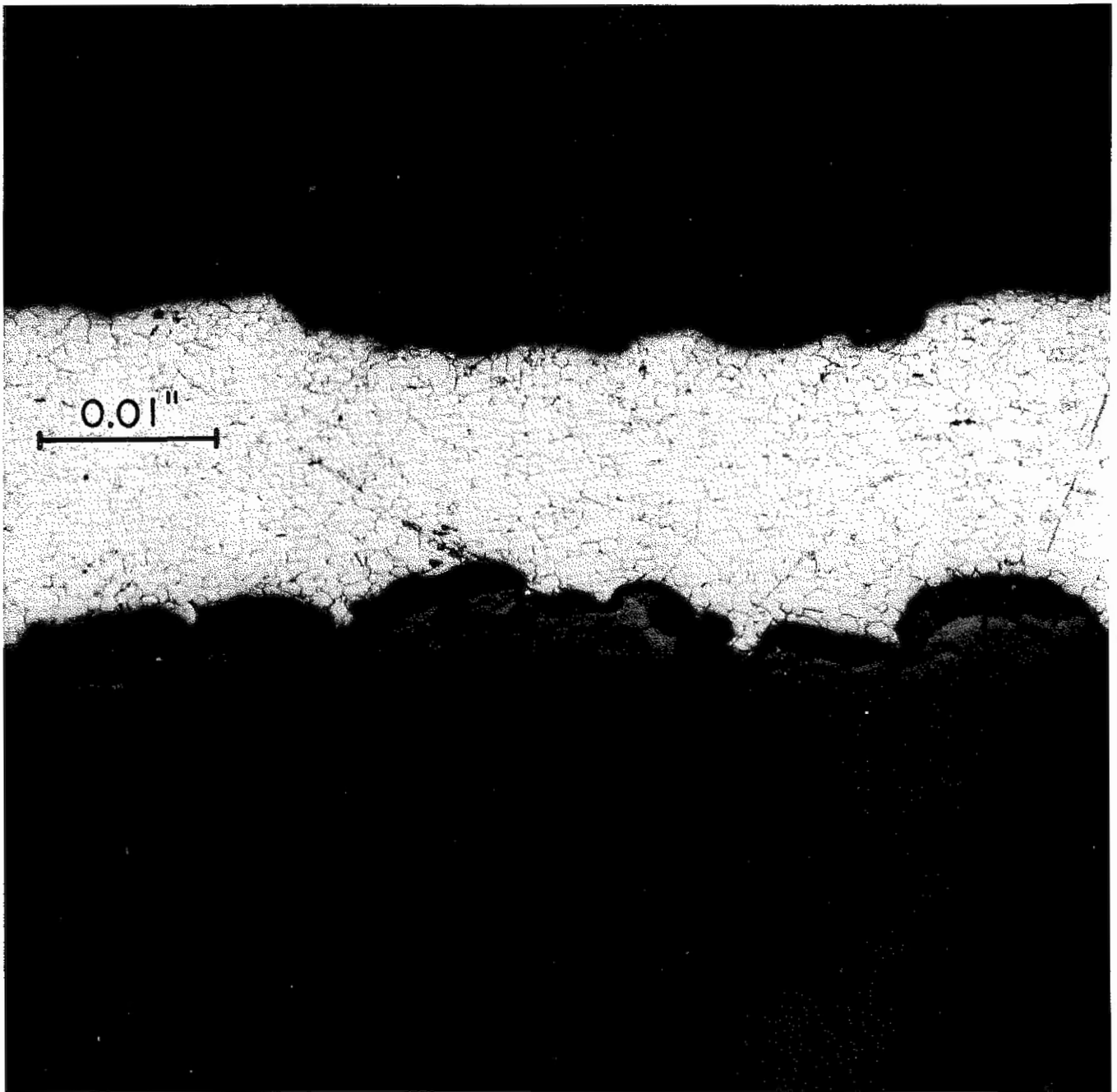


Figure 61. Micrograph of the Attack upon the Upper Container.



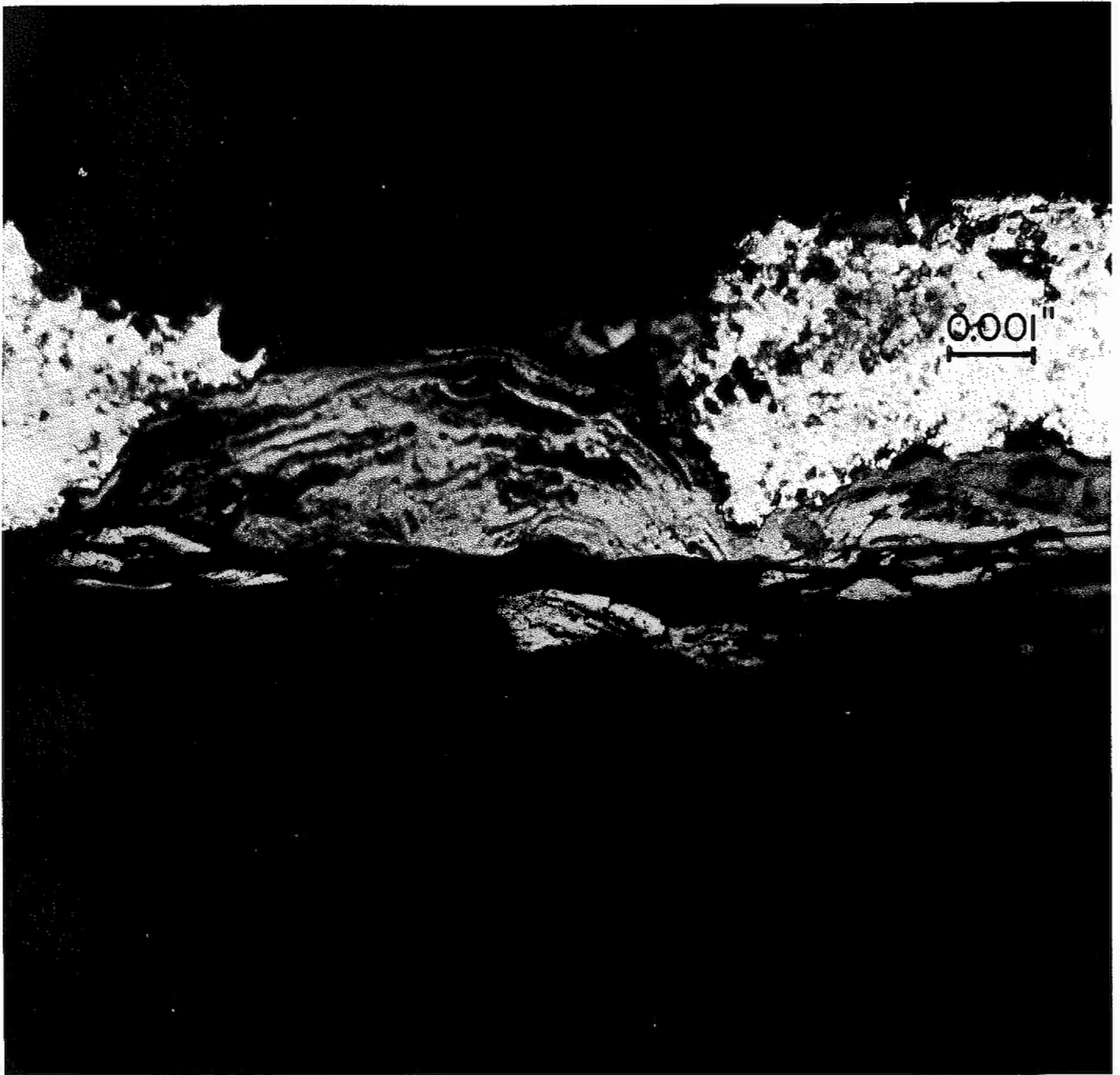


Figure 62. A Perforation Formed at the Upper Container Sheathing.

**TECHNICAL REPORT DATA**  
(Please read Instructions on the reverse before completing)

1. REPORT NO. EPA 520/1-82-009		2.		3. RECIPIENT'S ACCESSION NO.	
4. TITLE AND SUBTITLE Analysis and Evaluation of a Radioactive Waste Package Retrieved from the Atlantic 2800 Meter Disposal Site				5. REPORT DATE May, 1982	
				Date of Revision	
				6. PERFORMING ORGANIZATION CODE	
7. AUTHOR(S) P. Colombo, R. M. Neilson, Jr., and M. W. Kendig				8. PERFORMING ORGANIZATION REPORT NO. BNL 51102	
9. PERFORMING ORGANIZATION NAME AND ADDRESS Nuclear Waste Management Research Group Department of Nuclear Energy Brookhaven National Laboratory Upton, New York 11973				10. PROGRAM ELEMENT NO.	
				11. CONTRACT/GRANT NO. Interagency Agreement No. EPA-IAG-D6-0166	
12. SPONSORING AGENCY NAME AND ADDRESS Office of Radiation Programs U.S. Environmental Protection Agency 401 M Street, S.W. Washington, D.C. 20460				13. TYPE OF REPORT AND PERIOD COVERED Final	
				14. SPONSORING AGENCY CODE ANR-461	
15. SUPPLEMENTARY NOTES					
<p>16. ABSTRACT On July 31, 1976, an 80-gallon radioactive waste package was retrieved from a low-level radioactive waste dumpsite in the Atlantic, located at a depth of 2800 meters, 120 miles (190 Km) east of the Maryland-Delaware coast at coordinates 38°30'N, 72°06'W. This was the first such recovery of a radioactive waste package from an ocean dumpsite and was conducted by the EPA Office of Radiation Programs. The drum was transported to the Brookhaven National Laboratory where container corrosion, and matrix leach rate and degradation rate analyses were conducted. The drum was dumped approximately 15 years prior to recovery and was found to contain a sealed steel vessel containing some liquid and wound filter assemblies. The integrity of the concrete matrix had not degraded appreciably, and it is estimated that in the ocean dumpsite recovery environment it would require a minimum of 300 years before the concrete waste form would lose its integrity and provide no barrier to radioactivity release. The concrete waste form contained cesium-134, cesium-137, and cobalt-60 in both the concrete matrix and the inner steel vessel. The inner steel vessel did not leak; hence, the radioisotopes were contained. The estimated annual rate of leaching of the cesium-137 radioisotope measured in the concrete matrix was 3.7% per year.</p> <p>Corrosion attack on the metal container varied between the upper portion of the drum exposed to ocean water, and the lower portion of the drum exposed to sediment. General thinning attack appears to be the most important corrosion process. It is estimated that an 18 gauge mild steel drum in this ocean dumpsite would require 25-37 years before corrosion would cause the metal container to lose its effectiveness as a barrier to radioactivity migration.</p>					
17. KEY WORDS AND DOCUMENT ANALYSIS					
a. DESCRIPTORS		b. IDENTIFIERS/OPEN ENDED TERMS		c. COSATI Field/Group	
Ocean Dumping/Sea Disposal Radioactive Waste Disposal/Nuclear Waste Disposal Radioactive Waste Packaging-Concrete Deepsea Corrosion					
18. DISTRIBUTION STATEMENT  Unlimited Release		19. SECURITY CLASS (This Report) Unclassified		21. NO. OF PAGES 118	
		20. SECURITY CLASS (This page) Unclassified		22. PRICE	